Session IV

Detectors and facilities

Chairs: Ferenc Tarkanyi, Urszula Woznicka

Measurement of (n,xnγ) reactions at high precision

Jean-Claude Thiry,[1] **Catalin Borcea,**[3] **Philippe Dessagne,**[1] **Jean-Claude Drohé,**[2] **Erwin Jericha,**[4] **Habib Karam,**[1] **Maëlle Kerveno,**[1] **Arjan J. Koning,**[6] **Alexandru Liviu Negret,**[3] **Andreas Pavlik,**[5] **Arjan J.M. Plompen,**[2] **Chariklia Rouki,**[2] **Gérard Rudolf,**[1] **Mihai Stanoiu**[2]
[1]Université de Strasbourg, Strasbourg, France
CNRS, Strasbourg, France
[2]European Commission, Joint Research Centre, Institute for Reference Materials and Measurements, Geel, Belgium
[3]National Institute of Physics and Nuclear Engineering "Horia Hulubei", Bucharest-Magurele, Romania
[4]Technische Universität Wien, Atominstitut, Vienna, Austria
[5]Universtität Wien, Fakultät für Physik, Vienna, Austria
[6]Nuclear Research and Consultancy Group, Petten, The Netherlands

Abstract

The design of Generation IV nuclear reactors and the research of new fuel cycles require knowledge of cross-sections for different nuclear reactions. Our work is focused on the determination of the cross-sections of (n,xnγ) reactions occurring in these new reactors. The aim is to measure unknown cross-sections and to reduce uncertainty on present data relative to reactions and isotopes present in transmutation or regeneration processes.

The current study is relative to measuring ^{232}Th(n,n'γ) and ^{235}U(n,xnγ) reactions in the fast neutron energy domain (up to 20 MeV). The experiments are performed at GELINA (IRMM, Belgium) which delivers a pulsed, white neutron beam. The time characteristics of the beam enable us to measure neutron energies with the time of flight (TOF) technique. The neutron induced reactions (in this case inelastic scattering and (n,2n) reactions) are identified by online prompt γ spectroscopy with an experimental setup including 4 HPGe detectors. A double layered fission chamber is used to monitor the incident neutron flux.

As the precision is a key issue in these measurements, the detectors used in the experiment were studied extensively in order to reduce the uncertainties of the results to a minimum. Simulations and calibration experiments were realised and are presented.

Introduction

Knowledge of (n,xn) reactions is of crucial importance for the development of the new Generation IV nuclear reactors. These future systems will explore new energy domains and in order to optimise their design, the measurement of (n,xn) reaction cross-sections at a high level of precision is absolutely mandatory. Indeed, these reactions are an important energy loss mechanism, lead to neutron multiplication and production of radioactive isotopes.

The measurements are realised using the (n,xnγ) technique, for which a high precision experimental setup was developed and is presented here. It is meant to be used to probe reactions for which a high precision is required, such as for the ^{238}U(n,n') reaction cross-section, part of the NEA High Priority List [1]. The ultimate goal of developing these measurement techniques is to study (n,xn) reactions on ^{233}U, lacking experimental data, which is of upmost importance for the thorium cycle. For example, the ^{233}U(n,2n)^{232}U reaction leads in its decay to ^{208}Pb, emitter of a 2.6 MeV γ ray. Presence of such energetic photons has a major impact for the reactor core temperature, and therefore needs to be studied precisely.

Experimental setup

The experimental setup, shown in Figure 1, as well as the applied measurement techniques are treated in this section.

Figure 1: Experimental setup used at GELINA, FP16/30m

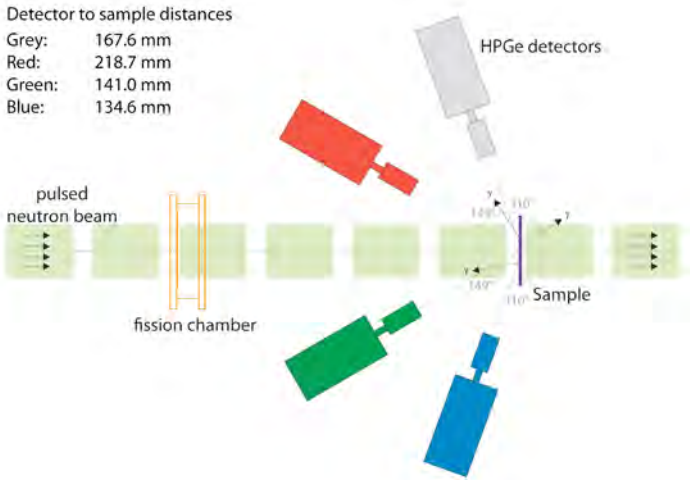

The (n,xnγ) technique

A sample enriched in ^{A}X isotopes is irradiated by a neutron beam inducing (n,xn) reactions, which produce $^{A-(x-1)}$X isotopes in excited states. Decay of these isotopes leads to emission of characteristic γ rays, witnessing a prior reaction. The intensity of these γ rays yields the cross-section of isotope production in a given excited state. The data can be used to validate theoretical codes, such as TALYS, which is able to predict (n,xnγ) reaction cross-sections (see *e.g.* ref. [2]).

The TOF technique

The experiments presented in this work were performed at the GELINA facility of the IRMM, Geel, Belgium, which produces a white, pulsed neutron beam using the (γ,xn) and (γ,F) reactions on a depleted uranium target. The energy domain of the produced neutrons ranges from a few keV up to several MeV [3,4].

The TOF technique is used to determine the incident neutron energy and the presence of a γ flash enables us to calibrate the time spectra. In order to obtain the best compromise between time (and thus neutron energy) resolution and flux intensity (resolution of 1 MeV at E_n = 20 MeV) the setup was installed at 30 m distance from the neutron source.

Flux monitoring

The uncertainties on the incident neutron flux (Figure 2) influence strongly the quality of the cross-section measurements. For this reason special effort has been made to obtain very precise flux data.

A fission ionisation chamber with a uranium sample is used to determine the neutron flux. The deposit, highly enriched in ^{235}U (>99.5%), is very thin: 324 μg/cm^2 and was made of vacuum evaporated $^{235}UF_4$. The effective thickness of the fission chamber was chosen between 6 and 7 mm, as this leads to the best ratio of fission fragment energy loss (signal) and radioactivity α particle energy loss (background noise), as explained later.

Figure 2: Differential neutron flux measured at FP16/30m at GELINA

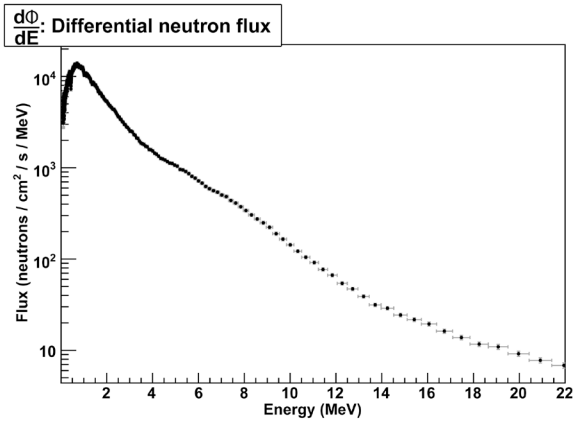

γ detection

4 High Purity Germanium (HPGe) detectors, referred to as *grey*, *red*, *green* and *blue* are used to observe the γ rays emitted by the created isotopes. These semiconductor counters are made of semi-planar crystals with depths ranging from 2 to 3 cm and surfaces between 10 and 28 cm^2. This type of detectors has been chosen as they allow for high energy resolution at low γ ray energy together with a good timing. In order to take into account the angular distribution of the emitted γ rays, they are placed at 110° and 149° with respect to the incident neutron beam. Backward angles were chosen to reduce dead time caused by the observation of events due to γ flash scattering, amounting up to 60% of the detections.

Efficiency of the fission chamber

As mentioned previously, the precision of the (n,xnγ) measurements is of upmost importance. This section treats the efforts made on reducing the uncertainty caused by the fission chamber. Indeed, this detector presents one of the major sources of error on the final results. For this reason, an extensive work was realised on the determination of the fission chamber efficiency.

Determination of the fission yield

An energy spectrum for the UF_4 deposit acquired during (n,xnγ) measurements at the GELINA facility is shown in Figure 3. In the low energy domain of the energy spectra one can see a very strong contribution coming from the α particle signals, which are due to the radioactivity of the uranium

foils. To the right, in the higher energy ranges one can observe events due to fission products in a double-humped shape.

Figure 3: Energy spectrum for the fission chamber deposit UF4 in its initial configuration: the gap between the electrodes is 8 mm with reverse biasing (HV on the deposit)

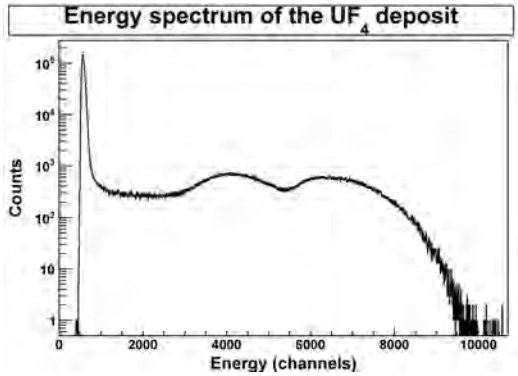

Separating the α particle signals from the fission events is a delicate process. In fact, the signal amplitudes generated both by the uranium decay and the neutron induced fissions have a respective upper limit value, *i.e.* their pulses are always weaker than a certain energy, but they do not have a lower limit. This means that the fission product signals share a part of their energy domain with the α particle signals which makes a strict separation between both types of signals very difficult. The only acceptable approach to achieve this goal is to apply an energy threshold to discard the α component and to correct for the portion of fission product signals lost.

Optimisation of the fission chamber configuration

As a threshold has to be applied to the energy spectra, it is important to configure the fission chamber in a way that as few events as possible are lost in this procedure. This means that we have to determine the configuration which leads to the best separation between α decays and fission products.

To achieve this, several measurements were performed. First, the thickness of the fission chamber was modified. Thicknesses of 6.5, 8 and 27 mm were chosen. The result is shown in Figure 4 (left). This comparison shows that the best configuration is to have a 6.5 mm gap between the anode and the cathode. Indeed, in this scenario the α particles are penalised with respect to the fission products. As their range is longer and their kinetic energy rather high, most of the energy loss occurs

Figure 4: Comparison of the different configuration possibilities of the fission chamber: (a) shows the effect of varying the effective volume of the chamber, (b) shows the effect of polarisation changes

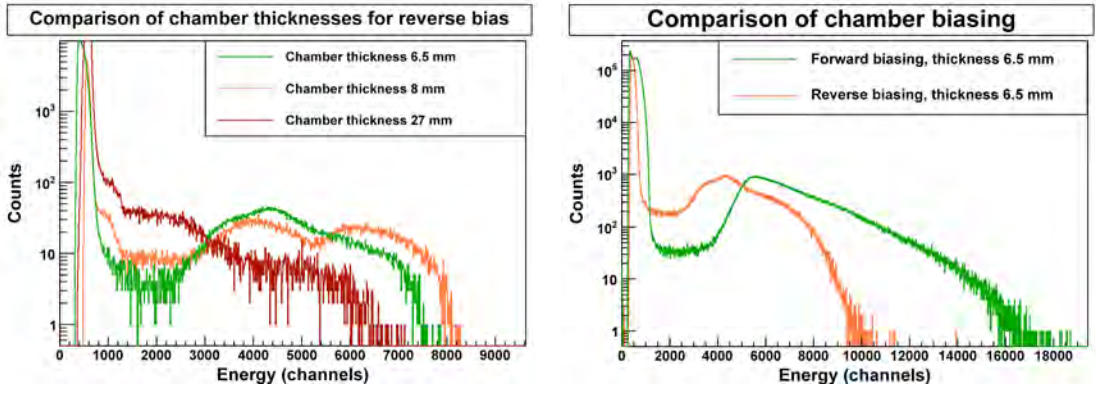

in the Bragg peak, whereas fission products lose their energy almost continuously. Increasing the volume thus means detecting more α particles, and filling up the valley between both contributions.

In a second study the impact of biasing was analysed. Figure 4 (right) shows the difference obtained when applying a reverse bias (HV on the deposit) or a forward bias (HV on the opposite electrode). In fact, the signal left in the fission chamber depends on the charge created, and thus the energy deposited, but also on the distance to the collection electrode. For this reason, fission products stopping in the chamber before reaching the opposite electrode create a larger signal in the forward bias scenario than in the reverse bias case. It is therefore preferable to apply forward biasing.

Correction for signal loss

In order to correct for signals lost, we distinguish between two different types. First, there are fission products created in the deposit without sufficient energy to leave the foil creating no signal at all. Secondly there are fission products producing a weak signal which is lost as it falls below the threshold in the energy distributions.

Whereas the first type can be corrected easily by applying well-known techniques [5,6], the second type cannot be corrected so easily. For this reason Geant4 [7] simulations were performed in order to reproduce the spectra and to show the behaviour of the fission products at low energy. The results in this region were however not satisfactory. Indeed, at very low energy, the energy loss of the fission products is not well known, which leads to a systematic difference between the simulated and measured spectra. Because of this, we cannot conclude how to extrapolate the fission product contribution towards low energies: A linear extrapolation to zero amplitude appears plausible, but there is no conclusive proof that this is adequate. In fact, for reverse biasing the simulations show that the expected loss is larger than would be inferred from a linear extrapolation while in contrast linear extrapolation is expected to be adequate for a forward bias. Again, given the imperfect nature of the simulations the situation is inconclusive.

Calibration measurements at PTB

As the previous correction strategies were not reliable, the fission chamber was calibrated using a monoenergetic (E = 8.4 MeV) neutron beam produced at the Physikalisch-Technische Bundesanstalt (PTB) in Braunschweig. The beam was well characterised by different reference measurements of high precision, including a recoil proton telescope (RPT) and a liquid scintillation detector [8]. The neutrons were produced through D(d,n)^{3}He reactions. Time of flight and energy information were saved in list mode files, enabling time gating on the acquired data, to eliminate neutrons with wrong energy, *e.g.* born through break-up reactions in the deuterium target or slowed down through scattering in the experimental hall. For the measurements several foreground runs were performed to obtain statistics of at least 10000 events in the fission chamber. Two series of background measurements were made: the first by placing a shadow cone between the neutron source and the detector to evaluate the indirect component of fission events generated and a second by taking the deuterium gas out of the target and bombarding the empty target with deuterons to estimate the amount of neutrons created by other mechanisms than that of the direct reaction.

After corrections for acquisition dead time and air attenuation, these measurements enabled us to determine the efficiency to detect a fission event in the ionisation chamber to be (94.4 ± 2.1)%, when applying a threshold in the middle of the plateau separating α particles and the main fission product contribution. Using this value, measured at 8.4 MeV, as a reference together with the corrections for events lost due to absorption in the foil [5,6], we can calibrate our efficiency curve shown in Figure 5.

Figure 5: Final efficiency values as a function of incident neutron energy

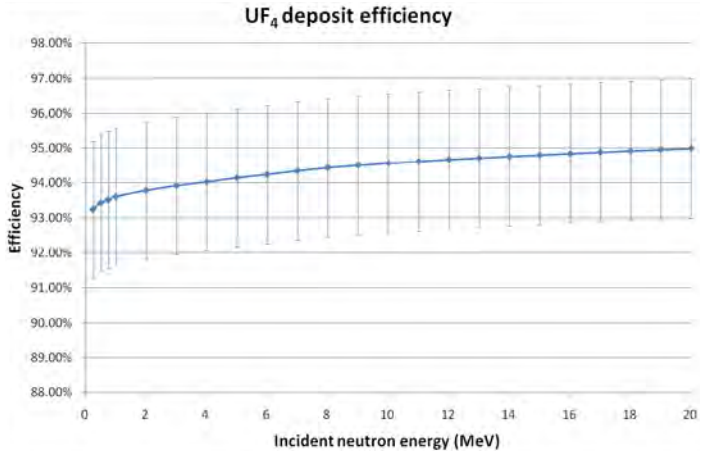

Efficiency of the HPGe detectors

Another large source of uncertainties comes from the evaluation of the γ-detection efficiency of the HPGe detectors. This section presents the work that has been realised on the determination of this quantity.

Efficiency computing method

The absolute photopeak-efficiency of a germanium detector in the case of extended samples depends on several parameters, which have to be taken into account in the total efficiency calculation. Besides the position of the detector with respect to the γ-ray emitting sample and the energy of the studied γ ray, these parameters also include:

- the shape of the γ-ray emitting sample (in our case this corresponds to the beam diameter of the order of 5 cm)
- the geometry of the crystal inside the detector
- the self-absorption $k_{E\gamma}$ of the γ rays inside the sample

Calibrations realised with a point source only are not sufficient in our case, as the studied sample is not point-like, *i.e.* the geometrical distributions of the emitted γ rays cannot be calculated at a satisfactory level. Another difficulty is introduced by the absorption of the γ rays inside the sample which is an important factor as the density and thickness of the used samples are rather high.

The best way to consider all these parameters is to measure the efficiency with calibrated sources and to compare these to Monte-Carlo simulations of the detector [9]. The procedure for this method is realised in several steps: First, the geometry of the crystal is determined and entered into a Geant4 simulation code. Then calibrated sources (point-like and extended) are placed at different spots of the sample position. The obtained results are compared to the simulated spectra. The differences in the yields are used to determine the dead layers of the crystal and to calibrate the simulation input. Once the simulation parameters are fixed, the second step consists of simulating the studied sample. For this purpose the geometry of the sample is entered into the simulation code and γ rays of the energies of interest are shot randomly within the sample. The ratio between the number of events in the photo-peak and the number of γ rays simulated is the absolute peak-efficiency of the detector.

Microfocus computer tomography of the detectors

As the precision of the constructor's specifications of the detector geometry was not reliable enough to perform accurate simulations, the internal crystal dimensions had to be verified. A non-destructive way to accomplish precise crystal measurements is to expose the detector to a radiative source. This was realised at the *Microfocus Computer Tomography* device of the *Department of Metallurgy and Materials Engineering* (MTM) at the *Katholieke Universiteit Leuven* (KUL).

A polychromatic X-ray source (Philips HOMX 161) operated at a voltage of 125 kV and a current of 0.28 mA, filtered by a 2 mm aluminium and a 1 mm copper shield [10], was used for the experiment. The data acquisition was realised through a CCD camera (Adimec MX12P) delivering 12 bits grey scale images at a resolution of 1024 × 1024 pixels, resulting in a voxel size of 110–150 µm. The detectors were placed on a rotating table and pictures were taken ever. 0.5°. The data were processed with the AEA Tomohawk software for 3D reconstruction.

With this configuration we were able to visualise the internal geometry of the detector. For the chosen beam energy, the detector cap was transparent, whereas the high density germanium crystal was not penetrated. Figure 6 shows the results of this experiment for the green detector. In this picture we can clearly recognise the germanium crystal held by an aluminium structure at the centre, surrounded by the detector cap. Knowing the precise dimensions of the cap, we were able to calibrate the experimental data and to determine the size of the crystal.

Figure 6: µ-ct analysis of the green detector, showing different cuts of the reconstructed data

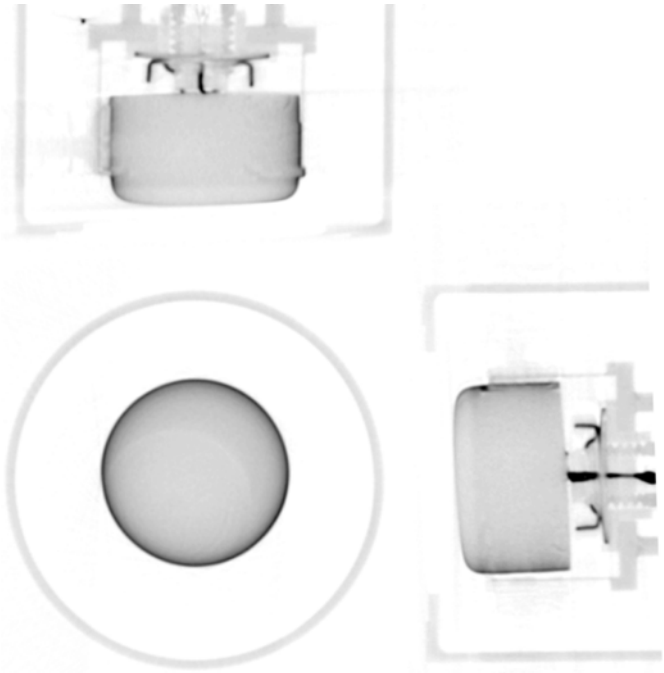

For the small crystals of the green and blue detectors we found that the diameter of the crystal was indeed a little smaller as the manufacturer specified. Moreover, the difficulties encountered in simulating the green detector could be explained by a wrong crystal to detector entrance window distance, which is in fact 3 mm longer than expected. The values determined here are in good agreement with the simulation results obtained by Geant4. Further investigations with the manufacturer also led to better specifications of the red and grey detectors, for which an agreement was found in the simulations.

Efficiency results

The efficiencies were simulated with the best fitted detector geometries and dead zone sizes obtained from the discussions above, and measurements were performed using different sources. The final experiment to simulation ratios of our calibration measurements are shown in Figure 7. In total 7 measurement series have been performed. A ^{152}Eu point source was placed at the centre position of the sample, and then displaced by 12 mm to the right, left, up and down. Two further measurements were realised with a ^{133}Ba point source and an extended ^{152}Eu source of 50 mm diameter at the centre position to check the previous results.

Figure 7: Experiment to simulation ratios for the efficiency calibrations for different source positions (see legends) of the four detectors

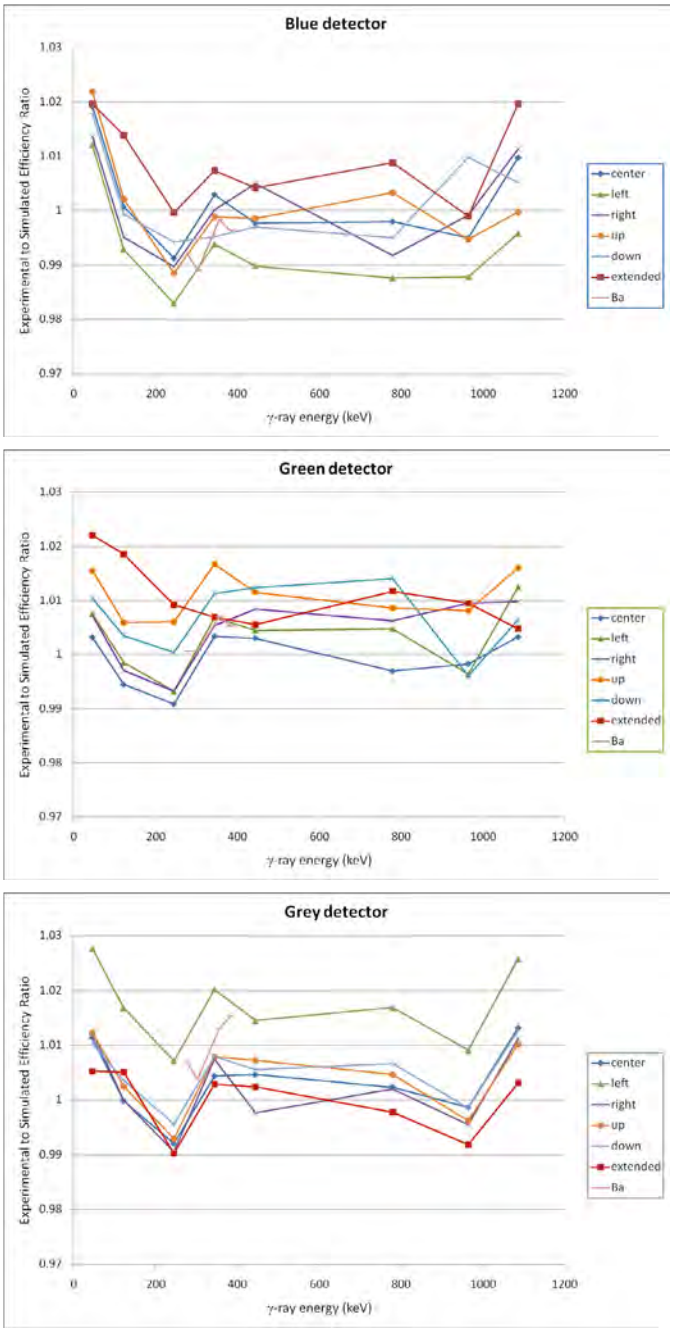

Figure 7: Experiment to simulation ratios for the efficiency calibrations for different source positions (see legends) of the four detectors *(continued)*

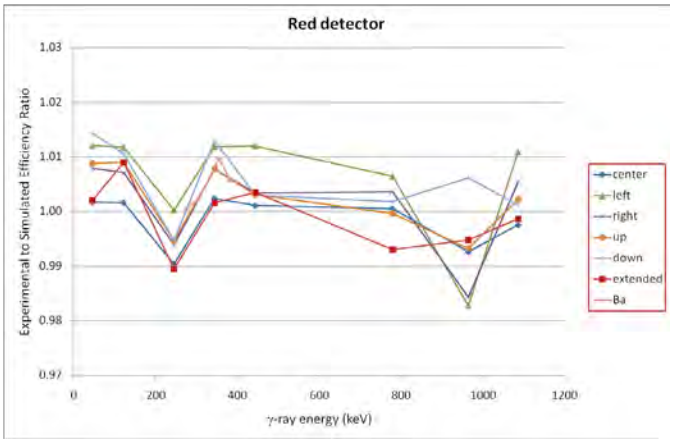

One can observe that the values obtained during the different measurement series all lie within a range of ± 2% with respect to the simulated values for the intermediate energy range (from 121.78 to 778.90 keV). For the low energy values, mainly the first point at 46 keV, the experimental values are differing a little more from the simulated ones. Indeed this region is more sensitive to dead zones and the rounding parameter at the front of the crystal as well as on the absorption of the detector window. The results for this domain are however sufficient for our needs.

The deviation between data and calculation in the intermediate energy domain can be explained by uncertainties on branching ratios and also by the fact that the simulations did not account for complete energy spectra. In fact, only the energies of interest were simulated, neglecting smaller energies rays due to background radiation. This can lead to small errors when subtracting the rays from the background. Such a particular deviation could me observed for the 244.7 keV ray, which is systematically lower experimentally than in the simulated spectra.

The differences between the measured series are mainly due to the position precision of the source. This can be observed best for the green line, corresponding to the "left" position of the source. For the detectors grey and red it is overestimated experimentally, whereas the detectors blue and green are showing an underestimated value. In fact, the grey and red detectors are positioned to the right-hand side (RHS) of the experimental setup, as described in Figure 1, and the blue and green ones to the left-hand side (LHS). As the experimental values are higher for the RHS placed detectors, this means that the source was placed too much to the right. This is confirmed by the fact that the outer detectors, *i.e.* the grey and the blue one, see a larger difference. Indeed as they are located at 110° they have a grazing angle to the target plane and a variation of the source position is seen more strongly as for the other detectors. Simulations show that a variation of 1% on this ratio of the grazing angle detectors corresponds to approximately 1 mm displacement.

Taking into account the variation of the different points simulated at different energies as well as the systematic uncertainties coming from the calibration sources used, this procedure enabled us to determine the γ efficiencies at uncertainties ranging between 2 and 3% in the energy domain of interest.

Conclusions

The aim of this work was to analyse all the different components used in the experimental setup to reduce the error to a minimum. This was achieved through an extensive analysis of the detection efficiencies of the used counters. For the fission chamber we were able to reduce the uncertainties on the efficiency to 2.1% and the Microfocus Computer Tomography helped to obtain uncertainties on the γ-detection efficiencies ranging between 2 and 3% depending on the photon energy.

With these efforts, the current experimental setup is able to measure (n,xnγ) reaction cross-sections at uncertainties of 5-6%, coming from the before mentioned efficiency uncertainties as well as from other errors due to target specifications and yield extraction. It has already been used to probe (n,n'γ) and (n,2nγ) reactions on ^{235}U and (n,n'γ), (n,2nγ) and (n,3nγ) reactions on ^{232}Th [11].

Acknowledgements

The authors thank the team of operators of the GELINA facility for the preparation of the neutron beam. This work was partially supported by the Integrated Project for European Transmutation (EUROTRANS).

References

[1] OECD/NEA, "Nuclear Data High Priority Request List", *www.oecd-nea.org/dbdata/hprl*.

[2] Mihailescu, L.C., *et al*., "A measurement of (n,xnγ) cross-sections for ^{208}Pb from threshold up to 20 MeV", *Nuclear instruments and Methods in Physics Research*, A811, 1 (2008).

[3] Tronc, D., J.M. Salomé, K. Böckhoff, "A new pulse compression system for intense relativistic electron beams", *Nuclear instruments and Methods in Physics Research*, A228, 217 (1985).

[4] Ene, D., *et al*., "Global characterisation of the GELINA facility for high-resolution neutron time-of-flight measurements by Monte Carlo simulations", *Nuclear instruments and Methods in Physics Research*, A618, 54 (2010).

[5] Budtz-Jørgensen, C., H.-H. Knitter, G. Bortels, "Assaying of targets for nuclear measurements with a gridded ionization chamber", *Nuclear Instruments and Methods in Physics Research*, A236, 630-640 (1985).

[6] Carlson, G.W., "The effect of fragment anisotropy on fission chamber efficiency", *Nuclear Instruments and Methods*, 119, 97-100 (1974).

[7] Allison, J., *et al*., "Geant4 – A simulation toolkit", *Nuclear Instruments and Methods in Physics Research*, A506, 250-303 (2003).

[8] Mosconi, M., *et al*., "Characterisation of Fission Ionisation Chambers using Monoenergetic Neutrons", *Proceedings of the EFNUDAT Workshop*, Cern, Geneva (2010).

[9] Deleanu, D., *et al*., "The gamma efficiency of the GAINS spectrometer", *Nuclear Instruments and Methods in Physics Research Section*, A624, 130 (2010).

[10] Kerckhofs, G., *et al*., "Validation of x-ray microfocus computed tomography as an imaging tool for porous structures", *Review of Scientific Instruments* 79(1), 1-9 (2008).

[11] Kerveno, *et al*., "Measurement of (n,xnγ) reactions of interest for the new nuclear reactors", *these proceedings*.

Modelling d-Be and d-C neutron sources for SPIRAL-2

Mitja Majerle,[1] **Stanislav P. Simakov**[2]
[1]Nuclear Physics Institute of the ASCR, Řež near Prague, Czech Republic
[2]Karlsruhe Institute of Technology, Karlsruhe, Germany

Abstract

SPIRAL-2 facility, which is currently under construction will produce intense white neutron spectra using deuteron beams (30-40 MeV) bombarding thick Be and C targets. The experimental data describing neutron production and induced radioactivity in these types were studied and data were fitted to phenomenological models to be used in future calculations concerning SPIRAL-2 and similar facilities.

Introduction

The future SPIRAL-2 facility, currently under construction at GANIL, Caen (France), will consist of a high-power superconducting driver LINAC delivering a high-intensity deuteron, proton and heavy ions beams [1]. Deuterons (30-40 MeV) bombarding thick Be and C targets will be used to produce an intense white neutron spectrum.

To predict the intensity and spectra shape of these neutron sources dedicated and validated computational tools and relevant cross-section data are needed. White energy neutron sources exploiting the irradiation of Be or C targets with deuterons were not sufficiently studied so far.

MCNPX calculations with built-in nuclear reaction models disagree with available experimental data up to factor of 2-3 [2], and we tried to get a more precise simulation for neutron yields from beryllium and carbon targets under deuteron bombardment by employing the stripping and compound models for deuteron-nuclei interactions. This approach was previously developed for the modelling of the d-Li neutron source and was implemented in the McDeLi code [3].

The radioactivity induced in Be and C type of targets was calculated with the EASY-2007 code package [4].

Available models and software for d-Be and d-C source modelling

The McDeLi code [3] is an extension to the MCNP code with a source subroutine fo1r the modelling of the neutron spectrum from the d-Li reaction. The approach used for the Li target can be applied to Be and C, and the adapted McDeLi code can be used to model the neutron production in these targets. The main modifications of the code include the substitution of ionization losses and nuclear parameters of the target materials. Free model parameters were also fitted to experimental data.

Evaluating and modelling experimental data for Be and C targets

The experimental data for reactions of deuterons on Be and C were collected from various experiments with thick targets that were performed from 1960's up to now, with the energies ranging from few MeV up to tens of MeV. The most common experimental method used was the Time-Of-Flight measurement (TOF), which can determine the neutron spectra from 0.2 MeV up to the energy of the deuteron beam. Figures 1 and 2 show the collected data in forward directions together with the values for Be and C targets modelled with the modified McDeLi code. Figures 3 and 4 show the total neutron yields in the forward direction together with modelled values. In Figures 5 and 6 the comparison of experimental and modelled values for other directions is shown.

The produced neutron spectrum consists of the forward oriented neutrons with the peak around half of the deuteron energy originating from the stripping process and of the isotropic neutron continuum at energies below 5 MeV from compound reaction, see Figure 6.

The experimental data are mainly focused on the peak of the stripping neutrons and several sets of measurements in this neutron energy region exist. The disagreement between different sets of measurements is around 30% for Be and 50% for C targets. The uncertainty of the modelled data is mainly caused by the disagreement between experimental data.

However, few experimental data describing the neutron spectrum below 3 MeV are available, and the accuracy of the modelled data in this neutron energy region is poor. The uncertainty can reach up to 100%. But, in forward directions and at deuteron energies of ca. 30 MeV, the contribution of neutrons below 5 MeV to the total neutron yield (and its uncertainty) is 10-20%.

The model predictions satisfactory describe the total neutron yield in forward direction for Be and C targets (Figures 3 and 4). These values concern mostly the neutrons from stripping process (most experimental spectra were integrated above few MeV threshold).

The angular distributions of neutrons from both types of targets seem to be modelled satisfactory. Drastic decrease of accuracy at larger angles is not expected (Figure 5 and 6).

Figure 1: Experimental (symbols connected with lines) and simulated (thick lines) spectral neutron fluences in the forward direction at different deuteron energies for Be target

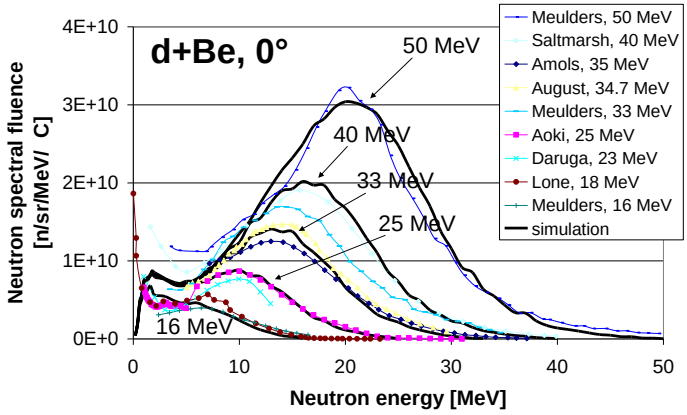

Figure 2: Experimental (symbols connected with lines) and simulated (thick lines) spectral neutron fluences in the forward direction at different deuteron energies for C target

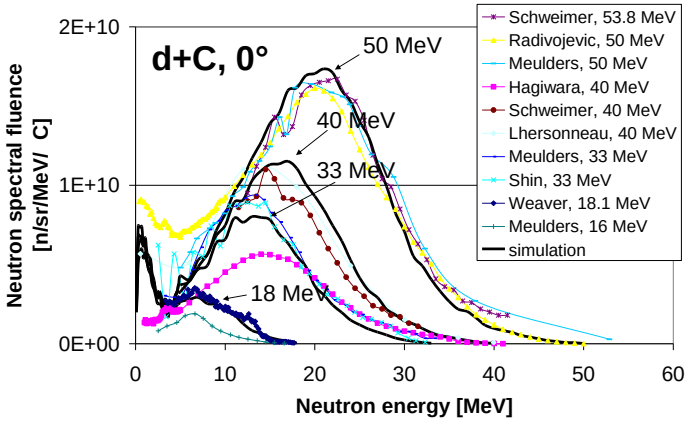

Figure 3: Total thick target neutron yield in the forward direction for different deuteron energies for Be target. Experimental (symbols) and modelled (thick line) values. Modelled values were obtained by the integration of the spectra from 5 MeV upwards.

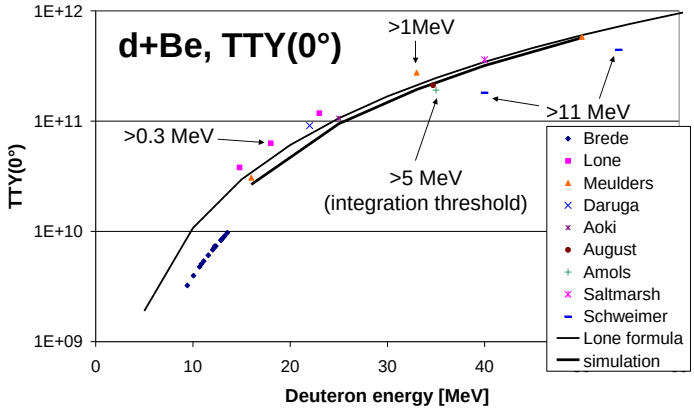

Figure 4: Total thick target neutron yield in the forward direction for different deuteron energies for C target. Experimental (symbols) and modelled (thick line) values. Modelled values were obtained by the integration of the spectra from 4 MeV upwards.

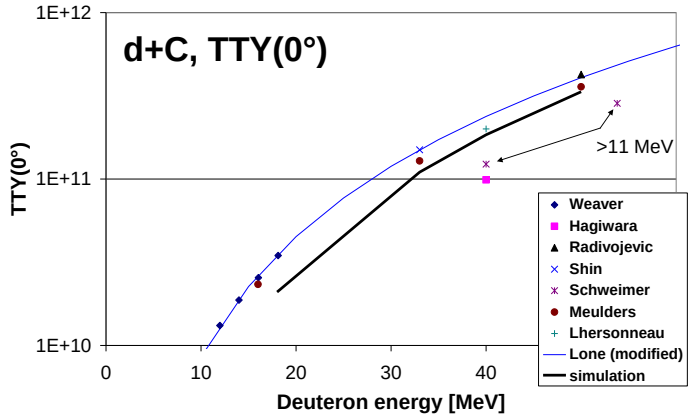

Figure 5: Angular distribution of the neutrons from Be target irradiated with 33 and 65 MeV deuterons. Experimental (symbols) and modelled (solid line) values.

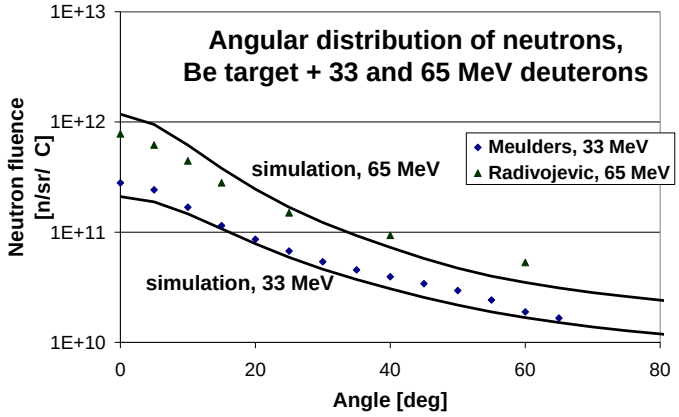

Figure 6: Neutron production at different directions for 50 MeV deuterons bombarding thick Be target. Experimental values (symbols) and modelled (solid line) values.

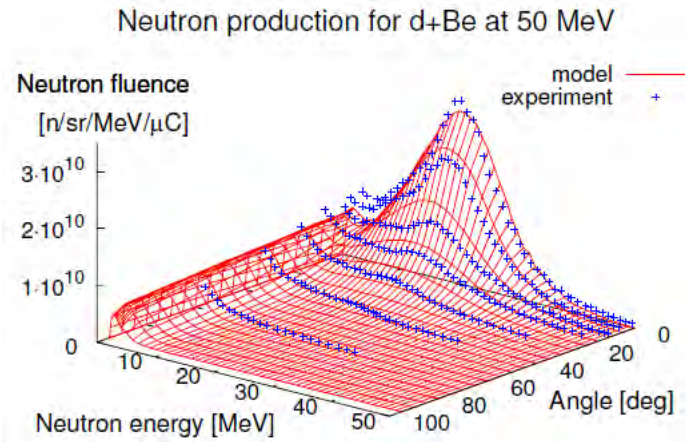

Figure 7: FISPACT calculated γ dose rate at 0.3 m distance from Be target after 10 days irradiation with 50 μA deuteron current at 40 MeV

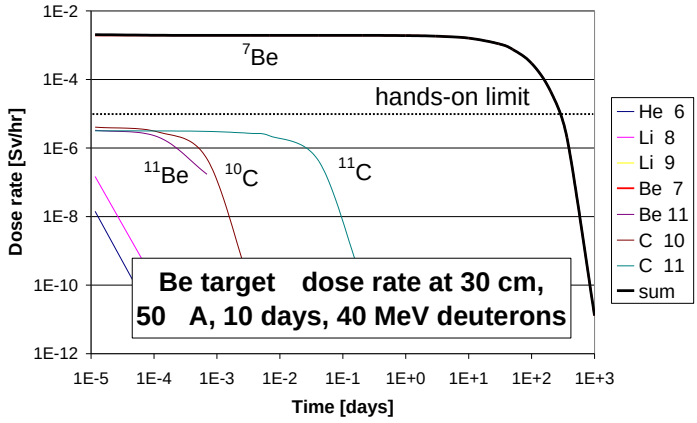

Figure 8: FISPACT calculated γ dose rate at 0.3 m distance from C target after 10 days irradiation with 50 μA deuteron current at 40 MeV

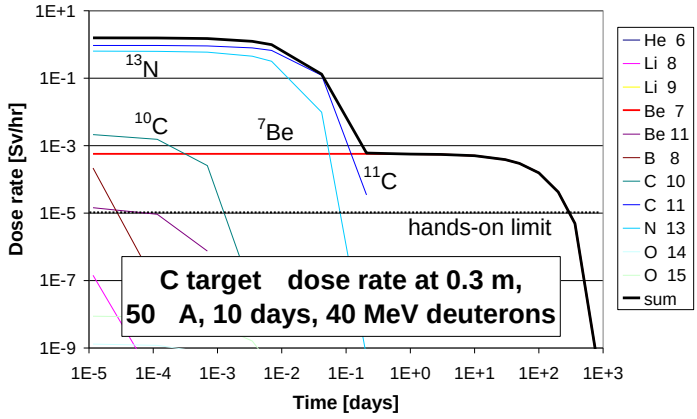

Estimation of the radioactivity induced in the Be and C targets

The number of radioactive nuclei and their γ dose rates after the irradiation were calculated with the code package EASY-2007 [4]. An irradiation of Be and C thick targets with 50 μA of 40 MeV deuterons during 10 days was assumed.

It was found that the radioactive isotope ^{7}Be contributes the highest γ dose rate from both targets. Cooling times before the γ dose rate decreases under hands-on limits at 0.3 m distance are in orders of years for the Be target (Figure 7) and months for the C target (Figure 8) after assumed irradiation period of ten days. Suitable target shielding and transport systems should therefore be considered for the target construction.

The calculated radioactivity of the Be target was compared to the values found in the EXFOR database. The agreement in the same order of magnitude was found, which is pointing out the disagreements between experimental cross-sections for thin (used in calculation) and thick targets.

Conclusion

SPIRAL-2 neutron sources consisting of Be and C targets bombarded by deuterons with energies around 30 MeV can be reliably modelled with a modified version of the McDeLi code which implements Serber stripping and compound reactions.

The experimental data for the neutron production in the Be and C targets bombarded with deuterons were extracted from several publications, and are modelled with an accuracy around 30% for Be and 50% for C targets above 5 MeV neutron energy.

The radioactivity of the targets after the deuteron irradiation was estimated with the EASY-2007 code package. It was found that ^{7}Be presents the major contribution to the γ dose rate in both types of targets, and that after a typical irradiation session the cooling times will be in the orders of months for C target and years for Be target. Transport and shielding systems should be therefore considered for the target construction.

Acknowledgements

The present work was finished during author's long term stay at the KIT. It was supported by the European Union in the frame of the SPIRAL2 Preparatory Phase FP7 project 212692.

References

[1] GANIL, *The scientific objectives of the SPIRAL 2 project*, Report available at *www.ganil-spiral2.eu* (2006).

[2] Herber, S., S.P. Simakov, U. Fischer, *D-Be and D-C Neutron Source Simulation by MCNPX*, Jahrestagung Kerntechnik, Dresden, CD-ROM Paper 812, INFORUM GmbH (2009).

[3] Wilson, P.P.H., *Neutronics of the IFMIF Neutron Source: Development and Analysis*, FZK Report, FZKA 6218 (1999).

[4] Forrest, R.A., J. Kopecky, *J. Nucl. Mat.*, 386-388, 878-881 (2009).

Present opportunities and future perspectives for experimental nuclear physics in Magurele

Nicolae Marius Marginean
"Horia Hulubei" National Institute for Physics and Nuclear Engineering
Bucharest-Magurele, Romania

Abstract

The contribution is an overview of the recent and the foreseen major investments in the field of nuclear physics research in IFIN-HH. In particular, the experimental infrastructure for nuclear physics made available during the last years at the TANDEM Laboratory of IFIN-HH will be presented, with emphasis on gamma spectroscopy, including a novel in-beam fast-timing infrastructure using a unique mixed array of $LaBr_3$:Ce and HPGe detectors.

The major development project for the Nuclear Physics research in Romania is the construction of the ELI Nuclear Physics pillar in the Magurele research campus. The present status of the ELI Nuclear Physics project will be presented, together with several research possibilities that will be opened by the construction of the facility.

Introduction

With a history extending over more than 50 years, the nuclear physics research in the "Horia Hulubei" National Institute for Physics and Nuclear Engineering (IFIN-HH), located in the Bucharest-Magurele campus, was continuously of the high level according to the scientific standards. Due to significant investments in the experimental infrastructure, IFIN-HH developed constantly during the last five years and started to become an important experimental infrastructure in Europe.

The TANDEM Laboratory

Since its commissioning in 1976, the TANDEM accelerator of IFIN-HH was intensively used for experimental research in fundamental nuclear physics. The maximum voltage originally was 7 MV and was later extended to 9 MV. In 2006 started a detailed program of modernization of the accelerator, and until 2010 all major components were replaced. The original charging system was replaced with a Pelletron chain system, which has an improved charging efficiency and is more reliable in operation. The accelerator tubes were changed with a new set with Titanium electrodes and spiral fields. The ion optics inside the accelerator was also improved, leading to ion transmission typically at the level of 90-95%. At present the TANDEM has three ion sources: a SNICS-II sputtering source for normal experiments requiring currents over 1 particle-nA on target, an AMS-dedicated MC-SNICS-II sputtering source, and a duoplasmatron alpha-particle source with charge exchange on Lithium. In 2009 was commissioned a fast beam pulsing system in nanoseconds range, consisting in a chopper with 5 MHz frequency and sub-divisions and a 25% packing buncher with pulse duration between 1 and 3 nanoseconds. The pulsing range of the accelerator is extended to the millisecond range using a chopper system constructed in the laboratory and installed on the "low-energy" side, between the ion sources and the accelerator. The modernization program leads to significant increase of the reliability in operation of the accelerator, and at present it works at the level of 5000-6000 hours of beam delivered per year. From 2009 the experiments at the IFIN-HH TANDEM are accepted after a peer-review from the recently established international Physics Advisory Committee (PAC) of the accelerator.

Besides the modernization of the accelerator, significant investments in the experimental infrastructure were made during the last years. At present there are six beam lines, most of them with dedicated experimental setups: a gamma spectroscopy and in-beam fast timing setup, one multi-purpose reaction chamber for RBS and ERDA material analysis techniques, one setup for the study of ionization processes via X-ray and charged-particle spectroscopy, one beam line equipped with a large reaction chamber and a high-granularity, 80 element neutron detectors array for the study of nuclear reaction mechanisms, one dedicated AMS beam line and one 0 degree magnetic separator for reactions in inverse kinematics. A relatively large number of different gamma and charged-particle detectors were also acquired, in the laboratory being available at present a number of 18 55% HPGe detectors, two 120% Clover HPGe detectors, 4 Germanium LEPS detectors, BGO anti-Compton shields and several Si E-ΔE telescopes of different sizes.

The Clover detectors together with two 55% HPGe were used to build a high-efficiency decay spectroscopy setup, used mostly to measure sub-barrier cross-section with the stack activation technique, and also for gamma spectroscopy in nuclei populated following beta decay.

The in-beam fast timing array

One of the gamma spectroscopy projects that allowed addressing research topics which complement the experiments performed at other experimental facilities and provides uniqueness to the IFIN-HH TANDEM Laboratory is the construction of a mixed HPGe-$LaBr_3$:Ce detectors array for in-beam fast timing experiments. Launched on the market during the last five years, the $LaBr_3$:Ce scintillation detectors provide the best gamma-ray relative energy resolution achievable with scintillators, between 2 to 3% depending on the size of the crystal. On the same time, these detectors have very good timing, with time resolution of about 160 picoseconds for 1.5"x1.5" cylindrical crystals and support very high counting rates. These characteristics make them ideal for in-beam measurements of excited states in nuclei produced in fusion-evaporation reactions, provided that the original complexity of the raw spectra is reduced by appropriate selections made using high-resolution HPGe detectors.

The "Fast Timing" array set up at the TANDEM Laboratory (Figure 1) can accommodate up to 8 $LaBr_3$:Ce detectors and 8 HPGe detectors, in a flexible geometrical configuration. The granularity of the array is suitable for in-beam measurements, where relatively long cascades of gamma transitions are produced in fusion-evaporation reactions. The HPGe detectors are standard cylindrical detector with 55% relative efficiency, and the $LaBr_3$:Ce are as follows: 3 elements cylindrical 2" × 2", 3 elements cylindrical 1.5" × 1.5", and 2 elements with truncated cone shape, 1" smaller diameter, 1.5" larger diameter and 1.5" height. The absolute detection efficiencies for 1.33 MeV are ~0.7% for HPGe sub-array and respectively ~0.5% for $LaBr_3$:Ce sub-array. Details about the electronic processing of the signals coming from the detectors and data analysis procedure can be found in reference [1].

Figure 1: The "Fast Timing" array at the TANDEM Laboratory in Magurele

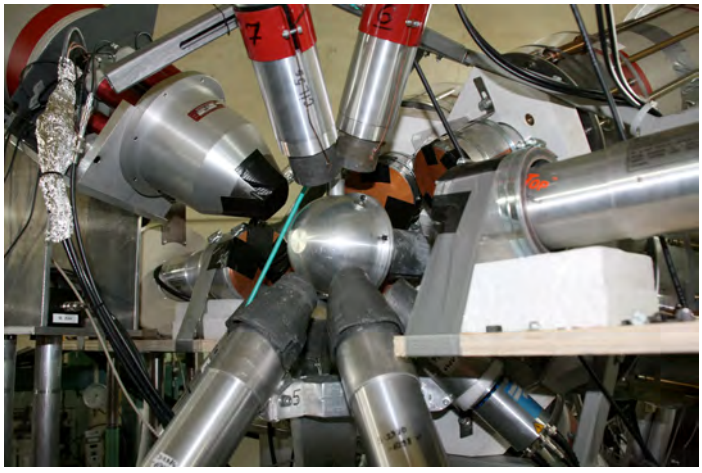

After building the in-beam fast timing setup, in the commissioning phase several test experiments were performed to investigate the performances of the apparatus. First, the lifetime of the yrast $7/2^+$ state in ^{107}Cd was re-measured, and the value obtained, 0.69(3) ns is in good agreement with the adopted value of 0.71(4) ns. Another test experiment aimed to approach the lower limit for the lifetimes that can be measured with the setup. From the systematic the lifetime of the first

Figure 2: Spectra illustrating the measurement of the first $3/2^+$ state in ^{199}Tl using the centroid shift method and the systematic of B(M1) and B(E2) for corresponding $3/2^+$ ® $1/2^+$ in odd-A Tl isotopes

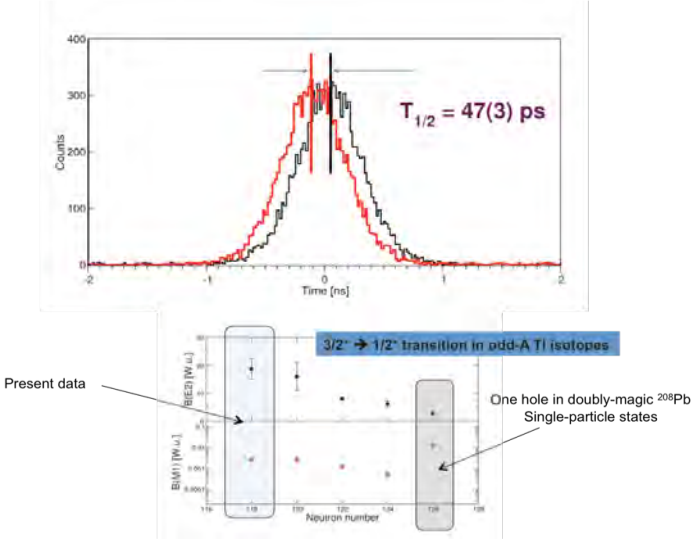

$3/2^+$ state of ^{199}Tl is expected to be ~100 ps or smaller, and since this nucleus can be easily populated using the ^{197}Au(α,2n) reaction, it was selected as test case. With the "Fast Timing" array we obtained for the half-life of the first $3/2^+$ state in ^{199}Tl the value of 47(3) ps, corresponding to a perfect agreement with the systematic of the M1 and E2 reduced transition for the same state in odd-A Tl isotopes (Figure 2).

These results demonstrated the sensitivity of the array, which can be used to measure in-beam half-lives from 20 nanoseconds down to the level of 50 picoseconds. The lower limit of this range overlaps with the upper limit for plunger measurements, and until the construction of the Bucharest "Fast Timing" setup was not covered by a dedicated in-beam gamma spectroscopy array. Respect to plunger method, the electronic timing method has no geometrical restrictions regarding the placement of the detectors relative to the beam axis, thus a better detection efficiency can be obtained, and consequently more precise experimental results. One should also consider the fact that lifetimes of hundreds of picoseconds were typically measured for states populated following beta decay with fast detectors placed in tight geometry. Using the in-beam fast timing technique one gain access to a multitude of excited nuclear states which are not populated in beta decay but are populated in reactions with light or heavy ions.

The "ELI Nuclear Physics" Project

Experimental techniques based on the use of conventional lasers are present in Nuclear Physics studies from decades, and proved to be extremely useful in the investigation of the properties of the nuclei. All of them are low-energy techniques and use the atomic electrons as a "bridge" to access information about the nucleus. During the last decade since one of the major scientific achievements obtained in the beginning of the 2000s was the experimental prove of the possibility to obtain radioactivity by hitting a target with a high-intensity laser beam. The high electromagnetic fields of the laser beam accelerate the electrons and the atomic nuclei from the target and several kinds of radiations are generated in primary and secondary processes: electrons, protons, heavy ions, X and gamma rays. Each of these is distributed in a specific energy range, strongly depending on the power of the laser source. At the present high-intensity laser facilities, with powers of ~1 PW or below, the energy transferred to protons or heavier ions is large enough to induce nuclear reactions. Processes as fusion-evaporation, fission or direct reactions, all induced by laser-generated secondary particles, have been observed. All these experimental discoveries triggered inside the Extreme Light Infrastructure (ELI) collaboration, which has the goal to construct a distributed experimental facility for physics with high-intensity lasers in Europe, the idea of building a dedicated pillar for nuclear physics studies. The site chosen for the nuclear physics pillar (ELI Nuclear Physics – ELI-NP) is the Bucharest-Magurele campus, near IFIN-HH and very close to the TANDEM Laboratory.

For the Extreme Light Infrastructure - Nuclear Physics facility two central instruments are planned:

1. A very high intensity laser beam, where two 10 PW lasers can be coherently added to the high intensity of 10^{23} – 10^{24}W/cm^2 or electrical fields of 2×10^{15}V/m.
2. A very intense, brilliant, very low bandwidth, high-energy γ beam, which is obtained by incoherent Compton back scattering of a laser light on a very brilliant, intense, classical electron beam.

A detailed description of the high intensity laser system, of the gamma beam and of the physics to be addressed at the ELI Nuclear Physics facility can be found in the White Book of the project [2]. In the following we will only briefly summarize them.

The high intensity laser system will consist of two lasers with 10 PW peak-pulse power, pulse width between 25-160 fs, pulse repetition rate between 1/10 - 1/60 Hz, contrast better than 10^{12}, and focused laser intensity $\geq 10^{23}$ W/cm^2. With coherent combination of the two lasers, intensities up to 10^{24} W/cm^2 might be achievable. These lasers will have the pulse power with one order of magnitude larger than the existing high intensity lasers, which have up to 1 PW. In order to reach these laser parameters, the most favourable solution for ELI-NP laser facility is to use OPCPA technology at the front-end and Ti:Sapphire high-energy amplification stages.

The Gamma Beam will be generated using a warm LINAC in X-band RF (120-180 MeV/m) plus 532nm laser, similar to MEGA-ray LLNL's project. This approach is based on the interaction of short

pulse lasers with relativistic electrons generated by a warm LINAC to create ultra bright mono-energetic gamma-ray beams. The scattered radiation is Doppler up shifted by more than 1,000,000 times and is forwardly directed in a narrow, polarized, tuneable, laser-like beam. The Gamma Beam of ELI-NP follows closely the MEGa-ray facility currently being constructed at LLNL. It will use the same X-band LINAC technology but extended from 250 MeV to 600 MeV and the same state of the art 120 Hz diode pumped laser technology but extended from 1 J to 10 J. It will duplicate as much as possible the control systems and hardware being developed for LLNL machine. The reflective laser for the production of γ-rays will run reliable at the high repetition rate of 120 Hz using diode pumping. By using a ring-down cavity for the laser pulse, within the macro-pulse of 120 Hz repetition rate, 100 micro-pulses can be realized, increasing the overall repetition rate to 12 kHz. The experiments envisaged with the γ source defined severe constraints for the parameters of the γ beam: bandwidth equal or higher than 10^{-3}, energy up to 19 MeV to access all GDR, total flux higher than 10^{13} photons/sec, peak brilliance higher than 10^{22} photons mm^{-2} $mrad^{-2}$ s^{-1} (0.1% BW)$^{-1}$ in order to improve the ratio effect-background.

At ELI Nuclear Physics facility will be possible to perform either experiments requiring the high intensity laser and the gamma beam synchronized on the target or experiments using only one of these systems. The facility will make possible a broad range of experiments addressing topics of high interests in the present time, as presented in the White Book of the project [2]. Due to the specific nuclear physics profile, it will be possible to develop and use complex, high sensitivity nuclear spectroscopic techniques to characterize the radiations emitted when the high intensity laser pulse interacts with the target. Using the recently observed Radiation Pressure Acceleration mechanism it might be possible to obtain bunches of accelerated ions with the density close to the density of the original solid matter. When such a dense bunch is stopped in a thick layer is possible to observe large deviations from the Bethe-Bloch formalism for the stopping of heavy ions in matter. The dense ion bunches created and accelerated with the high intensity laser might also be used to produce very exotic isotopes which cannot be produced at the projected radioactive beam facilities. With the high-resolution gamma beam it will be possible to investigate the fine structure of the dipole excitation in nuclei, the GDR and Pigmy resonances, and other aspects of nuclear structure. On the other hand, the intense and high-energy gamma beam can be used to produce high-quality positron beams, with many applications in the materials science.

The ELI Nuclear Physics project was from the beginning strongly supported by the Romanian Government. At present, the feasibility study is completed, and after the approval from the Romanian Government the funding application was send for pre-evaluation to the EC agency JASPER. The final approval of the project from European Commission is expected in summer 2011, and the construction phase to take place between 2012 and 2015.

References

[1] Marginean, N., *et al.*, "In-beam measurements of sub-nanosecond nuclear lifetimes with a mixed array of HPGe and $LaBr_3$:Ce detectors", *Eur. Physics Journal*, A 46, 329–336 (2010).

[2] *The White Book of ELI Nuclear Physics*, at *www.eli-np.ro*.

Effects of an energy broadened proton beam on the neutron distribution for the ^{7}Li(p,n)^{7}Be reaction near threshold

A.Shor,[1] G. Feinberg,[1,2] Y. Eisen,[1] M. Friedman,[2] A. Krása,[3] D. Berkovits,[1] G. Giorginis,[3] T. Hirsh,[1] M. Paul,[2] A. Plompen[3]
[1]Nuclear physics and engineering division, Soreq NRC, Yavne, Israel
[2]Racah Institute of Physics, The Hebrew University of Jerusalem, Jerusalem, Israel
[3]EC-JRC-IRMM, Geel, Belgium

Abstract

A common method for simulating the thermal neutron conditions in the stellar interior is based on the ^{7}Li(p,n)^{7}Be reaction near threshold energy. This method was pioneered at FZK, Karlsruhe, by Ratynski and Kaeppeler [1]. Maxwellian-averaged neutron capture cross-sections of mean energy 25 keV, relevant to the s-process nucleosynthesis, are measured at existing Van-de-Graaff (VdG) proton accelerators. Soreq NRC Applied Research superconducting linear Accelerator Facility (SARAF) phase 1 [2] is in its final stage of commissioning. Maxwellian averaged neutron capture cross-section measurements are planned to be conducted using a forced-flow closed-loop liquid-lithium target (LiLiT) [3]. The proton beam energy spread of RF linear accelerators, such as SARAF, is typically larger than the spread of proton beams of VdG accelerators. The energy spread of SARAF proton beam at 1912 keV is calculated to be of the order of 20-40 keV FWHM as compared to about 3 keV FWHM for VdG accelerators. For simulating the SARAF proton beam we performed an experiment at the IRMM-Geel VdG using a gold foil degrader positioned before the LiF target. This degrader shifts the mean proton energy to 1912 keV and it broadens the proton beam energy to values simulating the spread of the proton beam at SARAF. For calibrating the cross-sections we also performed a ^{7}Li(p,n)^{7}Be experiment without the gold foil degrader at a proton energy of 1912 keV. The VdG was operated in a pulse mode and the neutron energies were determined by time-of-flight measurements using ^{6}Li glass detectors. Detector efficiencies were obtained by Monte Carlo calculations. We present our study and compare the results for both narrow and broad energy proton beams. Comparison to calculations is also shown.

Introduction

A common method for simulating the thermal neutron conditions in the stellar interior is based on the ^{7}Li(p,n)^{7}Be reaction near threshold energy. This method was pioneered at FZK, Karlsruhe, by Ratynski and Käppeler [1]. Maxwellian-averaged neutron capture cross-sections of mean energy 25keV, relevant to the s-process nucleosynthesis, are measured at existing Van-de-Graaff (VdG) proton accelerators. Proton beams impinge solid targets of metallic lithium or LiF. Due to beam current limitations and heat removal limitations the neutron intensity is limited to about 109 n/s with an energy distribution peaking at 25 keV. This in turn limits the measurement of small neutron capture cross-sections in general and in particular capture cross-sections leading to short half life isotopes.

Soreq NRC Applied Research superconducting linear Accelerator Facility (SARAF) phase 1 [2] is in its final stage of commissioning. At the current stage the SARAF phase 1 RF linear accelerator will be able to accelerate protons up to energies of about 4 MeV and currents up to 3 mA. Maxwellian averaged neutron capture cross-section measurements are planned to be conducted using a forced-flow closed-loop liquid-lithium target (LiLiT) [3]. The neutron fluxes for the ^{7}Li(p,n)^{7}Be reaction near threshold are expected to be around 8×10^{10} n/s.

Figure 1: A schematics of the SARAF phase 1 accelerator

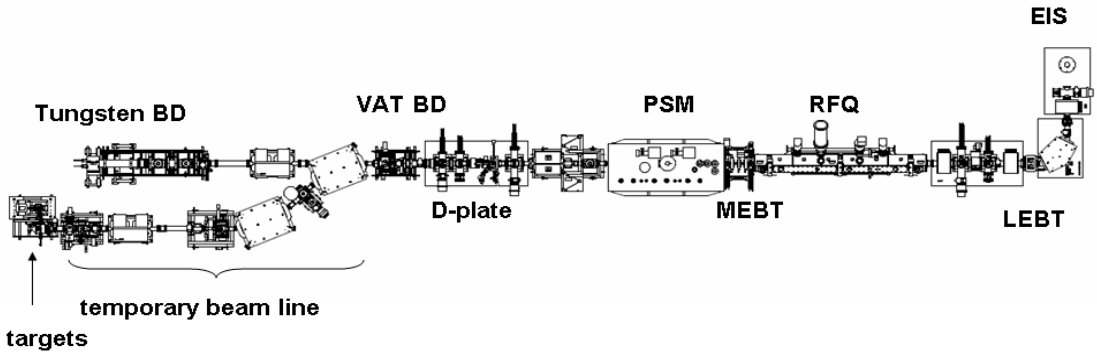

The proton beam energy spread of RF linear accelerators, such as SARAF, is typically larger than the spread of proton beams of VdG accelerators. The energy spread of the SARAF proton beam at 1912 keV is calculated to be of the order of 20-40 keV FWHM as compared to about 3 keV FWHM for VdG accelerators. Beam spread is a crucial parameter determining the high energy tail and the angular distribution of the outgoing neutrons in the reaction ^{7}Li(p,n)^{7}Be near threshold.

For simulating the SARAF proton beam we performed an experiment at the IRMM-Geel VdG using a gold foil degrader positioned before the LiF target. This degrader shifts the mean proton energy to 1912 keV and it broadens the proton beam energy to values simulating the spread of the proton beam at SARAF. For calibrating the cross-sections we also performed a 7Li(p,n)7Be experiment without the gold foil degrader at a proton energy of 1912 keV. The VdG was operated in pulse mode and the neutron energies were determined by time-of-flight measurements using 6Li glass detectors. Detector efficiencies were obtained by Monte Carlo calculations.

We present our study and compare the results for both narrow and broad energy proton beams. Results for both narrow and broad proton energy beams include: neutron energy distributions for emission angles in the 0°-80° range, average Maxwellian neutron energy, gold neutron capture cross-sections and number of neutrons per incident proton. The results of the narrow-energy beam are compared to results measured at FZK, Karlsruhe [1]. Also, all uncertainties of the measured quantities are discussed. A comparison to calculations is also shown.

SARAF RF linear accelerator

The high current SARAF accelerator phase 1 is now in the final stages of commissioning [2]. It will be capable of accelerating 3 mA of 4 MeV protons. Phase 1 is composed of an ECR ion source, an RFQ accelerator and 6 superconducting half wave resonators. Figure 1 is a schematic of the SARAF phase 1 accelerator capable of accelerating high currents of protons and deuterons to 4 and 5 MeV, respectively. Figure 2 is a schematic diagram of the prototype superconducting accelerator made of 6 cavities and the experimental beam line.

Figure 2: The superconducting module (left) and the experimental beam line (right)

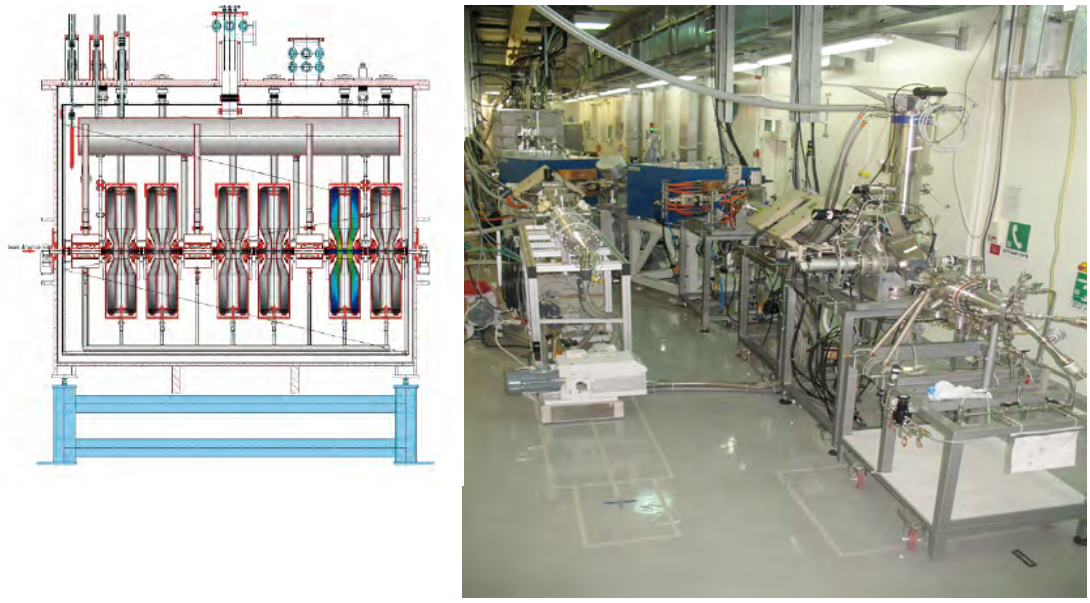

Figure 3: LiLiT liquid lithium target

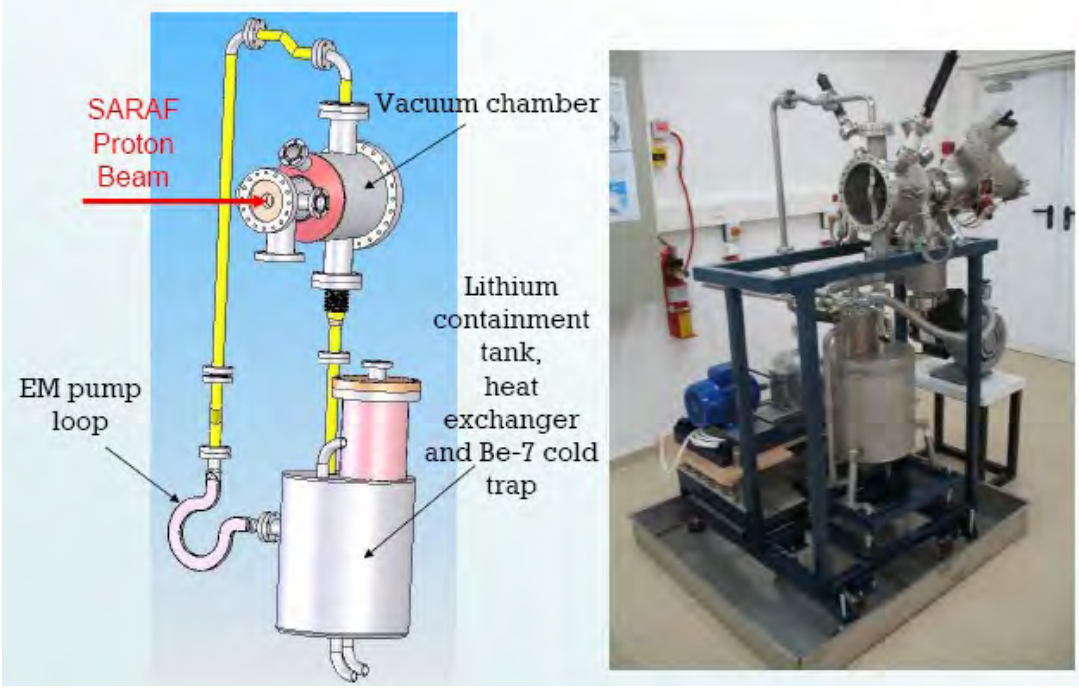

LiLiT liquid lithium target

The LiLiT target [3] is a windowless forced-flow closed loop liquid lithium target. The LiLiT setup is built as a loop circulating liquid lithium at a temperature of ~200° C and producing a jet (acting as the target) onto a thin concave supporting wall, driven by a rotating magnet inductive electromagnetic pump. The flow velocity is designed to be around 20 m/s. The liquid lithium is collected in a reservoir housing containing a heat exchanger with a mineral-oil closed loop. The target can holds currents up to 3.5 mA at proton energy of about 2 MeV.

Experiments at the IRMM VdG

The VdG

The IRMM VdG was operated in pulse mode at a frequency of 625 kHz. The proton pulse width was 1 to 2 ns. The pulse frequency limits the flight path of 1 keV neutrons to 70 cm. The average current was ~ 0.1 μA. Energy calibration of the VdG was checked periodically by a "neutron threshold curve" around the threshold (1881 keV) of the ^{7}Li(p,n)^{7}Be reaction. Initially it was calibrated using the resonance of the ^{27}Al(p,γ)^{28}Si reaction at 991 keV.

Experimental setup

The LiF targets were evaporated on a 1 mm copper plate. Their thickness was about 5 μm, much larger than the path length of a proton in the energy interval 1881 keV ≤ E_p ≤ 1912 keV. Two moveable ^{6}Li glass detectors were positioned at a distance 52 cm from the target and were moved in steps of 50. The dimensions of the detectors were: *(a)* 2" diameter by 1" thick, *(b)* 1" diameter by 0.5" thick. In addition, a ^{6}Li glass detector of diameter 2" by 1" thick was positioned at 12 degrees and at a distance 70 cm from target. The stability of the beam energy was continuously controlled by the end point of the monitor detector neutron time spectrum. The anode pulse of each ^{6}Li detector was split between a fast timing electronic channel and a slow energy electronic channel. List mode data were recorded in coincidence which enabled a 2D information of time-of-flight (TOF) versus energy. The electronic time resolution was 4 ns. Two other detectors were used as monitors: a 5" by 5" NaI and a neutron long counter. The experimental setup is shown in Figure 4.

Figure 4: Experimental setup of the 2 movable and one fixed monitor 6Li glass scintillation detectors

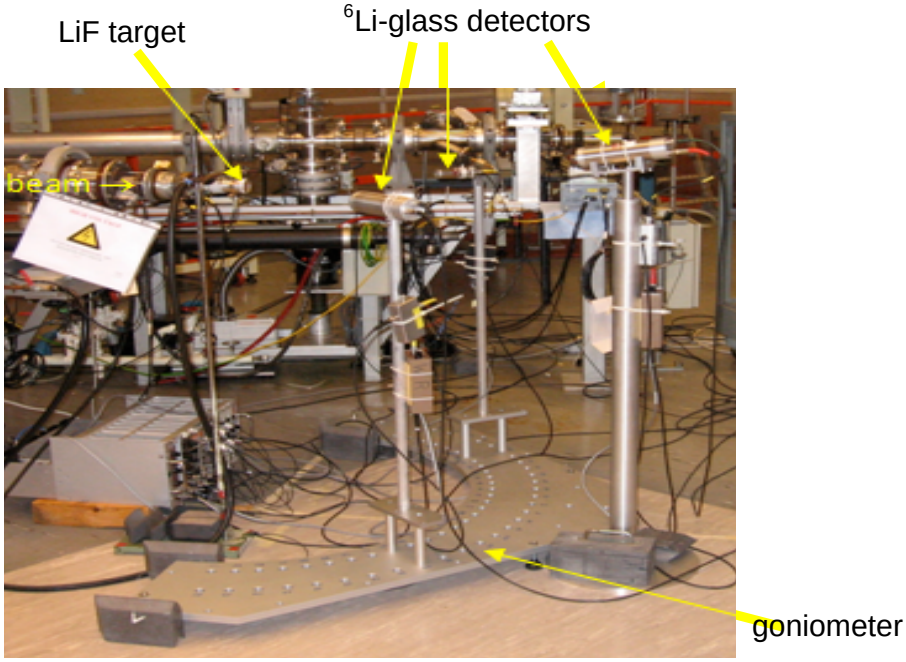

Experimental results

Measurements of the angular-energy distributions of the emitted neutrons were conducted for a narrow energy beam of standard spread σ ~ 1 keV and for a broad energy beam of σ~15 keV. Figure 5 displays a typical TOF spectrum showing the gamma peak (off-scale) to the right, and the neutron contribution at longer flight times to the left. The insert shows the gamma TOF distribution with FWHM ≤ 4 ns. The sources of gamma rays are the $^{7}Li(p,p'\gamma)$, $^{19}F(p,\alpha)^{16}O^{*}$ and $^{7}Li(p,\gamma)^{8}Be$ reactions (prompt peak), gamma rays produced upstream by protons striking accelerator components, and gamma-rays from neutrons captured in the room and from the natural background.

Figure 5 also shows a 2D scatter plot where TOF is the X-axis and pulse height (energy) is on the Y axis.

Figure 5: 2D display of energy versus TOF (right) and a TOF spectrum (left)

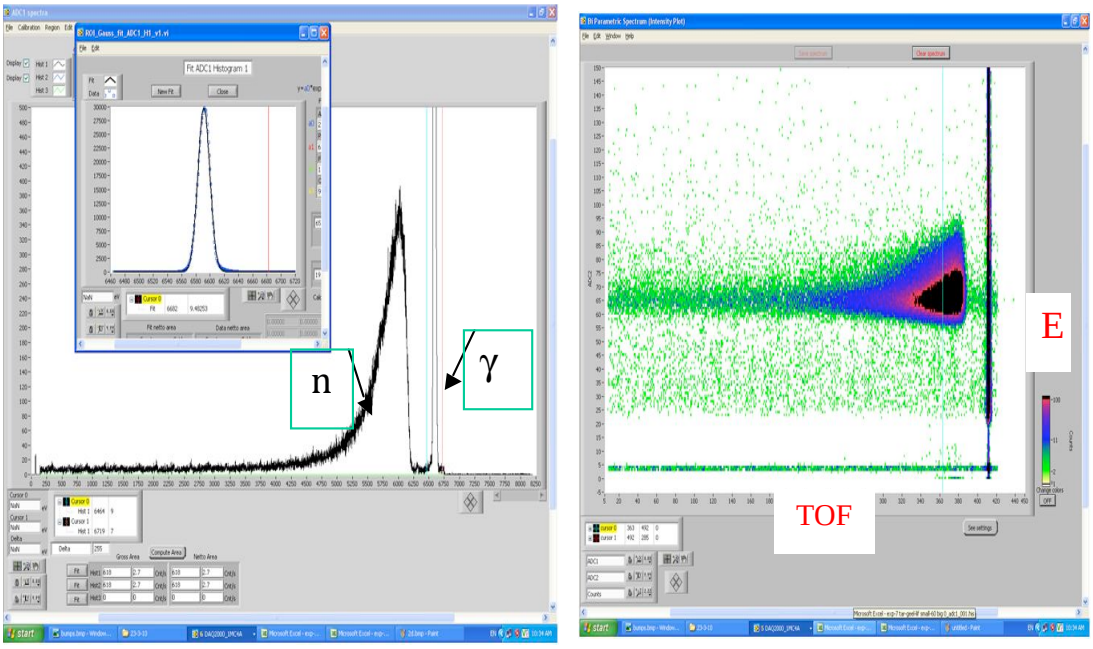

The broad energy beam was achieved by bombarding 2093 keV protons on a 2 μm thick Au foil positioned in front of the LiF target as shown in Figure 6. The gold foil shifted the beam energy down to 1912 keV with the expense of beam broadening due to straggling estimated to be σ(E)~15 keV.

Figure 6: Generating a broad energy beam by a 2 μm thick gold foil

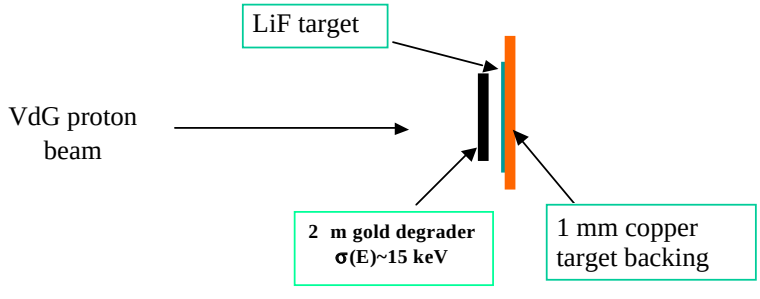

The steps conducted to obtain the energy distribution of the neutrons were as follows:

- Selecting a 2D window for the neutrons;
- Converting time of flight to neutron energy;
- Subtracting background from scattered gammas and neutrons;
- Correcting for efficiency of the detectors for each neutron energy;
- Correcting for solid angle of each detector;
- Sum all energies at all angles to obtain the integral energy distribution.

The energy spectra obtained for the narrow and broad energy beams are displayed in Figure 7.

Figure 7: Energy distributions for narrow-energy (blue) and broad-energy (green) proton beams. Also a comparison to a semi-Maxwellian energy distribution with kT=25 keV (red)

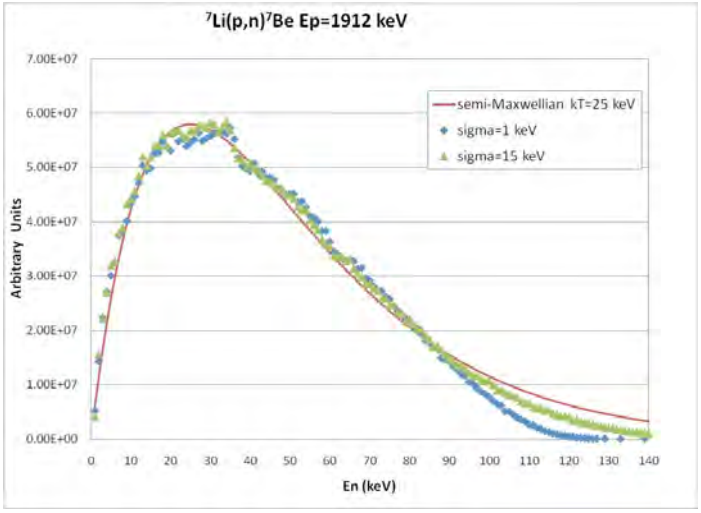

Figure 8: Energy distributions for narrow-energy proton beam and a comparison to Ratynski-Käppeler data [1] and to a semi-Maxwellian energy distribution with kT=25 keV

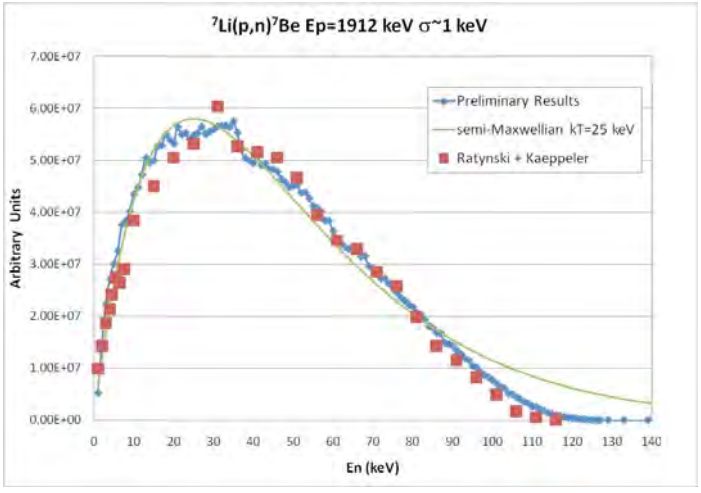

Figure 8 compares the narrow beam energy distribution to that obtained by Ratynski and Käppeler [1] and a semi-Maxwellian with kT=25 keV.

It is clearly seen from Figure 7 that the energy spectra for the narrow and broad beams peak nearly at the same energy close to 25 keV. However the energy distribution for the broad beam has a larger tail to higher neutron energies. Figure 8 shows that the rise of the neutron energy distribution for the present data shifts slightly to lower energies as compared to the data presented in ref. [1].

Uncertainties in the determination of energy distributions

The uncertainties in the data reduction analysis are as follows:

- Neutron energy
  - $\Delta E/E=2\ \Delta t/t$ where t is the time of flight;
  - The detector thickness affects the uncertainty more at the higher neutron energies than the lower ones;
  - Δt has an electronic component ~ 4 ns FWHM;
  - $\Delta t/t$ (at 1 keV) ~ 0.4%, $\Delta t/t$ (at 60 keV) ~ 2.7%;
  - Δt has an error of 5% (1" detector) due to the thickness.
- ^{6}Li Detector Efficiency
  - Multiple scattering inside the detectors mainly occurs due to oxygen and silicon nuclei composing the glass;
  - Multiple scattering affects more the efficiency of a thicker and larger size ^{6}Li detector;
  - Multiple scattering changes the path length of the neutron, thus affects the flight time till an absorption with ^{6}Li occurs.
- Multiple scattering of stray neutrons and gamma rays (background subtraction)
  - The neutron energy distribution has a random background of neutrons and gamma rays. It was assumed that the background is equal at each time bin and is equal to the background between the gamma flash and the neutron end point as shown in Figure 5. This background increases the uncertainty in data reduction of the neutrons and especially affects the low energy neutrons having lower statistics.

Gold activation cross-sections

The uncertainties in the data reduction analysis are as follows:

Experimental gold activation, ^{197}Au(n,γ)^{198}Au, cross-sections for the integral neutron distribution were also measured for the narrow-energy and broad-energy beams and for cone angles ~60° and ~80°. Figure 9 shows the geometrical positions of the planar gold foils. The gold foils were positioned at 1 mm and 5 mm from the target and their diameters were 18 mm and 22 mm respectively. The procedure for deriving the cross-sections was a three step process as follows:

a. Measure the ^{7}Be activity of the target, extract the number of emitted neutrons due to the reaction ^{7}Li(p,n)^{7}Be. Accurate current integration was essential.

b. Measure the activity of the gold foils and correct the activity for the number of neutrons emitted to a cone covered by the gold foil to the total number of neutrons. Scattering by the copper target backing is taken into account.

c. Correct the experimental activity measured using the planar gold foils to an expected activity of a hemispherical foil with the aid of Monte Carlo calculations and then estimate the gold activation cross-sections.

Activity measurements of both ^{7}Be and ^{198}Au were conducted using a low background HPGe detector.

Figure 9: Experimental setup for measuring the gold activation cross-section (not to scale)

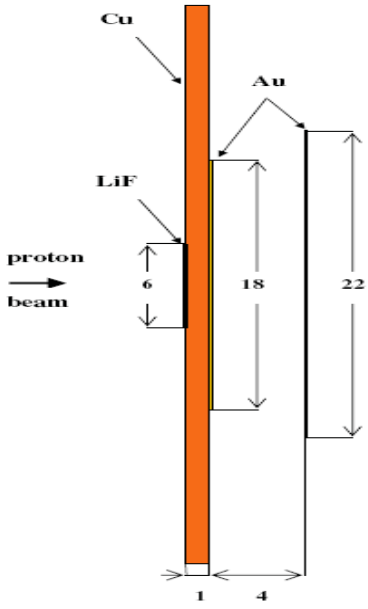

Table 1 shows the correction factors applied to correct the gold foils activity from a planar to hemispherical shape. The correction factors were obtained using the Monte-Carlo code SimLiT [5] for the ^{7}Li(p,n)^{7}Be neutron production and the GEANT4 Monte Carlo code for the transport of the outgoing neutrons from the ^{7}Li target till they interact via the (n,γ) reaction with the gold foil. The calculations take into account the varying effective thickness of the Au target with scattering angle and the scattering of neutrons by 1 mm copper backing of the target.

Table 1: Correction factors applied to modify the experimental activity of the planar gold foils to the expected activity of a hemispherical shape gold foils

	Narrow beam	Broad beam
Target 1	1/1.25	1/1.32
Target 2	1/1.17	1/1.07

Table 2: Experimental gold activation cross-sections and comparison to FZK result

	Narrow beam	Narrow beam FZK [1]	Broad beam
Target 1 cross-section (mb)	596±12	586±8	652 ±12
Target 2 cross-section (mb)	582±12		607±20
Average cross-section (mb)	589±12	586±8	630±16

Table 2 shows the experimental ^{197}Au(n,γ)^{198}Au cross-sections averaged over the neutron spectrum obtained from the proton beams with narrow and broad energy. A comparison to the cross-section cited by Ratynski and Käppeler [1] is also given for the narrow beam and good agreement is observed.

We also calculated from the ^{7}Be activity the number of neutrons/proton in the ^{7}Li(p,n)^{7}Be reaction generated for both narrow and broad beams. In Table 3 we compare these ratios to our calculations with SimLiT code [5] and to the PINO code [4]. It is seen that the results of the SimLiT Monte Carlo code [5] are in decent agreement with experimental results.

Table 3: Experimental and calculated neutron/proton ratios and comparison to calculations

	Narrow beam	Broad beam
Experiment	(1.10±0.02) x 10^{-6}	(1.36±0.03) x10^{-6}
Calculated (SimLiT [5])	1.17 x 10^{-6}	1.20 x 10^{-6}
Calculated (PINO [4])	0.9 x 10^{-6}	0.9 x 10^{-6}

Conclusions

- The energy distribution for the broad-energy beam of σ=15 keV is similar to that of the distribution of the narrow energy beam and they peak nearly at the same energy. The broad-energy distribution has a tail extending to higher energies than that of the narrow-energy beam.
- The neutron distribution of the broad-energy beam better matches a Maxwellian flux distribution of kT=25 keV.
- The neutron energy distribution for the narrow-energy beam is slightly shifted to lower neutron energies compared to that measured by Ratynski and Käppeler[1].
- The ratio between the average gold activation cross-section for the broad-energy beam and that of the narrow-energy beam is (1.070±0.035).
- The gold activation cross-section for the narrow-energy beam agrees well with that measured by Ratynski and Käppeler [1].
- It was necessary to incorporate Monte-Carlo calculations to complement the experimental data analysis for estimates of:
  - Multiple scattering inside the detector;
  - The change of path length of the neutron in the detector which is reflected in change of flight time;
  - The efficiency of the detectors;
  - Scattering of neutrons in the 1 mm copper target backing;
  - The angular distribution of the neutrons impinging the gold foils;
  - Removal of neutrons from the expected cone by the 1 mm copper backing of the LiF target.

Acknowledgements

The authors would like to thank Mr. E. Tsuk for his valuable assistance in producing the LiF targets and the operators of the IRMM VdG accelerator for many extra hours they devoted in providing the conditions necessary for these experiments.

References

[1] Ratynski, W., F. Käppeler, *Phys. Rev.*, C37, 595 (1988).

[2] Weissman, L., *et al.*, LINAC 2010, Tsukuba, Japan (2010).

[3] Feinberg, G., *et al.*, *Nucl. Phys.*, A827, 590C (2009).

[4] Reifarth, R., *et al.*, "PINO – A Monte Carlo program for ^{7}Li(p,n)^{7}Be near threshold", *Nucl. Instr. Methods*, A608, 139 (2009).

[5] Friedman, M., *et al.*, "SimLiT – A Monte Carlo program for ^{7}Li(p,n)^{7}Be near threshold", to be published.

Future neutron data activity on the neutron source IREN

N.B. Janeva,[2] **Yu.V. Grigoriev,**[1,3] **N.A. Gundorin,**[1] **Yu.D. Mareev,**[1] **Yu.N. Kopatch,**[1] **N.T. Koyumdjieva,**[2] **L.B. Pikelner,**[1] **I.N. Ruskov,**[1,2] **V.N. Shvetsov,**[1] **P.V. Sedyshev,**[1] **Sh. Zeinalov**[1]
[1]JINR, Dubna, Moscow region, Russia
[2]INRNE BAS, Sofia, Bulgaria
[3]FSUE "SSC RF–IPPE", Obninsk, Kaluga region, Russia

Abstract

The global energy demand continues to rise and nuclear power has a potential to be part of the solution of energy problem. Complete and accurate information about the nuclear reactions ensures developing and operating nuclear reactors to reach high efficiencies and adequate safety standards. This demands many nuclear data of improved quality, including covariance nuclear data and correlations. The new neutron source IREN (1 stage) has been put in operation at the end of 2009. The first stage includes the construction of the LUE-200 linear accelerator and non multiplying target. The first measured TOF spectra have been presented recently. The facility is in continuous completion and improvement (according to the full version in the project). The program for neutron data investigation on the IREN neutron source is in preparation. The measuring targets for neutron cross-sections TOF spectra would be selected between isotopes of construction materials, fission products and minor actinides. Now the experimental facilities are in preparation – detectors, innovative electronics equipment and systems for data acquisition and analysis.

Neutron data needs

Complete and accurate information about the nuclear reactions ensures developing and operating nuclear reactors to reach high efficiencies and adequate safety standards. The next generation general purpose Evaluated Nuclear Data Files – ENDF/B-VII.0, JEFF-3, BROND-3 of recommended nuclear data for advanced nuclear science and technology applications contain data primarily for reactions with incident neutrons.

Nuclear data needs are determined by national priorities in present and future plans of nuclear energy production. Here we present only some considerations about data needs at present and taking into account possibilities of the neutron source IREN. High burn-up fuels, thermal and fast reactors lifetime extension, transmutation of structural materials, improvement data for fission products and taking into account increasing the contribution of minor actinides. The main direction of national Russian strategy is closed fuel circle with fast reactors as the base of technological platform. Mainly minor actinides nuclear data fission cross-sections for Pu, Am and Cm isotopes, Am isotopes capture cross-section. These data are necessary for minor actinides transmutation to decrease nuclear waste radiotoxicology, for Th-U fuel cycle – the basic reserve for involving Th in nuclear power.

The NEA SG-26 working group stimulates selected measurements that answer generally accepted high-precision nuclear data needs, such as those identified by the recent on nuclear data needs for advanced reactors and ADS, as categorized in the High-Priority Request List for nuclear data.

Resonance region is important for advanced fuel cycle applications. Advanced fuel cycle will be closed thereby requiring that spent nuclear fuel be reprocessed to produce new fuel for nuclear reactors. The nuclear data for many of the actinides anticipated in the fuel reprocessing streams are not well known. Moreover, the safety basis for efficiently sized equipment, in terms of inventory and through put, will require the demonstration of acceptable margins of subcriticality. The minor

Figure 1: IREN upper accelerator hall

actinides data such as capture cross-section, fission cross-section, fission neutron yields, and fission product yields plays important roles as their concentration of the minor actinides become large. The traditional fast reactor model employs the separated plutonium as fuel. But the Gen-IV fast reactors will use mixed minor actinides to achieve the proliferation resistance goal. This means that the initial concentration of americium and curium will be not ignorable. The differences of data in major libraries are still significant. The resonance data in hundreds eV up to thousands eV region will play important role when the temperature of reactor increase.

IREN neutron source

The full-scale scientific research complex IREN will comprise a 200-MeV linear accelerator LUE-200 with a beam power about 10 kW, and subcritical multiplying target. The characteristics of the full-scale complex IREN (integral neutron yield 10^{15} n/s and pulse width 0.6 μs) will allow it to rank among the best neutron sources of such class. The realization of the project is conducted in several stages. The first stage includes the construction of the LUE-200 linear accelerator and non-multiplying target. This will make possible to carry out experiments which require precision neutron spectroscopy in the energy range from fractions of eV to few keV already at the first stage of IREN.

The first stage of the IREN neutron source has been put into operation at the beginning of 2009 [1].

At the end of 2009 the facility reached the following parameters:

- Energy of the accelerated electrons – 30 MeV;
- Peak current – 3 A;
- Pulse width – 100 ns;
- Repetition rate – 50 Hz;
- Beam power – up to 400 W;
- Target – non multiplying W;
- Integral neutron yield – about 10^{11} n/s.

Figure 2: Neutron flux density at 10 m flight path of IREN source. Calculated (solid squares) and measured (open circles).

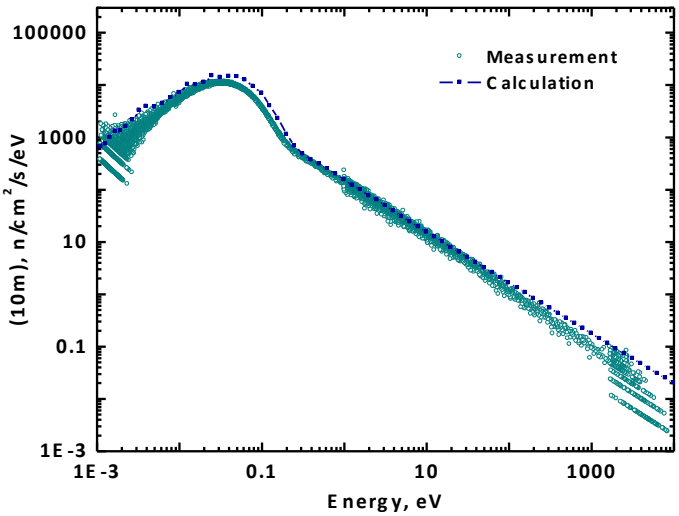

The parameters of the extracted neutron beam are estimated on the base of the experiment on neutron transmission through tantalum filter sample 2 mm thick (*Figure* 3). This element has strong resonances in total cross-sections in the energy region from eV to keV. This experiment has been performed in optimal background conditions.

Figure 3: Neutron transmission through Ta foil, measured with liquid scintillator detector. Experimental points and SAMMY [2] fit.

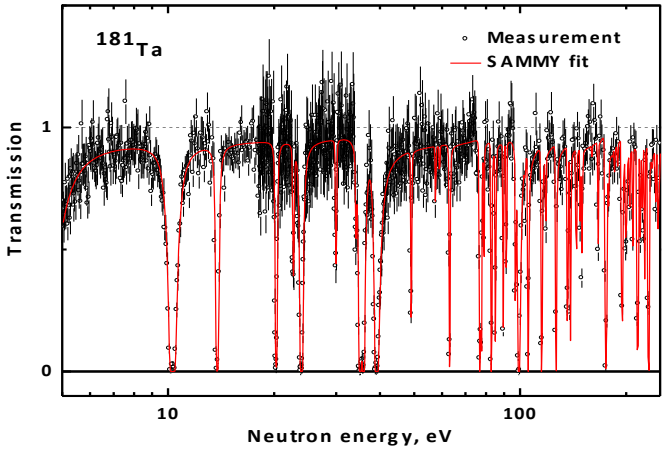

Figure 4: Liquid scintillator detector counts vs. neutron energy at IREN 60 m flight path. Sample – natural Cu foil. Time channel width – 250 ns.

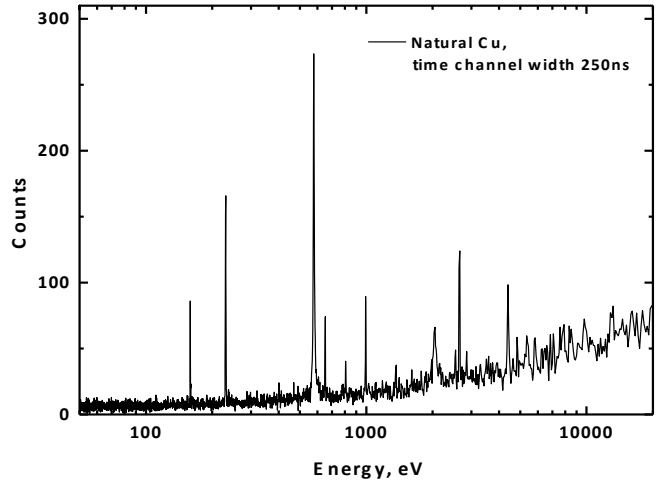

The measured spectrum shows the reached wide energy interval.

FLNP operates also 2 neutron producing facilities: IBR-2 – a pulsed fast reactor which after modernization will be put into operation in few months; electrostatic neutron generator EG-5 for producing fast neutrons.

Experimental methods and facilities

Ultimate goal of any neutron data measurement is the obtaining of a set of resonance parameters for a given nucleus. Average, group and point-wise cross-sections can be reconstructed from these parameters for the required energy region using modern calculation techniques [2]. In order to extract

the resonance parameters in the most precise and unambiguous way, it is necessary to measure a set of different cross-sections for the given nucleus: total (transmission), capture, scattering, fission etc. In FLNP JINR a complex of experimental set-ups is under construction, which will allow to measure simultaneously or sequentially different neutron cross-sections at the IREN facility. The core of the experimental complex will be the 4π detector system "Romashka". This is a modern version of the 4π multisectional scintillation detector applied first in neutron spectroscopy by G.V. Muradyan [3] He gave this name to the detector with allusion to a special shape of scintillators (like a flower Daisy). This was a starting period of the multiplicity (of gamma quanta and neutrons per act of neutron-nucleus interaction) spectrometry method that insures many important results in precise measurement of resonance neutron cross-sections and their functions, parameters and spins of resonances etc. On the *Figure 6* is presented one of the first systems Romashka.

Figure 5: 4π - multidetector system ROMASHKA

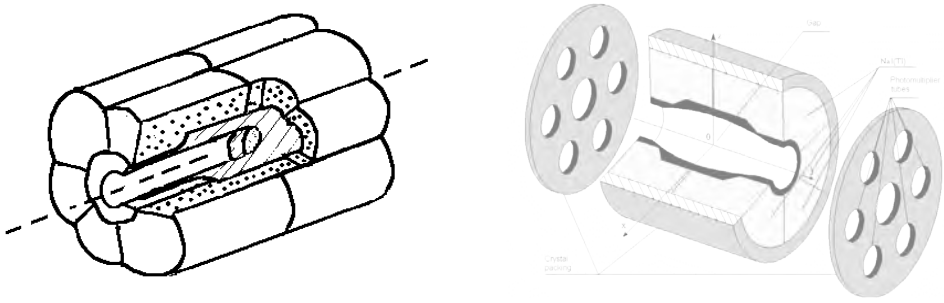

Figure 6: Detector system "Romashka". The inner diameter is 180 mm. Total length of the sensitive part is 400 mm.

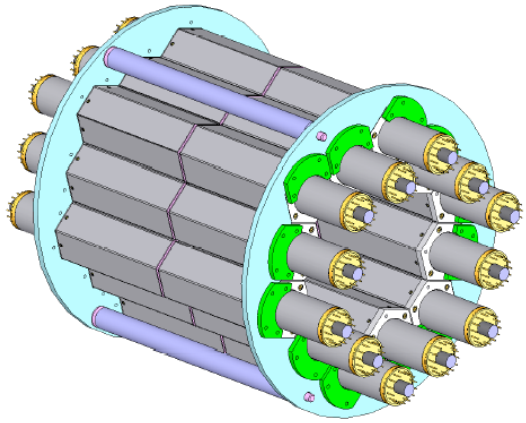

This detector is assembled from 12 scintillators NaI(Tl) which are divided on two halves of 6 crystals. The crystals measure in total is 16.6 l NaI(Tl) and they are placed in a cylinder with the outside diameter 30 cm. The scintillations of each crystal are seen through a light guide by a photomultiplier tube. We intend to use this detector for some auxiliary measurements on IREN.

The basic configuration of core multiplicity detector consists of 24 NaI hexagonal crystals 200×78×90 mm equipped with modern photomultipliers and digital readout system. For specific measurements it can be supplemented by HPGe detectors for gamma-ray spectroscopy and Stilbene scintillator crystals for measuring fast neutrons.

Rather large inner diameter of 180 mm can allow for measurements with big targets which may partially compensate low neutron intensity from IREN. The following quantities can be measured using "Romashka" in combination with other auxiliary detectors:

Capture cross-section measurements

The most direct and obvious application of the 4π gamma-ray detector in the field of neutron data is the measurement of the capture cross-section. The target is placed in the centre of the detector, and the gamma-ray detection count rate is measured as a function of the neutron time of flight. Although the efficiency of the detector is rather high, but it's not 100%, so some corrections should be applied in order to account for the variation of gamma-ray spectra and multiplicities for different isotopes and to extract the absolute value of the cross-section. A reference target with well-known cross-section should be used for normalization purpose. Gamma-ray multiplicity can be used as an additional parameter to increase the accuracy of the obtained data.

We have high-efficiency γ-detector based on liquid scintillator which detects the neutrons via γ-quanta cascades followed by neutron capture in a special converter within detector. The replacement of converter with target sample allows the use of detector for registration of neutron capture reactions. Overall detector design consists of 6 sections which surround cylindrical empty volume along the neutron beam. The total length of detector assembly is 700 mm with inner and outer radii 300 and 730 mm respectively. Each section has a volume of 35 litres (210 litres for entire assembly). Inner surface of each section is covered with titanium oxide. Liquid scintillator represents a mixture of toluol with PPO (4 g/litre), POPOP (0.5 g/litre). Scintillator contains also $B(OCH_3)_3$ (about 50% of toluol) for decreasing of neutron lifetime in scintillator. Every section is equipped with two PMT which are attached to a section's front and back sides. This detector has been used for various experiments in fundamental and applied neutron physics. The photo the detector from its back side is shown on Figure 7.

Figure 7: Liquid scintillation detector for investigation of neutron transmission and capture reactions. 1-cap of individual PMT. 2-empty volume for the samples or converter, 3-safety siphones.

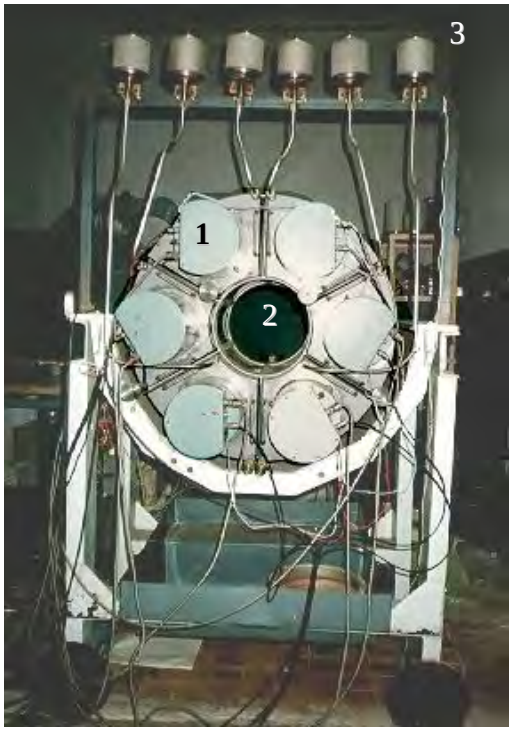

Total cross-section (transmission) measurements

The same detector can be used for transmission measurements. In this case the investigated target is placed in front of the detector, and in the centre of the detector a special converter is inserted. The converter consists of several rare-earth isotopes with high density of resonances, so that the resulting capture cross-section curve is rather smooth and the efficiency of conversion is rather high. The transmission is measured using standard sequence of measurements: without target and with targets of different thicknesses.

Fission cross-section and α coefficient measurements

Fission cross-section can be measured with "Romashka" using multiplicity method [3, 4]. It exploits the fact that gamma-ray multiplicities for the fission process (typically 8-10) are significantly different from the capture process (typically 2-3). The multiplicity parameter can be used, after proper calibration and normalization, for simultaneous measurement of these two processes in one experiment for a fissioning target. Reference targets with known capture/fission cross-sections should be also used for normalization purposes. In addition, in FLNP JINR there are a number of specially designed fast ionization chambers which can be placed in the centre of "Romashka" and used as an additional external trigger for the fission cross-section measurements. The multiplicity method is especially useful for the α coefficient measurements, which is the ratio of capture to fission cross-sections.

Neutron and gamma emission from fission.

Addition of digitization electronics provides new features to gamma multiplicity measurements like pulse height and time peak-off evaluation from the individual pulses. Application of digital signal processing (DSP) algorithms reduces coincidence resolution down to the nanosecond scale (~1ns). Combination of time peak-off method with pulse height correction of detected multiplicity events dramatically suppresses the background as it was demonstrated in prompt fission neutron measurements [5].

Evaluation methodology

In the resolved resonance region the resonance analysis of experimental data will be performed by the code SAMMY Multilevel R-Matrix Fits to Neutron Data Using Bayes' Equations.

For appropriate application of multiplicity method the necessity of using the codes GEANT and MCNP is obvious.

For unresolved resonances we can apply our code HARFOR and continue the investigations of neutron strength function energy structure [6].

Measurement and analysis of the experimental data of neutron transmission in dependence of sample thickness will give additional information for energy structure in the unresolved region.

The code NJOY will be explored for validation of the evaluation.

Start-up of Nuclear Data program

For development of Nuclear Data program on IREN we are using information for national requirement of neutron data from IAEA documents and especially the priority list of key materials identified by SG26 for advanced reactor systems [7]:

- 19 actinides (cross-section covariances, nubar covariances) in priority order:
  - ^{235,238}U, ^{239}Pu;
  - ^{237}Np, ^{240,241}Pu, ^{241,242m,243}Am;
  - ^{232}Th, ^{233,234,236}U, ^{238,242}Pu, ^{242,243,244,245}Cm.
- 34 structural, moderator and coolant materials (cross-section covariances) in priority order:
  - ^{16}O, ^{23}Na, ^{52}Cr, ^{58}Ni;
  - ^{1}H, ^{12}C, ^{28}Si, ^{90,91,92,94}Zr, ^{206,207,208}Pb, ^{209}Bi, ^{4}He, ^{6,7}Li, ^{9}Be, ^{10}B, ^{15}N, ^{19}F, ^{27}Al, ^{56,57}Fe, ^{155,156,157,158,160}Gd, ^{166,167,168,170}Er.

A possible candidate for starting and testing measurements of nuclear data seems to be natural Gadolinium, namely measurements of natural Gd neutron capture cross-section, transmission and self-indication.

Gd with very big thermal neutron cross-section is important for the nuclear technology new type nuclear fuel fabrication. So called "Gadolinium" fuel became popular ultimately.

Gd with very big thermal neutron cross-section and big magnetic moment is applicable in medicine for neutron capture therapy and nuclear magnetic resonance

Acknowledgements

The authors would like to thank professors G.V. Muradyan and A.A. Lukyanov for their very important support in development of nuclear data activity on IREN.

References

[1] Belikov, O.V., *et al*., *Journal of Physics G Conference Series*, V 205 (2009).

[2] Larson, N.M., *Updated Users' Guide for SAMMY: Multilevel R-Matrix Fits to Neutron Data Using Bayes' Equations*, ORNL Report, ORNL/TM-9179/R5, Oak Ridge National Laboratory (2000).

[3] Muradyan, G.V., *et al*., Preprint 2634 Kurchatov Atomic Energy Institute, Moscow (1976).

[4] Muradyan, G.V., "The Multiplicity spectrometry", *Atomic Energy*, 50 (6), 394 (1981).

[5] Zeynalov, Sh., *et al*., "Recent results from investigation of prompt fission neutron emission on spontaneous fission of ^{252}Cf", *these proceedings*.

[6] Koyumdjieva, N., N Janeva, A.A. Lukyanov, "Cross-section structure of 232Th in the unresolved resonance region", *J. Phys. G: Nucl. Part. Phys.,* 37**,** 075101 (2010).

[7] Nuclear Energy Agency (NEA), "Uncertainty and target accuracy assessment for innovative systems using recent covariance data evaluations", *International Evaluation Co-operation*, Vol. 26, NEA/WPEC-26, OECD/NEA, Paris (2008).

Development and validation of ALEPH Monte Carlo burn-up code

Alexey Stankovskiy, Gert Van den Eynde, Tim Vidmar
SCK·CEN, Mol, Belgium

Abstract

The Monte-Carlo burn-up code ALEPH is being developed in SCK·CEN since 2004. Belonging to the category of shells coupling Monte Carlo transport (MCNP or MCNPX) and "deterministic" depletion codes (ORIGEN-2.2), ALEPH possess some unique features that distinguish it from other codes. The most important feature is full data consistency between steady-state Monte Carlo and time-dependent depletion calculations. Recent improvements of ALEPH concern full implementation of general-purpose nuclear data libraries (JEFF-3.1.1, ENDF/B-VII, JENDL-3.3). The upgraded version of the code is capable to treat isomeric branching ratios, neutron induced fission product yields, spontaneous fission yields and energy release per fission recorded in ENDF-formatted data files. The alternative algorithm for time evolution of nuclide concentrations is added. A predictor-corrector mechanism and the calculation of nuclear heating are available as well. The validation of the code on REBUS experimental programme results has been performed. The upgraded version of ALEPH has shown better agreement with measured data than other codes, including previous version of ALEPH.

Introduction

The growing of computing power caused sustainable growth of the share of Monte Carlo codes in nuclear reactor research and development. These Monte Carlo codes can provide the most accurate locally dependent neutronics characteristics in realistic 3-D geometries of any complexity. However, they still have had limited applicability to follow the evolution of the system neutronics characteristics with time. There is a variety of Monte Carlo burn-up codes developed worldwide: MONTEBURNS [1], MCB [2], MOCUP [3], CINDER'90 incorporated into MCNPX [4], MVP [5], Serpent [6], MURE [7], EVOLCODE [8]. The common principle of these codes is steady-state Monte Carlo calculation of neutron fluxes and spectra followed by solving the system of Bateman equations for a given time step using the reaction rates calculated from these fluxes and spectra. Then the nuclide concentrations are updated and passed to Monte Carlo driver for recalculation of fluxes and spectra, etc. This procedure repeats up to the end of the irradiation and/or decay history. As a rule, these codes wrap around general purpose Monte Carlo radiation transport codes (MCNP [9], MCNPX) and depletion codes (ORIGEN [10], CINDER'90 [11]). However, some of them use built-in depletion modules (MCB, Serpent). The method of coupling is often is realized as a set of scripts which complicates its utilization by non-experienced users.

The general-purpose burn-up code ALEPH merging MCNP(X) Monte-Carlo radiation transport and ORIGEN-2.2 [10] depletion codes is being developed in SCK·CEN since 2004 [12,13]. Belonging to the same category of shells coupling Monte Carlo transport and "deterministic" depletion codes, ALEPH possess some unique features that distinguish it from other codes. The most important feature is full consistency of cross-section data. The same unionized cross-section tables (*i.e.* cross-sections are linearized on the same energy grid) for a given nuclide are used for Monte Carlo transport and subsequent depletion calculations. The reaction rates are calculated at the beginning of each time step using the fluxes and spectra calculated by MCNP(X). ALEPH allows the user to change materials, temperature and geometry after each time step to reflect the irradiation conditions. Finally, the code is easy to use since it requires only several extra cards in MCNP(X) input file. The validity of ALEPH has been confirmed for different types of problems [14,15,16].

However, since ALEPH invokes ORIGEN-2.2 to perform time evolution calculations, it retains all limitations inherent to ORIGEN. This concerns the accuracy of matrix exponential method to solve Bateman equations and limited number of nuclear data involved.

The upgraded version of ALEPH code is free from these limits which makes it powerful and flexible burn-up tool.

Modifications to ALEPH

Several principal modifications have been made to ALEPH code: extending the nuclear data set, adding an alternative to ORIGEN method of obtaining nuclide concentrations, enabling the predictor-corrector mechanism, and calculating of heating due to neutrons, photons and decay. Besides that, some minor corrections were made in order to improve the code performance and facility of use.

Nuclear data

Major improvement concerns nuclear data treatment. ORIGEN-2.2 is capable to treat only limited number of reactions (radiative capture, fission, (n,2n),(n,3n),(n,p) and (n,α)). However, the number of open reaction channels can be significantly higher and increases drastically for the problems involving energies higher than characteristic to nuclear reactors, such as in accelerator driven systems (ADS). The auxiliary utility, ALEPH-DLG [13] wrapping around NJOY code [17] was modified to be able to build the nuclear data library containing nuclide production cross-sections up to 1 GeV. The library can be constructed for a set of temperatures from basic general-purpose evaluation (JEFF-3.1.1 [18], ENDF/B-VII [19], or JENDL-3.3 [20]). Then it is extended to higher number of nuclides and reactions per target nuclide by adding the data from TENDL-2009 library [21]. TENDL-2009 contains ~2000 neutron files and ~1200 proton files for the nuclides with half-lives greater than one second. The upper energy limit in these files is either 200 MeV for the majority of stable and important unstable nuclides or 60 MeV for short-lived isotopes. Actinides, however, have upper limit 20 MeV. Final step is extension to higher energies using HEAD-2009 activation data library [22].

HEAD-2009 library contains neutron and proton induced data for 684 stable and unstable nuclides in the primary particle energy range 150 MeV to 1 GeV.

Proton induced reactions can play an important role in investigating the time behaviour of spallation and activation products in an ADS. The capability to treat proton data was added to ALEPH. To summarize, the new library constructed by ALEPH-DLG consists of ~2000 neutron files and ~1200 proton files for individual nuclides with half-lives greater than a second. Files contain up to ~2000 reaction cross-sections with upper energy limit 1 GeV.

Since the number of reactions for an individual nuclide can be rather high, significant efforts were directed to accelerate the cross-section averaging over the spectrum produced by the MCNP(X). The algorithm of averaging in ALEPH and format of activation data storing (PENDF tapes generated by NJOY code) were found to be ineffective. The format of activation data files was changed to ACE (A Compact ENDF) dosimetry type [4,9] where only reaction cross-sections are recorded. A unique energy grid is employed for all neutron and proton induced reactions on all nuclides in the library. Tests have shown that the total time to get one-group averaged cross-sections for most complex problem (involving all reactions for all nuclides in the library, *i.e.* about 460,000 neutron and proton induced reactions) is comparable to the time to process ~3000 neutron reactions for most complex problem handled by previous version of ALEPH.

At the beginning of each time step ALEPH was updating only cross-sections in ORIGEN library, moreover, the cross-sections of reactions leading to metastable states remained unchanged. All other information, such as neutron fission product yields and radioactive decay data was not updated. The modified version of ALEPH is capable to use almost all data supplied in basic libraries, namely radioactive decay data (*e.g.* JEFF-3.1.1 radioactive decay file contains information for 3851 nuclides), total recoverable energy per fission of fissile nuclides, spontaneous neutron fission product yields, and direct neutron and proton fission product yields.

Method to obtain concentrations

ORIGEN-2.2 uses matrix exponential method to solve the system of first-order ordinary differential equations. It is clear however that the expansion series have limited accuracy due to round-off error, and, due to stiffness of a general system, short-lived nuclides must be removed from the system and treated separately (in ORIGEN-2.2, by Gauss-Seidel iterative technique) [23]. Modern computers, however, allow applying more precise methods of solving the stiff systems of first-order differential equations with constant coefficients. The implicit Runge-Kutta method of order 5 (Radau IIA, three stages) [24] with step size control and continuous output has shown reasonable performance and stability when solving the system containing up to ~4000 equations for all known nuclides. This algorithm has then been incorporated in the code. Typical running time strongly depends on the size of the system and for majority of the problems is not competitive with matrix exponential method (minutes versus seconds or even milliseconds). However, this is still significantly less than the MCNP(X) running time to obtain fluxes and spectra. A simple parallelization was implemented and could be invoked in case the number of burnable materials exceeds the number of CPU allocated to the problem (assuming that MCNP(X) runs in parallel mode). This reduces significantly the total computational time for huge problems with numerous burnable materials. ORIGEN-2.2 can still be used in ALEPH if the speed rather than quality is required.

Predictor-corrector algorithm

Previous version of ALEPH did not use any predictor-corrector mechanism. It should be noted however that predictor-corrector will obviously slow down the code since additional steady-state Monte Carlo calculations of fluxes and spectra are required. The best option from the quality/performance point of view remains the fine binning of irradiation history, however it is not always possible to properly define it. This situation is somehow similar to the variance reduction technique inside Monte Carlo code itself: the best variance reduction is simply higher statistics, but for some problems such increase is not feasible.

In order not to severely overburden memory consumption, the approach from MCNPX [4] which originates from MONTEBURNS [1] was adopted for ALEPH. The fluxes and spectra are calculated at the beginning of time step, and then the concentrations are obtained at the half of the time step.

Using these concentrations, the fluxes and spectra are recalculated and finally the concentrations at the end of time step are computed on the basis of new fluxes and spectra. ALEPH takes the responsibility whether to apply predictor-corrector or not by comparing the nuclide concentrations and reaction rates at the beginning and end of time step.

Nuclear heating

The ALEPH-DLG utility was modified in order to provide the neutron and photon heating numbers (kerma-factors) in the ALEPH data files. Using these total kerma-factors, the energy release rates by neutrons and photons in the material could be calculated at the beginning of each time step by folding these numbers with neutron and proton fluxes, accordingly. Then they are integrated over the time together with decay energy release rates to get the total energy release in the material during the given time step.

Recoverable energy per fission or capture event

It is a customary to use the total power of the system or specific power per material when describing irradiation history. However, this power must be converted to flux in order to obtain the reaction rates for the right side of Bateman equations. The ALEPH uses the following ratio to get the flux value at the beginning of time step after steady-state Monte Carlo calculation:

$$\phi = 6.242\times10^{18}\frac{P}{\left(F\sum_i w_i Q_{fi} + C\sum_i w_i Q_{ci}\right)}\varphi_{MCNP}, \quad (1)$$

where P is specific power of a given material in MW, F and C are the numbers of fission and neutron capture events occurred in the material per source particle simulated in MCNP(X) calculation, Q_{fi} and Q_{ci} are energy releases per fission and capture events on nuclide i, w_i stands for the atomic fraction of nuclide i in the material, and φ_{MCNP} is the track length estimate of neutron flux in MCNP(X) calculation normalized to source particle. The values of recoverable energies per fission and capture events are taken from ENDF/B evaluations. If the recoverable energy per fission event is not provided in nuclear data files, the ORIGEN-2.2 approximate formula is used [10]:

$$Q_{fi} = 1.29927\times10^{-3}Z_i^2\sqrt{A_i^2} + 33.12, \quad (2)$$

where Z_i and A_i are charge number and atomic mass of nuclide i. The user however can alternatively input the desired value of recoverable energy per fission.

The implementation of the changes to ALEPH allows concluding that all the limitations related to nuclear data treatment and method to perform depletion calculations are eliminated, and possible final uncertainties in nuclide concentrations will depend on the original nuclear data uncertainties only.

Besides major improvements some minor corrections were done, such as the possibility to follow time evolution of different material types (fuel, moderator, clad, etc.) in the same code run. The improved version of the code contains significantly reduced number of commands extra to standard MCNP(X) input than its predecessor.

Validation of modified ALEPH

The GDF Suez Company requested to validate ALEPH by comparison with the experimental data from the REBUS study [25], which they had acquired, and not with the MALIBU [26] or ARIANE [27] experiments, for example. It was therefore decided to undertake the validation study using the data from the REBUS experiment [28].

The REBUS experiment

REBUS [28] was an international programme aimed at providing an experimental database for validation of reactor physics codes used for burn-up credit estimations. As part of the experiment, several UO_2 fuel elements were irradiated for four full cycles in a commercial PWR at the Neckarwestheim NPP in Germany. The rods from the fuel assembly from this power plant then underwent first a gamma spectroscopy scan to determine their burn-up profile and later a radiochemical analysis, during which the majority of the radionuclides of interest, in particular, to code validation were determined with high precision. The REBUS experiment actually considered two different reactors and two different types of fuel, but it was assumed that the uniform nature of the flux in a large commercial power reactor should make simulations relatively straightforward.

Reliable data was also available on the geometrical and material properties of the fuel assembly. Its position in the reactor core, however, was not known and neither was the history of any possible reshuffling. This limited the simulation options to the fuel-assembly level (as opposed to a possible full-core calculation).

The power history had been calculated at the Neckarwestheim NPP applying a licensed deterministic code for this type of reactors from the Siemens Company, which used the reactor's thermal output as a normalization factor. A separate computer code was used for the calculation of the fuel and moderator temperature history, whereas the data on the changing boron concentrations over time was available experimentally.

Model

The approach from [28] adopted 53 time steps of power history. The boric acid in the system was kept constant at the average value and a single, constant temperature was used for the moderator, the cladding and the fuel. The initial fuel composition was adjusted for the typical presence of ^{234}U, the percentage of which was not specified in [28]. Assuming that the fuel was enriched by gas diffusion, the process of enrichment in ^{234}U is similar to the one of ^{235}U. One quarter of the 18x18 assembly was modelled, with reflective boundaries on two sides to mimic the symmetry of the system and the white boundaries on other sides to simulate an infinite assembly array. The model has no division of the fuel elements in the vertical direction, but each of the fuel pins was burnt separately (*i.e.* was a different material in ALEPH parlance). A sketch of the model is shown in Figure 1.

Figure 1: a) Model of fuel pin. The cladding thickness is 2.8 mm.
b) Assembly model. The UO_2 pins are coloured in yellow.

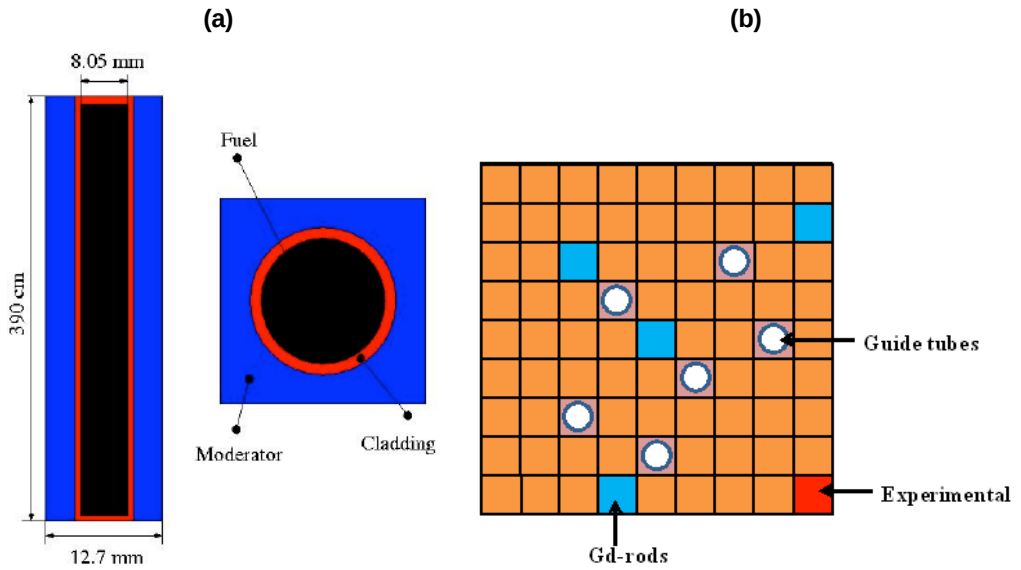

Three different pin types were present in the assembly model: the UO_2 fuel pin from Figure 1, a, the UO_2-Gd_2O_3 pin and the empty guide-tube pin.

In addition to ALEPH itself, the results obtained with the 2-D deterministic code WIMS [29] recalculated to the reference date of the measurements have been used for validation. Calculations were also done using a pure ORIGEN-2.2 model, for which high-burn-up PWRUE libraries [10] matching the experimental conditions were employed. Finally, results of MALIBU experiment [14] were also considered.

Discussion

The results of the comparison of nuclide concentrations are shown in Figure 2. They can be deemed satisfactory and comparable in quality with the ones from a previous verification attempt of the original ALEPH code [14], which used the MALIBU program data. It has to be borne in mind, of course, that the MALIBU program considered a very different reactor core setup, fuel composition and burn-up history, so that any comparison can only be qualitative.

Figure 2: Deviation of calculated nuclide concentrations from experimental data

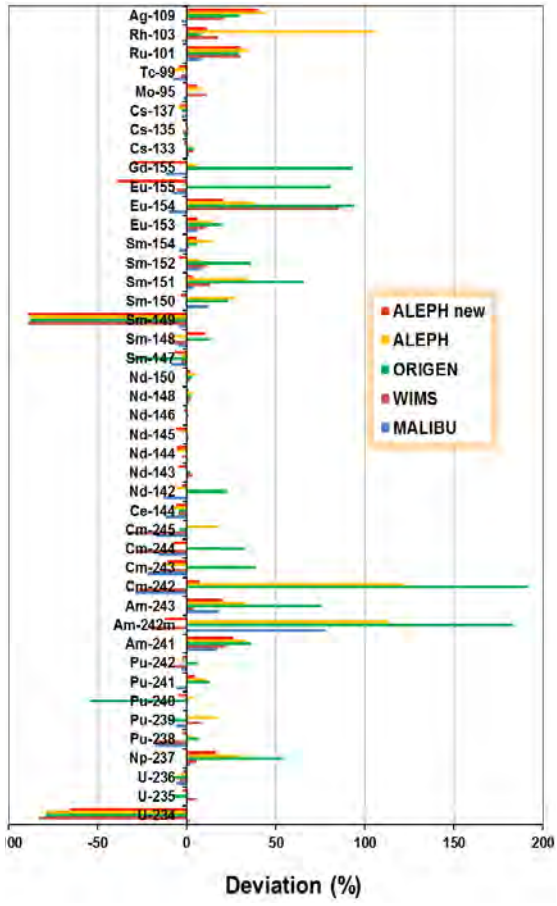

The quantitative analysis was performed using two deviation criteria useful to perform statistical analysis when the values differ by several orders of magnitude:

$$F = 10^{\sqrt{\frac{1}{N}\sum_{i=1}^{N}(\lg C_i^{exp} - \lg C_i^{calc})^2}}, \tag{3}$$

$$H = \sqrt{\frac{1}{N}\sum_{i=1}^{N}\left(\frac{C_i^{exp} - C_i^{calc}}{\Delta C_i^{exp}}\right)^2}, \tag{4}$$

where N stands for the total number of experimental points C_i^{exp} and C_i^{calc} are the experimentally measured and calculated nuclide concentrations, and ΔC_i^{exp} represents the experimental error. The F criterion allows estimating adequately and reliably the correlation closeness between calculated and experimental data, while H accounts for experimental error [30]. The deviation factors are shown in Table 1.

Table 1: Calculated deviation factors

Code	F	H
MALIBU	1.146	0.137
WIMS	1.595	0.245
ORIGEN	1.722	0.491
ALEPH	1.598	0.341
ALEPH new	1.495	0.204

The results of calculations with modified ALEPH code show improvement with respect to the related calculations by original ALEPH. It is observed from Figure 2 that very large discrepancies for Am and Cm isotopes found for ALEPH are no longer present among the results of calculation with upgraded ALEPH. It should be noted that the experimental error attributed to most of AM and Cm isotopes was quite high, reaching 36% for Cm-242. The concentrations for the major actinides are within 5% deviation from measured data. The ^{234}U concentrations in the initial fuel compositions remain uncertain. Another isotope with a substantial discrepancy, ^{237}Np, has a rather large experimental uncertainty attached to its value. This is a positive outcome of using a complete and consistent set of nuclear data both in MCNP(X) and in the depletion calculations.

The concentrations of fission products vary in quality with the nuclides present in higher amounts generally yielding better results and with the nuclides most important from the waste management point of view, such as ^{135}Cs and ^{99}Tc, showing a satisfactory match. The same is true of ^{137}Cs, which was used for experimental gamma scanning, aimed at burn-up profile determination. The agreement with

Figure 3: Neutron induced FP yields from different libraries and codes. The total sum over all FP is 2.

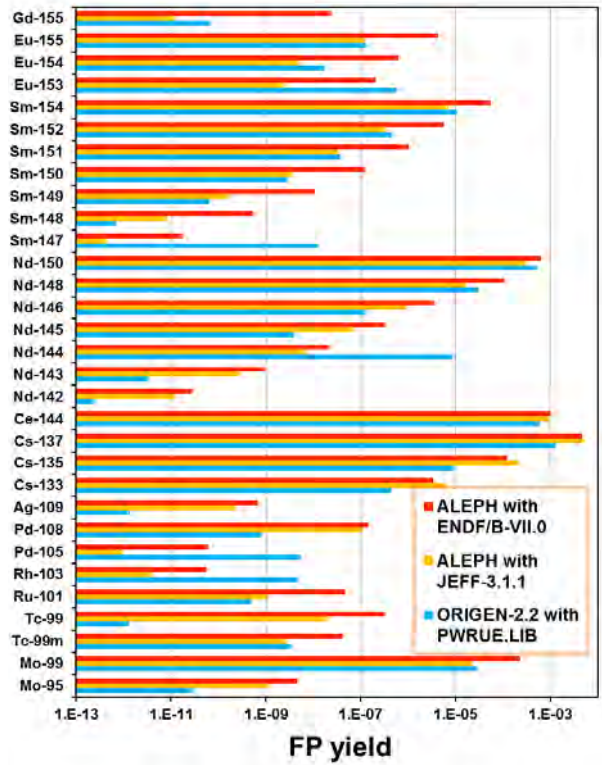

the experimental data is very good for the Nd isotopes, which testifies to the correct burn-up values used in the model. The results of most of the Sm isotopes are disappointing, however, as are those of Pd isotopes. This is attributed to results calculated with both ALEPH versions, as well as with ORIGEN-2.2. The reason is neutron induced fission product yields. They differ significantly between ORIGEN-2.2 libraries and libraries used by upgraded ALEPH code (the calculations with FP yields from JEFF-3.1.1 and ENDF/B-VII were performed). For some nuclides the difference in FP yields is as high as several orders of magnitude which is vividly seen from Figure 3. It should be noted that in the standard ENDF evaluated files, as a rule, the FP yields are given only for thermal point, fast spectrum averaged and for 14 MeV. Thus the folding with neutron spectrum becomes one of the main sources of final uncertainty.

To summarize, the general trend is an overestimation of the calculated concentrations and the differences with the experimental data which exceed the uncertainties of the latter. However, for the current requirements of the nuclear industry, the achieved accuracy can be deemed satisfactory.

Conclusions

Two principal features of ALEPH Monte Carlo burn-up code, a nuclear data library covering neutron and proton induced reactions, neutron and proton fission product yields, spontaneous fission product yields, radioactive decay data, total recoverable energies per fission, and numerical solution of Bateman equations make this tool flexible and powerful. The area of application ranges from single pin model to full-scale reactor model, including such specific facilities as accelerator driven systems. In addition, the format of the input file used to describe the model and the irradiation conditions has been greatly streamlined, making introduction of errors in the parameters of the simulation much less likely.

The code has been validated on REBUS experimental data. There is notable improvement with regard to original version of ALEPH, ORIGEN-2.2 and WIMS codes. The fission products are generally overestimated which is attributed to the uncertainties in direct fission product yield data. However, the deviations from experimental data satisfy the current requirements.

References

[1] Poston, D.L., H.R. Trellue, *User's Manual, Version 2.0 for MONTEBURNS Version 1.0*, LA-UR-99-4999, Los Alamos National Laboratory (1999).

[2] Cetnar, J., *et al.*, "General solution of bateman equations for nuclear transmutations", *Ann. Nucl. En.*, 33, 640 (2006).

[3] Moore, R.L., *et al., MOCUP: MCNP-ORIGEN2 Coupled Utility Program*, INEL-95/0523, Idaho National Engineering Laboratory (1995).

[4] Pelowitz, D.B., *MCNPX User's Manual, Version 2.6.0*, LA-CP-07-1473 (2008) and Pelowitz D.B., *et al., MCNPX 2.7.C Extensions*, LA-UR-10-00481, Los Alamos National Laboratory (2010).

[5] Mori, T., *et al.,* "Development of the MVP Monte Carlo Code at JAERI", *Trans. of the ANS*, 84, 45 (2001).

[6] Leppänen, J., *Serpent Progress Report 2009*, VTT-R-01296-10, VTT Technical Research Centre of Finland (2010).

[7] Meplan, O., *et al., MURE, MCNP Utility for Reactor Evolution - User Guide - Version 1.0*, IPNO-09-01, IPN Orsay (2009).

[8] Gonzalez, E., *et al.,* "EVOLCODE: ADS Combined Neutronics and Isotopic Evolution Simulation System", *Proc. Int. Conf. MC'99*, Madrid, p. 963 (1999).

[9] Booth, T. E., *et al.,* (X-5 Monte Carlo Team), *MCNP – A General Monte Carlo N-Particle Transport Code, Version 5, Volume II: User's Guide*, LA-CP-03-0245, Los Alamos National Laboratory (2003).

[10] Croff, A.G., *A User's Manual for the ORIGEN2 Computer Code*, ORNL/TM-7175, Oak Ridge National Laboratory (1980).

[11] Wilson, W.B., *et al.,* "CINDER'90 code for Transmutation Calculations," *Proc. Int. Conf. on Nuclear Data for Science and Technology*, Trieste, p. 1454 (1997).

[12] Haeck, W., B. Verboomen, *ALEPH 1.1.2 – a Monte carlo Burn-up Code*, BLG-1003, SCK·CEN, Belgium (2006).

[13] Haeck, W., B. Verboomen, *ALEPH-DLG (Data Library Generator) – Creating a General Purpose Validated Application Library for MCNP(X) and ALEPH*, BLG-1002, SCK·CEN, Belgium (2005).

[14] Haeck, W., B. Verboomen, "An Optimum Approach to Monte Carlo Burn-up", *Nucl. Sci. Eng.,* 156, 180 (2007).

[15] Schubert, A., *et al.,* "Extension of the TRANSURANUS burn-up model", *J. Nucl. Mat.,* 376, 1 (2008).

[16] Chandler, D., *et al.,* "Validation of a Monte Carlo based depletion methodology via High Flux Isotope Reactor HEU post-irradiation examination measurements", *Nucl. Eng. Des.,* 240, 1033 (2010).

[17] MacFarlane, R.E., D.W. Muir, *The NJOY Nuclear Data Processing System, Version 9*1, LA-12740-M, Los Alamos National Laboratory (1994).

[18] Nuclear Energy Agency (NEA), *The JEFF-3.1.1 Nuclear Data Library*, JEFF Report 22, OECD/NEA, Paris (2009), and *The JEFF-3.1 nuclear data library*, JEFF Report 21, OECD/NEA, Paris (2006).

[19] Chadwick, M.B., *et al,* "ENDF/B-VII.0: Next Generation Evaluated Nuclear Data Library for Nuclear Science and Technology", *Nuclear Data Sheets*, 107, 2931 (2006).

[20] Shibata, K., *et al.,* "Japanese Evaluated Nuclear Data Library Version 3 Revision-3: JENDL-3.3", *J. Nucl. Sci. Technol.,* 39, 1125 (2002).

[21] Koning, A.J., D. Rochman, *Consistent TALYS-based Evaluated Nuclear Data Library including covariance data*, JEFF Project, JEF/DOC-1310, NEA Data Bank (2009).

[22] Korovin, Yu., *et al., High Energy Activation Data Library (HEAD-2009)*, LA-UR-10-01397, Los Alamos National Laboratory (2010).

[23] Gauld, C., O.W. Hermann, R.M. Westfall, *ORIGEN-S: SCALE system module to calculate fuel depletion, actinide transmutation, fission product buildup and decay, and associated radiation source terms, SCALE6 Manual*, ORNL/TM-2005/39, Version 6, Vol. II, Sect. F7, Oak Ridge National Laboratory (2009).

[24] Hairer, E., G. Wanner, *Solving Ordinary Differential Equations. Stiff and Differential-Algebraic Problems*, 2nd ed., Springer Series in Comput. Math., Vol. 14 (1996).

[25] Baeten, P., *et al.*, "The REBUS Experimental Programme for Burn-Up Credit", *Proc. 7th Int. Conf. on Nuclear Criticality Safety* (2003).

[26] MALIBU Program, *Radiochemical analysis of MOX and UOX LWR fuels irradiated to high burn-up*, Technical proposal MA2001/02, Belgonucleaire, Brussels, Belgium (2004), and Boulanger, D., *et al.*, "High burn-up PWR and BWR MOX fuel performance: a review of Belgonucleaire recent experimental programs", *Proc. Int. Meeting on LWR Fuel Performance*, Orlando, Florida, USA (2004).

[27] Lippens, M., *et. al.*, "Source Term Assessment: The ARIANE Programme", *Proc. 8th Int. Conf. on Environment Management* (2001).

[28] Lance, B., *REBUS International Programme, REBUS-PWR Final Report*, Ref. No. File 0501320/221-1 (RE 2005/37), SCK·CEN, Belgium (2006).

[29] Serco Assurance, *WIMS8a ANSWERS Software Package, A general Purpose Neutronics Code*, Serco Assurance (previously AEA Technology).

[30] Korovin, Yu., *et al.*, "Evaluation of activation nuclear data in the energy region 150 MeV to 1 GeV", *Proc. Int. Conf. On Nuclear Data for Science and Technology ND2007*, Nice, France, p.1175-1178 (2008).

Automatic dosimeter for kerma measurement based on commercial PIN photo diodes

V. Kushpil,[1] **S. Kushpil,**[1] **Z. Huna**[2]
[1]NPI of ASCR, Rez near Prague, Czech Republic
[2]CVUT, Prague, Czech Republic

Abstract

A new automatic dosimeter for measurement of radiation dose from neutron and ionization radiation is presented. The dosimeter (kerma meter) uses commercial PIN diodes with long base as its active element. Later it provides a maximal dependence of the minority carriers life time versus absorbed dose. The characteristics of the dosimeter were measured for several types of commercial diodes. Device can be useful in many environmental or industrial applications.

Introduction

In result of wide application of different types of semiconductor's detectors in modern experimental nuclear physics today, stands up a new requirement to improve detectors reliability. The irradiation changes the properties of semiconductor materials due to the generation of defects, hence parameters of the detectors may be considerably changed. To investigate sensitivities of parameters of detectors under irradiation, the neutrons, protons and electrons are used. During the process of detectors irradiation the absorbed dose must be measured and the process of measurement must be as simple as possible.

The PIN diodes are used as a device for measurement of dose from fast neutrons and charged particles since 1959 [1]. But for the precise measurement of absorbed dose few important parameters must be controlled. They are the temperature, time interval after irradiation of the diode and also the parameters of test signal (amplitude of current and pulse width). Recent progress in developing the embedded systems allows to create simple and reliable devices which are easy to use. Measurements can be automated enough and it is possible to do all important corrections of data to output results in units of dose. In this article we describe the device for measurement of dose by measurement of forward voltage on PIN diode for given constant current. The device called RM20 has been developed in frame of bachelor-ship's work.

Short theory for optimal application RM20

The principle of application of PIN diode for measurement of absorbed dose is simple enough and described in works [2], [3]. Let us consider the PIN diode as it is shown in Figure 1. The total forward voltage can be presented in a form (1) (where V_{fw} is total forward voltage, V_{pn} – junction voltage, V_{rb} – voltage on resistance of part of i-type silicon).

$$V_{fw} = V_{pn} + V_{rb} \tag{1}$$

According to work [4] we can present dependencies for each component of total voltage using the semiconductor's detector parameters as (2)

$$V_{fw} = V_{pn} + V_{rb} = \varphi_T \cdot \ln\left[\frac{I(t) \cdot N_d(\Phi)}{e \cdot S \cdot N_i^2 \cdot \sqrt{D_n \cdot \tau_n}}\right] + \varphi_T \cdot \ln\left[\frac{I(t) + B(N_t[\Phi])}{A(N_d[\Phi]) + B(N_t[\Phi])}\right] \tag{2}$$

The dependencies of the minority carriers life-time and resistance of silicon on the neutron dose can be obtained from [4] and where $\varphi_T=(k_o \cdot T/e)$, k_o –Boltzmann constant, T - temperature, Φ-fluence, N_d is concentration and D_n diffusion length, τ_n time of life for majority carriers in i-Si, I(t)- forward current at time t, S- area of P-N junction, N_i – intrinsic carriers concentration for Silicon,

Figure 1: The structure and equivalent circuit of PIN diode

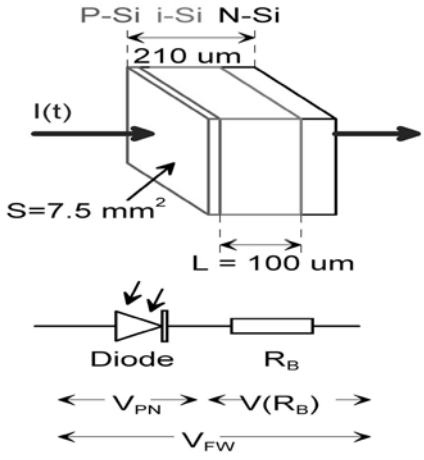

e- charge of electron, K_{nd} and K_{nt}– coefficient of dependencies for concentration of majority carriers and for traps with energy 0.6eV versus absorbed dose (N_{d0}, N_{t0} - concentrations before irradiation), also

$$A(N_d[\Phi]) = e \cdot \sqrt{\frac{D_n}{\tau(\Phi)}} \cdot \frac{N_i^2}{N_{d0} \cdot \exp(-K_{nd} \cdot \Phi)} \quad \text{and} \quad B(N_t[\Phi]) = e \cdot \frac{L}{2} \cdot N_i \cdot N_{t0} \cdot \exp(K_{nt} \cdot \Phi)$$

We can use a commercial PIN photo-diode BPW34 [6] to estimate influence of dose on each component of equation (1). The results of calculation are presented on Figure 2. According to work [5] we can estimate the temperature of passive part of diode for given pulse width of current. To simplify we assume that process of cooling of diode does not play important role and that temperature of full diode is the same as temperature of passive part of diode (the part of i-type silicon). Differential equation describing the process of heating of diode in this case can be presented in form (3).

$$\frac{dT}{dt} = \frac{\rho_n(T)}{C \cdot p \cdot S^2} \cdot I^2(t) \tag{3}$$

where $\rho_n(T)$ - resistivity of silicon (I-part), C- specific heat of silicon, p- density of silicon, I(t) forward current of diode in time t, L- length of passive part of diode, S - area of diode. The results of numeric solution are shown in Figure 3. Accurate measurement of V_{FW} is possible if the power dissipation before irradiation and after irradiation are the same (it means that diode is under the same temperature). If serial resistance of i-type region before irradiation is R_{bo} and its resistance after irradiation is R_{bi} and R_{bi}/R_{bo}= k from equilibrium of power dissipation we can obtain a relation of currents $I_i=I_o*k^{1/2}$. From experimental data we have got upper limit of k (for diode BPW34 k up to 60). In case k equals 49 we can obtain that the power dissipation for current 1mA for 60ms will be the same as for current 7mA for pulse length 20ms.

Figure 2: Results simulation of BPW34 for V_{FW} from neutron fluence

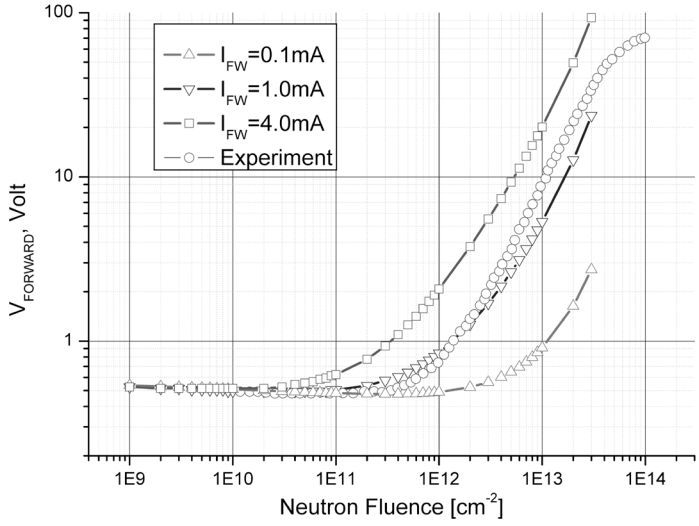

Short remarks about results of simulation are shown in Figures 2 and 3. The simulation of dependence of forward voltage versus dose (Figure 2) was obtained for assumption that during irradiation in silicon only single trap level was born with energy ½ of energy gap of silicon. It could explain big errors in calculation in comparison with experimental data. The dependencies presented in Figure 2(b) can be used for estimation of length of pulse of current for diodes with known resistance of the base after irradiation. We can conclude that for application of calibration for diode from article [6] is necessary to use the same parameters of the test signal and temperature of ambient. The error of measurement will increase with increasing absorbed dose and with increasing variation of temperature of ambient.

Figure 3: Results of simulation of temperature of P-N junction for BPW34

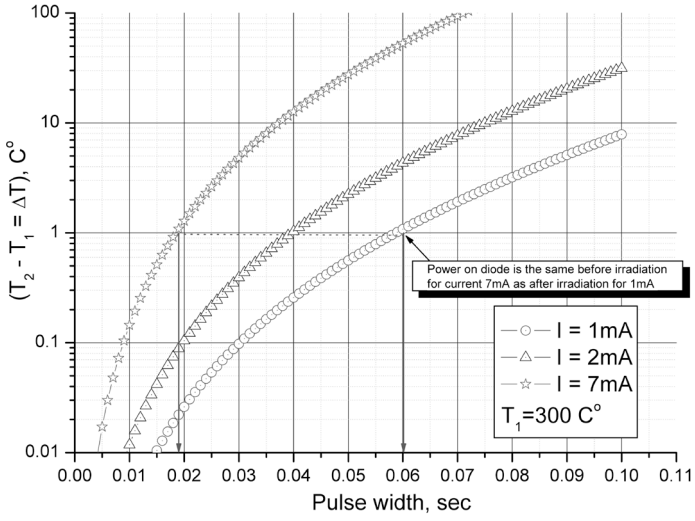

Dosimeter hardware, firmware and software

The dosimeter was developed as simple system with manual control to read the forward voltage drop across PIN diode and as the system controlled by external personal computer. In mode of PC control the dosimeter allows online monitoring of the diode that is under investigation and then to display data in form of fluence of neutrons. The dosimeter can be used in many fields of control and calibrations of detectors and radiation hardness of detectors and also for studying different materials under high radiation doses. Let us describe the basic hardware and software components of dosimeter.

Hardware

The complete circuit block diagram is shown in Figure 4. Other main functions are incorporated in the dosimeter: Current generator (Curr. Gen.) allows to set stable current for investigated diode in range 1-99mA with step 1 ± 0.1mA by digital switches DSW1, DSW2. High voltage supply (HVS) allows to generate 25 V DC for current generator. 12 bit ADC allows to measure voltage drop on diode in range 0-5VDC with accuracy ± 10mV. Temperature sensor (T sens.) to measure temperature in range -20 + 80 C with accuracy ±0.25C and resolution 0.06 C. Source of reference voltage 1.25 VDC for calibration of ADC. The connections of modules are build on analog switches SW1..5. Control module based on MCU Atmega8 from ATMEL Co. allows to control all measurement processes and output results of measurement on LCD display. The MCU allows to communicate with external PC also.

Figure 4: The complete circuit block diagram of RM20

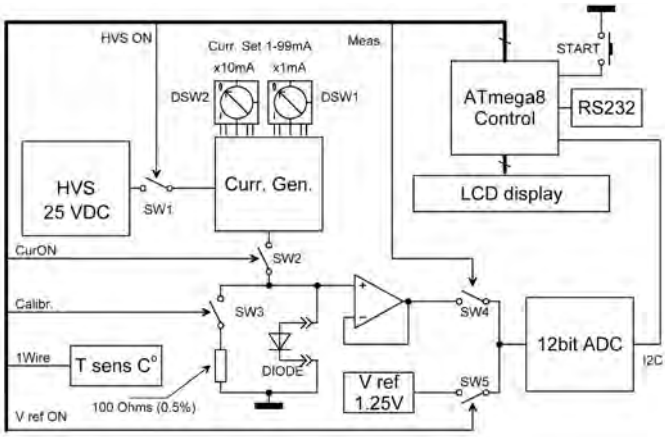

Firmware

The firmware for MCU Atmega8 was created using BASCOM AVR Basic. The diagram of algorithm of measurements is shown in Figure 5. In regime of manual control only one push button is used for measurement. Every time before the measurement is used the calibration when the reference voltage is measured by 12bit ADC. When the push button "START" is pressed for more than 2 seconds, the dosimeter will switch to remote control mode. The current version of firmware measures the voltage without conversion to units of fluence.

Figure 5: The algorithm of measurements realized by firmware of dosimeter

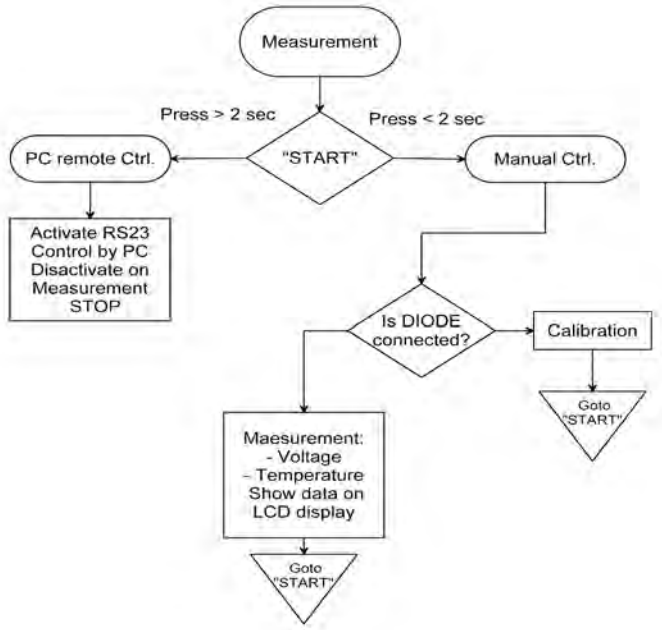

Software

The software for control and graphic user interface (GUI) for dosimeter was created in environment of Lab Windows CVI. External control extends the usage of the radiometer. First of all using external software we can use dosimeter for online monitoring of studied diode. Then we can use embedded functions for sending of alarm messages. We can select maximum limit of temperature and maximum of measured voltage (fluence). When the maximum of selected value is reached the short message can be sent to defined e-mail address. For calibrated diodes we can apply corrections for self-annealing, correction for long cable resistance and for fluctuation of temperature during experiment. For known spectrum of radiation we can use recalculation using NIEL hypothesis.

Conclusion

The RM20 kerma meter is a practical device for application in wide area of nuclear physics experiments. The current version of kerma meter is optimized commercial PIN diode BPW34 and Si-1, Si-2 [7] as active elements. Automatic corrections have been used for recalculation of dose in case of influence of self annealing for BPW34. Automatic optimization and correction can be used for adjustment of pulse width for BPW34 and Si-2. The RM20 can be controlled manually or by computer. This allows RM20 to be used for remote monitoring of absorbed dose and for calibration of new types of diodes.

Acknowledgements

I would like to acknowledge Dr. M. Mejerle for permanent interest to this work and for fruitful discussions and remarks. This work was supported by the Ministry of Education of the Czech Republic (grant LC 07048).

References

[1] Mengali, J., *et al.*, *Proceedings of the Second Conference on Nuclear Radiation Effects on Semiconductor Devices, Materials and Circuits*, Sept. (1959).

[2] Swartz, J.M., M.O. Thurston, "Analysis of the Effect of Fast-Neutron Bombardment on the Current-Voltage Characteristic of a Conductivity-Modulated *p-i-n* Diode", *Journal of Applied Physics*, Vol. 37 (2), pp.745-754 (1966).

[3] Raj Korde, *et al.*, "The effect of neutron irradiation on silicon photodiodes", *IEEE Transactions on Nuclear Science*, Vol. 36 (6), pp. 2169-2175 (1989).

[4] Rosenfeld, A.B., *et al.*, "PIN diode with a wide measurement range of fast neutron doses", *Radiation Protection Dosimetry*, Vol. 33 (1), pp. 175-178 (1990).

[5] Tasca, D.M., "Pulse modes in failure power semiconductor", *IEEE Transactions on Nuclear Science*, Vol. 17 (6), pp. 364-372 (1970).

[6] Ravotti, T., *et al.*, "BPW34 commercial p-i-n diodes for high-level 1-MeV neutron equivalent fluence monitoring", *Proc. of the European Conference on Radiation and its Effects on Components and Systems, RADECS 2007*, Sept. (2007).

[7] *www.cmi.cz/index.php?lang=1&wdc=352*.

Angular-energy spectra of neutrons in selected locations at the Wendelstein 7-X stellarator

Grzegorz Tracz, Krzysztof Drozdowicz
The Henryk Niewodniczański Institute of Nuclear Physics,
Polish Academy of Sciences, Krakow, Poland

Abstract

Extensive angular-energy distributions of neutron currents expected from deuterium fusion in the Wendelstein 7-X stellarator have been calculated by means of the Monte Carlo method. The MCNP5 code has been employed. A simplified model of the W7-X fusion reactor, developed at the Max-Planck-Institut für Plasmaphysik, has been utilised to carry on computer simulations. Five cylinders above the stellarator have been modelled additionally. They will contain radiation detectors. The obtained spectra are to be used by the PTB Braunschweig to design five sets of neutron and gamma dosimeters and detectors. The counters are to provide information concerning both thermonuclear plasma diagnostics and dosimetry.

The neutron spectra have been calculated in nine angle bins, 10 degrees each, for bottom, lateral and top surfaces of an every individual cylinder. Due to a poor statistics in case of the lateral and especially top surfaces, the mesh-based weight windows technique of variance reduction has been employed. Solely particles entering the cylinders, at any point of the relevant surface, have been taken into account for all calculations. In the source model only 2.45 MeV neutrons from D-D reactions have been taken into account. Because of a non-central location of the W7-X in the experimental hall, the angular spectra are different in the case of the lateral and top surfaces, while for the bottom surfaces almost identical for all cylinders. The 2.45 MeV neutron peak is well visible for currents across the bottom surfaces. It decreases for the lateral surfaces and through the top surfaces it actually vanishes, because of absence of near reflecting surfaces in surroundings. Thermal and epithermal neutrons predominate in the energy distributions across all surfaces. In every case, the current of neutrons crossing any surface perpendicularly is noticeably higher than the current of neutrons moving almost parallel to this surface.

Introduction

The Institute of Nuclear Physics Polish Academy of Sciences in Krakow, as a member of the Association Euratom-IPPLM (Poland), is engaged in an international cooperation with the Max-Planck-Institut für Plasmaphysik (IPP) in Germany. The Polish scientific network „Neutrons-Emission-Detection" manages the project "*Neutron diagnostic for pulsed plasma source*". The foregoing paper supplements the mentioned study.

The Wendelstein 7-X stellarator [1,2] is currently being constructed at the IPP branch in Greifswald. Contrary to the tokamaks, the stellarators have effectively steady state magnetic field because internal plasma currents are minimized and the equilibrium is actually provided exclusively by the external magnetic field. The W7-X stellarator is intended to employ plain deuter plasma though deuterium-tritium synthesis is also possible. Namely, two fusion reactions, $^{2}D(d,n)^{3}He$ and $^{2}D(d,p)^{3}T$, occur with more or less the same probability. Therefore, the tritons of the 1 MeV energy from the latter reaction can fuse with the deuterons. The deuterium density is expected to be much higher than concentration of the tritons in the W7-X, so spectra of neutrons emitted from the stellarator ought to be dominated by 2.45 MeV neutrons from the $^{2}D(d,n)^{3}He$ reaction. The tritium-tritium reactions, $^{3}T(t,2n)^{4}He$, because of an even lower probability, have been neglected in this study, too.

Neutrons produced in fusion reactions enable to evaluate the ion temperature, which is a fundamental parameter in plasma diagnostics. Moreover, safety precautions require knowledge of the neutron field around the stellarator. The Technical University (PTB) in Braunschweig is going to design and build a set of neutron and gamma detectors, which will be located above the W7-X stellarator (Figure 1). The assumed height and diameter of the cylindrical counters are h = 180 cm and d = 100 cm, respectively. Centres of the cylinders are placed 290 cm above the equatorial surface of the stellarator at a ring of 770 cm radius, while the average major radius of the plasma is 550 cm. The axis of each cylinder is defined by the radii 550 cm and 770 cm, thus the tilt of the neutron counters is about 37.185 degrees. This arrangement – called "long counters positions" – is a refinement of an old configuration. Previously the counters were to be placed perpendicularly to the equatorial surface of the W7-X stellarator. Owing to the cant, the distance detectors-plasma can be decreased and the dimensions of the cylinders increased.

Figure 1: Computer visualization of positions of the neutron counters (red cylinders) above the Wendelstein 7-X stellarator (courtesy of A. Weller)

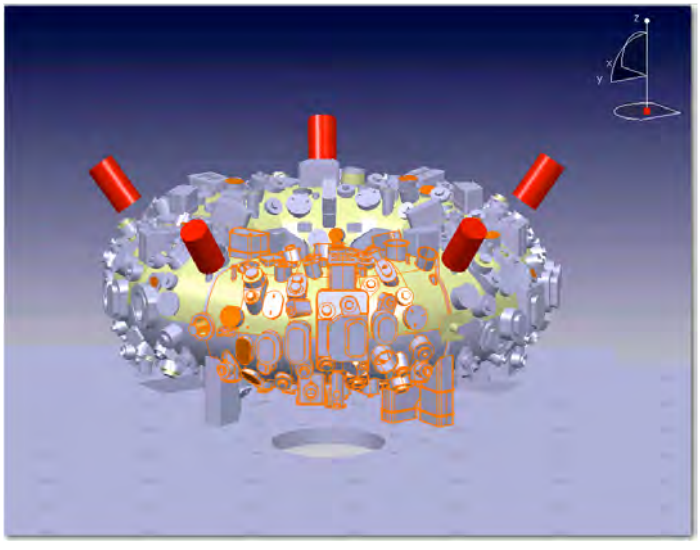

Monte Carlo calculations

Optimization of arrangement of detectors inside the cylinders is going to be based on Monte Carlo calculations of neutron spectra for particles entering the counters. The angular-energy distributions have been computed for bottom, lateral and top surfaces of all five cylinders using the MCNP5 code [3]. The neutron source has been modelled as a ring of the 550 cm radius, which is equal the effective major radius of plasma. All the spectra presented in the paper have been calculated assuming 10^{16} n/s emitted from plasma in D-D reactions. As mentioned above, the D-T reactions have been neglected. Therefore, the most probable initial neutron energy has been 2.45 MeV (Gaussian fusion spectrum at the temperature of ~ $4.64 \cdot 10^{7}$ K).

A cross-section of a simplified CAD model of the W7-X is presented in Figure 2. It contains barely major elements of the stellarator, while details are neglected. Even such a model is too complex to

Figure 2: Cross-section of a simplified CAD model of the Wendelstein 7-X stellarator (courtesy of IPP Greifswald)

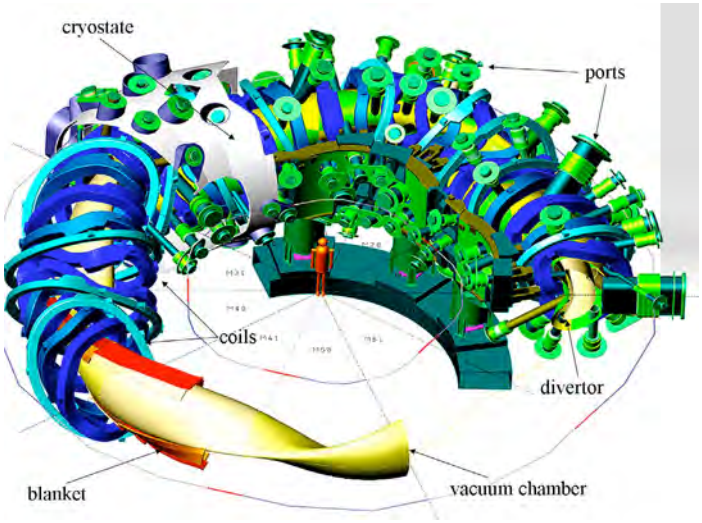

Figure 3: MCNP model of the W7-X. A horizontal section (plane z = 0 cm) through the torus shows the coils, the cooling system and the support structure (MCNP input file through the courtesy of IPP Greifswald)

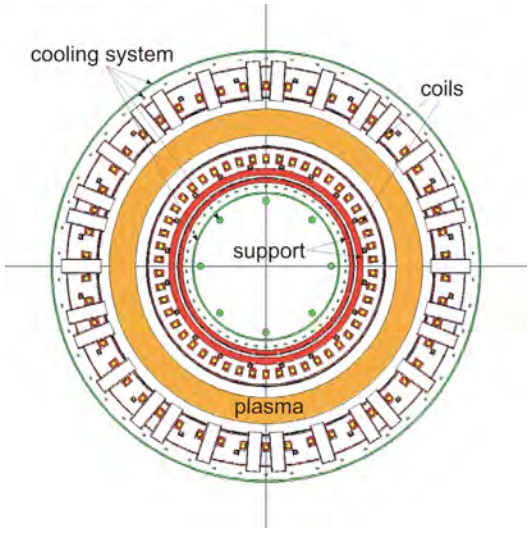

introduce into the MCNP since the code allows to use only surfaces of the first and second order to model geometry. In order to define precisely, for instance, poloidal coils (the blue ones in Figure 2) they must have been divided into many small pieces of "simple enough" shapes, what is time consuming. The MCNP model of the stellarator is a simplification of the real construction. The complicated shapes of varying dimensions – like coils, cryostat, supporting structure and plasma – have been "averaged" and modelled as structures of mean measurements corresponding with a specific W7-X component [4,5]. A horizontal cut of the W7-X in the MCNP model is presented in Figure 3 whereas the horizontal section of the stellarator hall at the level of centres of the cylinders is shown in Figure 4. Since the stellarator is placed non-centrally in the experimental hall, distances of the cylinders from individual concrete walls differ considerably.

In spite of the simplification, the Monte Carlo geometrical model is still extremely complex and calculations have required very long runs to obtain reliable results. The mesh-based weight windows technique of variance reduction [3] has been employed to decrease relative errors. The method in question requires several runs in order to achieve a "good enough" set of weight windows. When the weight windows seem to be optimal, a very long MCNP job can be run. In the foregoing

Figure 4: The layout of neutron counters in the experimental hall (plane z = 290 cm)

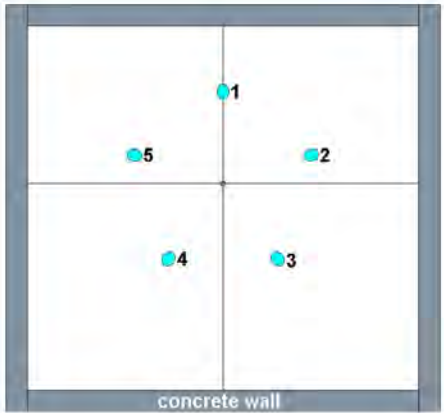

Figure 5: Sketch of angle bins at the cylinder surfaces used in the calculations. All values are in degrees

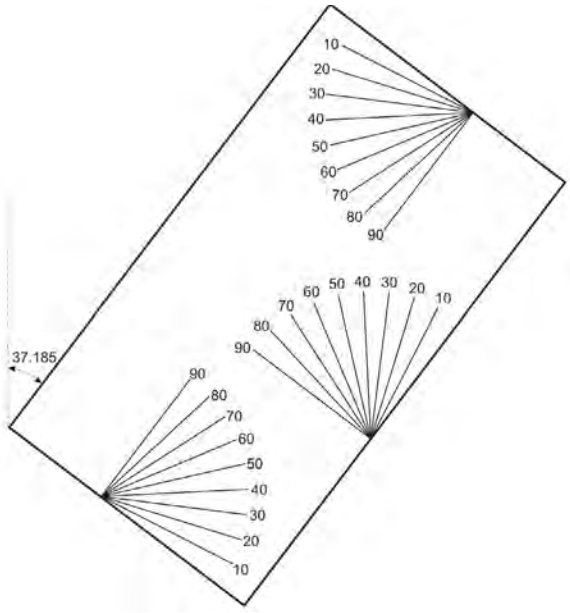

simulations the relative errors of neutron spectra across the bottom and lateral surfaces of the cylinders appear to be satisfactory and the results are reliable. In the case of the top surfaces it is extremely hard to reduce variance, *i.e.* increase validity of results, for solely neutrons scattered on air molecules and concrete walls or ceiling (situated far from the stellarator) can enter the cylinders inwards. Optimization of the mesh-based weight windows has been carried out for the detector labelled "1" (Figure 4), because only one tally can be optimized in the MCNP code in one series of runs. Naturally, the code user can select any of the detectors, but the long-lasting optimization procedure has to be carried on again.

The angular-energy neutron spectra have been calculated in nine equal (in two dimensions) angle bins, 10 degrees each. As already mentioned, only particles entering the cylinders, at any point of the relevant surface, are taken into account for all calculations presented in the paper (Figure 5).

Results

Angular distributions of neutron currents crossing the bottom, lateral and top surfaces of the cylinders are shown in Figures 6, 7 and 8. As expected, in the case of the bottom surfaces the currents are almost the same for all the counters because they are situated relatively close to the W7-X stellarator (Figure 6). Neutrons scattered on air as well as on the hall walls and the ceiling

Figure 6: Angular distributions of neutron currents across the cylinder bottom surfaces

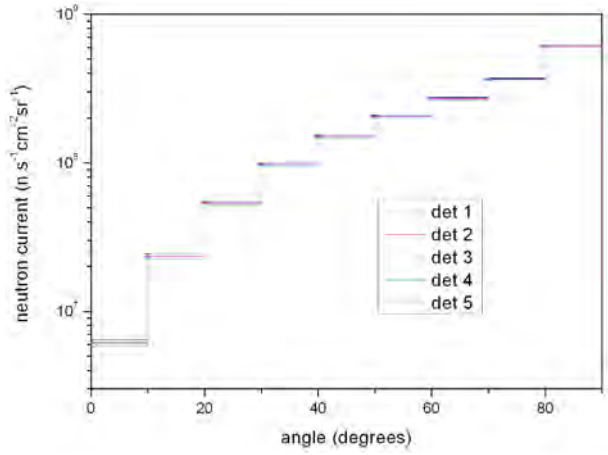

Figure 7: Angular distributions of neutron currents across the cylinder lateral surfaces

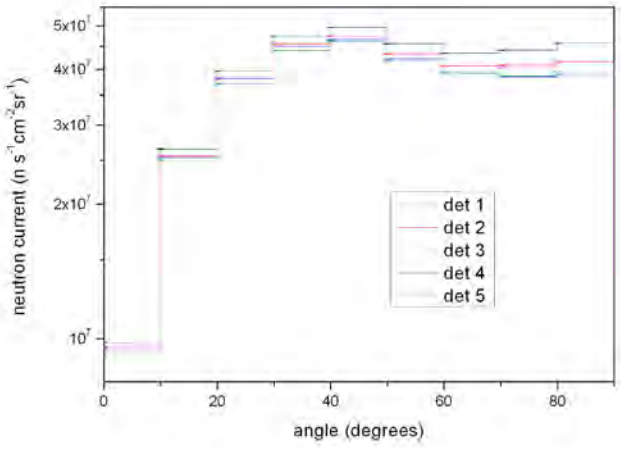

Figure 8: Angular distributions of neutron currents across the cylinder top surfaces

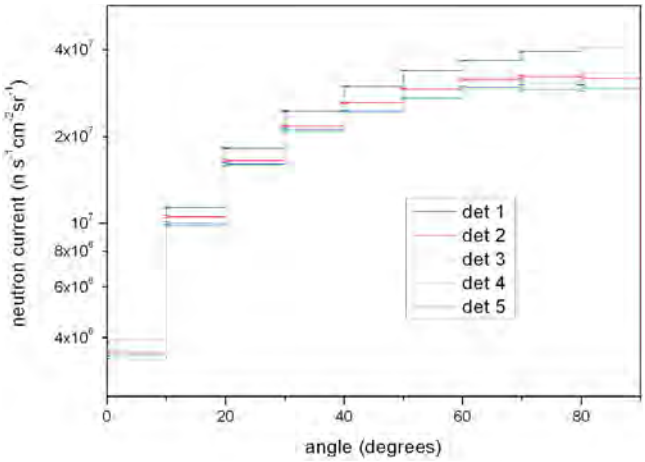

Figure 9: Angular distribution of current ratio for the top surfaces of detectors "1" and "3"

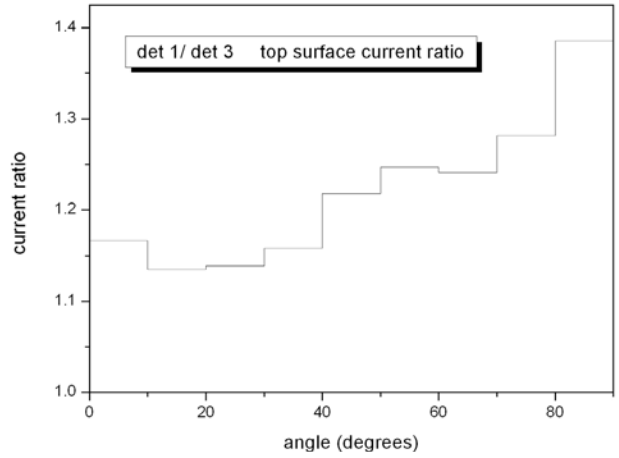

Figure 10: Neutron currents across the cylinder bottom surfaces (80÷90 deg)

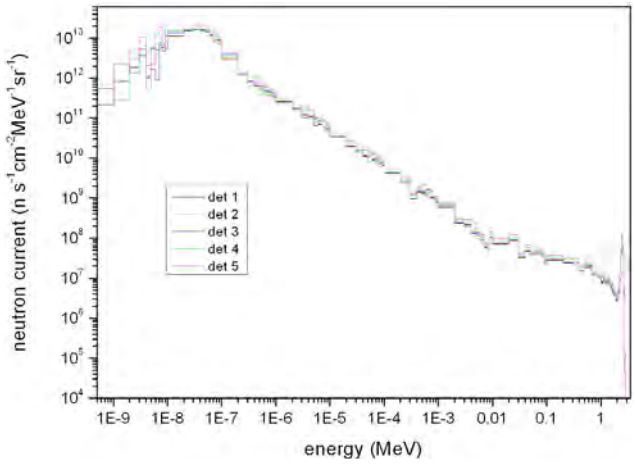

dominate the spectra for the lateral and especially the top surfaces. Distance from the concrete wall to detector "1" is shorter than from detectors "2" and"5", whereas detectors "3" and "4" are located at the longest from the wall. Accordingly, neutron currents in the case of detector "1" are higher than for detectors "2" and "5", while the least currents have been calculated for detectors "3" and "4" (Figures 7 and 8). For all surfaces neutron current increases as the angle grows, particularly for the bottom surfaces due to stellarator nearness. An instructive example is presented in Figure 9. Namely, angular distribution of current ratio of neutrons crossing the top surfaces of detectors "1" and "3". This is the case for which the effect of distance to the hall walls is remarkable visible, particularly for 80÷90 deg angle bin. Energy spectra of neutrons crossing (almost) perpendicularly the top, bottom and lateral surfaces are showed in Figures 10, 11 and 12.

The 2.45 MeV neutron peak – associated with non-scattered neutrons from the D-D fusion – is well visible in the case of the bottom surfaces (Figure 10). The peak decreases for all the lateral surfaces (Figure 11), whereas in the case of the top surfaces it vanishes (Figure 12) due to lack of particles moving in the proper direction. For all the surfaces, including the bottom ones, neutron currents are maximum for thermal energies. Thus, the spectra are dominated by particles scattered on stellarator elements as well as on walls and ceiling of the experimental hall.

As explained above, the most reliable results have been obtained for detector "1". Because of that, it has been chosen to present distributions of neutron currents for various angle bins across

Figure 11: Neutron currents across the cylinder lateral surfaces (80÷90 deg)

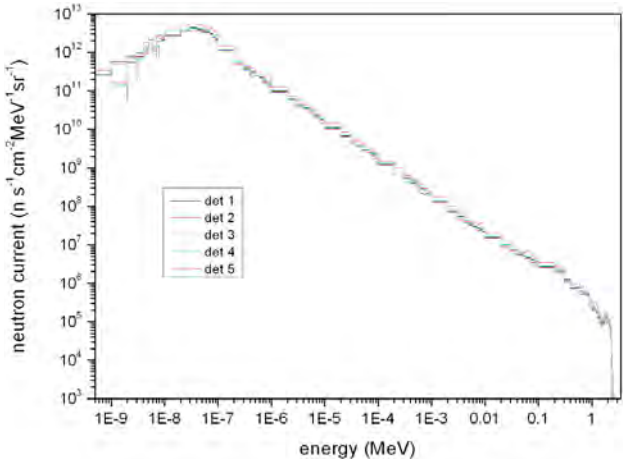

Figure 12: Neutron currents across the cylinder top surfaces (80÷90 deg)

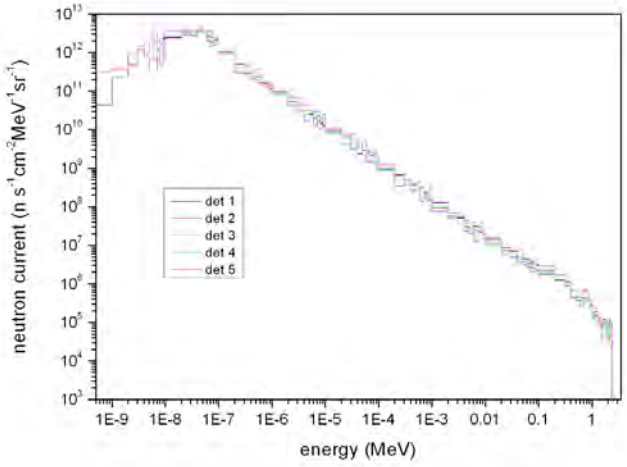

Figure 13: Distributions of neutron current across bottom surface (detector "1")

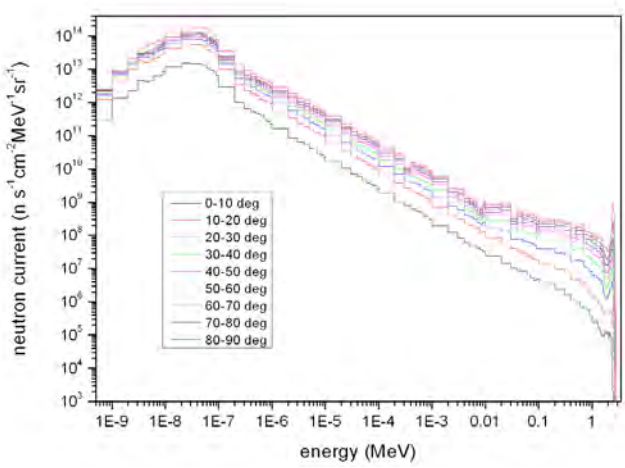

Figure 14: Distributions of neutron current across lateral surface (detector "1")

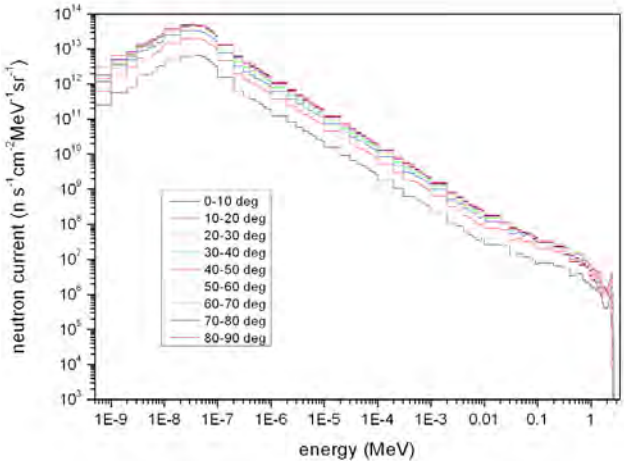

Figure 15: Distributions of neutron current across top surface (detector "1")

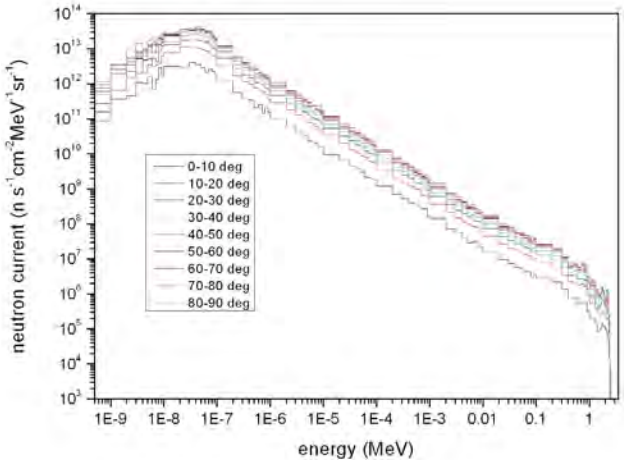

Figure 16: Ratio of perpendicular (80÷90 deg) to parallel (0÷10 deg) neutron current across the cylinder bottom surface (detector "1")

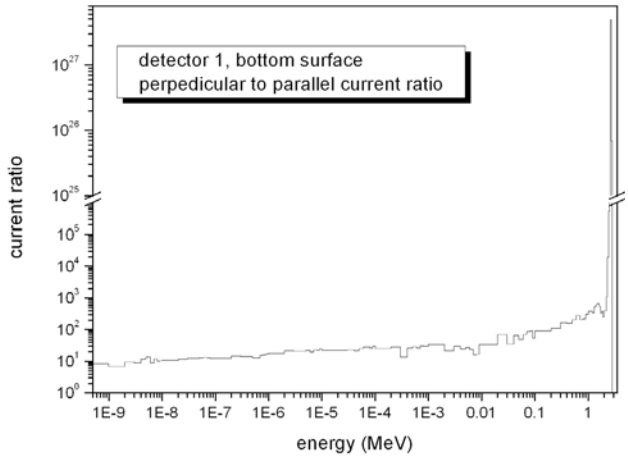

the top, lateral and bottom surfaces (Figures 13, 14 and 15). The behaviour of the 2.45 MeV peak is similar like previously. Neutron currents are the lowest for particles crossing the surfaces almost in parallel (0÷10 deg) and they gradually increase when the angle mounts, what corresponds to the total angular distributions of neutron currents (Figures 6, 7 and 8). The absolute values of neutron current are the highest for the bottom surface and the least for the top surface.

Ratio of the perpendicular to parallel neutron current across the bottom surface of detector "1" is presented in Figure 16. For thermal neutrons it is roughly 10 and then the ratio increases with energy. The rise becomes noticeable for fast neutrons and is extraordinary high for the 2.45 MeV peak. This effect is obvious since non-scattered particles from plasma cross the bottom surface at high angles. Probability that uncollided neutrons get through the bottom surface almost parallel is trifling.

Acknowledgements

The study has been partly supported by the Association Euratom-IPPLM (Poland).

The authors are very grateful to Doctors J. Junker, F. Herrnegger and F. Grünauer who have developed the MCNP model of the W7-X stellarator for years. We also acknowledge the assistance of Dr. A. Weller and Dr. R. Burhenn from the IPP.

References

[1] Beidler, C., *et al.*, "Physics and Engineering Design for Wendelstein 7-X", *Fusion Technology* 17, 148-168, (1990).

[2] Wolf, R.C., the Wendelstein 7-X Team, "A stellarator reactor based on the optimization criteria of Wendelstein 7-X", *Fusion Engineering and Design* 83, 990-996, (2008).

[3] X-5 Monte Carlo Team, *MCNP - A general Monte Carlo N-particle transport code, Version* 5, Los Alamos National Laboratory, LA-UR-03-1987, (2003).

[4] Junker, J., A. Weller, *Neutrons at W7-X*, IPP Report, Max-Planck-Institut fur Plasma-physik, Garching, IPP-2/341, (1998).

[5] Herrnegger, F., *et al.*, "Neutron field in the Wendelstein-7-X hall", *Fusion Engineering and Design* 66-68, 849-853, (2003).

From nGy to MGy – new TL dosimetry of complex radiation at high-energy accelerators and thermonuclear fusion facilities

Barbara Obryk, Pawel Bilski, Maciej Budzanowski and Pawel Olko
Institute of Nuclear Physics, Polish Academy of Sciences, Krakow, Poland

Abstract

One of the well known advantages of thermoluminescence (TL) detectors made of lithium fluoride doped with magnesium, copper and phosphorus (LiF:Mg,Cu,P) is their very high sensitivity to ionizing radiation. LiF:Mg,Cu,P detectors enable measurements of radiation doses from tens of nanograys up to a few kilograys, when the total saturation of the signal of the so-called main dosimetric peak (at about 220°C) occurs. In 2006 for the first time we observed unprecedented high-temperature emission of LiF detectors heated to temperatures up to 600°C, after exposures to radiation doses ranging from 1 kGy to 1 MGy. For quantification of the glow curve shape changes of LiF:Mg,Cu,P detectors in this range of doses and determination of the absorbed dose, the high temperature coefficient (UHTR) was defined. This newly established dosimetric method was tested in a range of radiation qualities, such as gamma radiation, electron and proton beams, thermal neutron fields and in high-energy mixed fields around the SPS and PS accelerators at CERN. A number of dosimetric sets with LiF:Mg,Cu,P detectors are currently installed around the LHC at CERN. The new method for ultra-high dose range monitoring with a single LiF:Mg,Cu,P detector, which is capable of covering at least twelve orders of magnitude of doses, can be used for dosimetry at high energy accelerators and has great potential for accident dosimetry in particular.

Introduction

There are many kinds of technology impact on the environment. Many facilities that are being built in recent years pose a challenge to radiation protection and dosimetry; dosimetric measurements appropriate for their environment monitoring need to cover a very wide range of doses. These facilities are high-energy accelerators developed for research and hadron therapy of cancer (which number is rapidly growing) as well as thermonuclear fusion technology facilities which hopefully shall contribute to energy production in future helping the climate change mitigation. Among them is the largest high-energy accelerator (the Large Hadron Collider, LHC, at CERN) which started its operation in 2009. The crucial milestone in the development and implementation of the nuclear fusion technology is going to be the ITER (International Thermonuclear Experimental Reactor), which is being under construction at Cadarache (France), and which will generate fast neutron fluxes 1000 times larger than in the largest installation up to date (JET - Joint European Torus). These technologies produce complex radiation fields in the vicinity of installations. From the radiation protection point of view all these facilities require measurements of environmental doses of mixed radiation [1]. These radiation fields typically consist of charged hadrons, muons, neutrons as well as photons and electrons with energy spectrum extending from fractions of eV to several hundreds of GeV. The intensity of this radiation may be very high [2]. Monitoring the radiation field around such facilities may require several thousands dosimetric devices, because of its dimensions and complex distributions of radiation [3]. A solution to this problem will require application of a dosimetric system that consists of passive dosimeters, mainly alanine, RPL [4] and TLDs [5].

The thermoluminescent dosimeters (TLD) are well developed technology in the field of passive radiation sensors, already widely used [6,7]. LiF:Mg,Cu,P detectors are the most suitable material for environmental radiation monitoring due to their high sensitivity, low background, suitable energy dependence and long-term stability [8,9]. They are able to measure doses at the level of tens of nanogray [10] and are becoming a standard in the modern environmental TL dosimetry [11]. Nevertheless, such sensors have not yet been applied in the radiation environment as it is presented by the technologies mentioned above. The response of lithium fluoride thermoluminescent detectors is known quite well for typical types of radiation such as photons, neutrons and beta particles, but there is only limited knowledge about their response to complex mixed radiation fields, such as those expected around *e.g.* the LHC, especially in a high-energy range. By exposing TL detectors to a well-defined mixed high-energy radiation field better knowledge and understanding of their response to these fields has been achieved. The experiments in a known mixed radiation environment were conducted at the CERN-EU high energy reference field facility (CERF), providing radiation fields similar to those expected around the Large Hadron Collider (LHC) and behind the LHC's shielding walls [12]. Measurements in this experiment were performed in both the lower (mGy) and the higher (1-150 Gy) range of doses [5]. For the latter range, in addition to the experiment, Monte Carlo simulations were performed giving good agreement for high energy mixed fields. Tests at doses up to tens of kGy were also done at the CERN's PS-IRRAD6 facility providing mixed high-energy particles, up to now. They are still under evaluation, however, preliminary results are very promising.

In addition, new behaviour of high sensitive thermoluminescent detectors (LiF:Mg,Cu,P) at high [13] and ultra-high doses [14] has been recently discovered, which allows using these detectors for measurements of doses from tens of nanograys up to several hundred kGy [15]. The most important finding is the appearance of a new peak of light emission from detectors exposed above 50 kGy [14, 15]. After having discovered the unexpected behaviour of LiF:Mg,Cu,P detectors at very high doses, a detailed study of the response of LiF sensors to specific radiation types was carried out. Comprehensive measurements of their response after photon, electron, proton and thermal neutron high-dose irradiation were completed, and the results confirmed the high-dose behaviour of LiF:Mg,Cu,P detectors [14-17]. In this way it was confirmed that the dynamic range of these detectors is meant to cover very broad range of doses.

Materials and measurements

Materials and readout methods

The response of different LiF-based TL detectors was extensively investigated for the purpose of high-dose high-temperature testing during the last few years. Efforts concentrated on high sensitive LiF:Mg,Cu,P (MCP-N), ^{7}LiF:Mg,Cu,P (MCP-7), ^{6}LiF:Mg,Cu,P (MCP-6) detectors, equivalent to TLD-100H, TLD-700H, TLD-600H, respectively. However, standard LiF:Mg,Ti (MTS-N), ^{7}LiF:Mg,Ti (MTS-7), ^{6}LiF:Mg,Ti (MTS-6), equivalent to TLD-100, TLD-700 and TLD-600, respectively, were also tested in order to observe differences in their response. All detectors were developed and produced at the Institute of Nuclear Physics (IFJ), Krakow.

The standard annealing cycle was applied; for MCP detectors 240°C for 10 minutes, and for MTS detectors 400°C for 1h followed by 100°C for 2h. The readout was performed with the MICROLAB Manual Reader-Analyzer RA'94, with a bialkali photomultiplier tube, at temperatures up to 600°C with a linear heating rate of 2 K/s. To reduce the high-dose TL signal to PMT a filter was applied in order to avoid malfunctioning during the high-dose readout.

Measurements/Irradiation

Detectors were tested at high doses of photons up to 500 kGy; ^{60}Co sources at the IFJ, Saclay and KAERI were used [13-15]. The tests with a 10 MeV electron beam were carried out at the Institute of Nuclear Chemistry and Technology, Warsaw, with doses ranging from 5 kGy to 1 MGy [16]. Also the tests with a 25 MeV proton beam at the Maier-Leibnitz Laboratory in Garching, Germany, were performed in order to check the behaviour of the glow curve in the high-dose region after irradiation with heavy particles (with LET more than an order of magnitude higher than in previous experiments) [15]. In addition, irradiations with 24 GeV/c protons (up to 1 MGy) were done in CERN's Proton Synchrotron IRRAD1 facilities [17]. The occurrence of the peak "B" (a high-temperature peak) in the MCP's glow-curve of MCPs resulting from high-dose irradiation was confirmed but it was not observed for MTS detectors [17]. Also the behaviour of LiF:Mg,Cu,P and LiF:Mg,Ti detectors at high and ultra-high thermal and epithermal neutron doses up to 1 MGy was investigated at the TRIGA Mark II reactor at the Reactor Research Center of the Jožef Stefan Institute (JSI) in Ljubljana. The results of all these irradiations confirmed the high-dose behaviour of the MCP detectors.

High temperature LiF:Mg,Cu,P emission

The shape of the MCP's glow-curves is practically identical when they result from doses ranging from nanograys to a kilogray. However, significant changes of this shape have been discovered at high and very high doses, as an outcome of all the experiments mentioned above. High temperature peaks start to grow at doses above one kilogray and continue to grow up to doses about 50 kilogray when a completely new, well separated peak, called peak "B" (see Figure 1), appears in the MCP's

Figure 1: LiF:Mg,Cu,P glow-curves resulting from 10 MeV electron irradiation

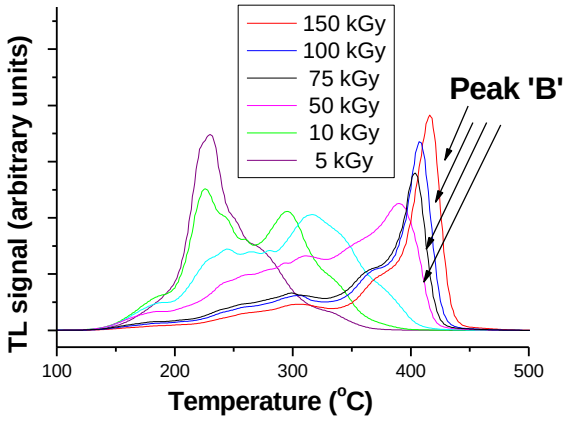

glow-curve beyond 400°C, and its position shifts towards higher temperatures with increasing dose (*e.g.* from 405°C at 50 kGy to 470°C at 500 kGy for gamma irradiation results) in contradiction to standard TL models [18].

TL emission of highly irradiated LiF:Mg,Cu,P detectors is very complex, especially in the region of very high doses. It was also found that above 20 kGy the TL emission spectrum changes, shifting towards longer wavelength [14,19].

New method

The standard TL method of dose measurements in the range of doses up to 1 kGy in exploiting the integrated signal of the main peak (with necessary correction for saturation of this peak for doses higher than 1 Gy), so for this purpose the TL signal is usually integrated up to 250°C.

Glow curves in the range from 1 kGy to 1 MGy

The results of the investigation of the LiF:Mg,Cu,P detectors' behaviour in the high and ultra-high dose range revealed a number of possible glow-curve parameters that could be used for high-dose calibration. There was a pattern observed indicating that the glow curve shape is similar for three well defined temperature regions, see Figure 2.

Figure 2: The regions of integration of TL signal: 0-250°C, 250-350°C and 350-550°C

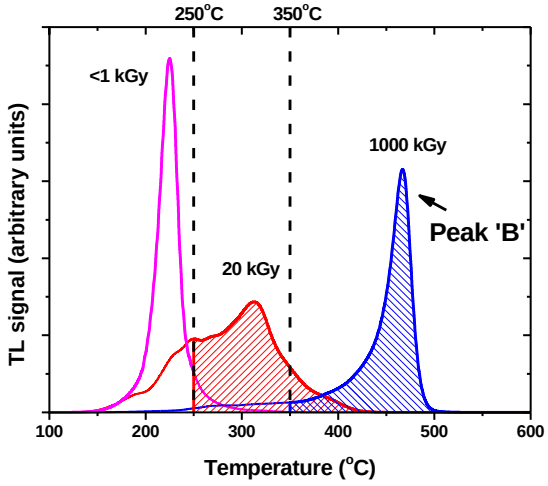

Ultra-high temperature ratio (UHTR)

The so called "ultra-high temperature ratio" was defined as a ratio of the integrated TL signal for temperatures above the temperature T_x, to the total integrated TL signal:

$$UHTR(T_x) = \frac{\sum_{T=T_x}^{T_{max}} I_T}{\sum_{T=T_{min}}^{T_{max}} I_T} \quad (1)$$

where I_T denotes TL signal at temperature T; T_{min} and T_{max} are minimum and maximum temperatures of the readout, respectively [20,21].

Regions of TL signal integration for determining the UHTR(250) and UHTR(350) parameters are shown in Figure 2, while Figure 3 presents UHTR(250) and UHTR(350) values resulting from the two types of irradiation, *i.e.* electrons and protons. A good agreement of these results enables us to fit

calibration curves for both parameters. It has been found that UHTR(250) is a good dose estimator for doses from 1 kGy to 1 MGy, while UHTR(350) can evaluate well doses higher than about 50 kGy, *i.e.* in the region of the doses where the high-temperature peak "B" grows.

Figure 3: UHTR(250) and UHTR(350) for MCP detectors as a dose function (proton irradiation-triangles; electron-circles) [20]

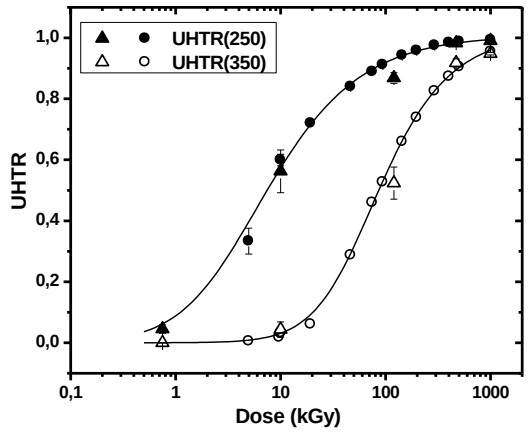

Ultra-high dose range dosimeter

The configuration of the TL dosimeter that was developed to measure doses within a very broad dynamic range is shown in Figure 4. In addition to the MCP-N or MCP-7 ultra-high dose range detector, the RADOS dosimeter slide is equipped with a pair of MTS-7 and MTS-6 TL detectors (^{7}Li- or ^{6}Li-enriched). Thanks to this pair of detectors, such a dosimeter can also detect thermal and epithermal neutrons in addition to photons and other ionizing particles. In order to simplify the readout procedure of MCP-N/MCP-7 detectors, the MTS-N standard detector is used as a dose "indicator" that allows estimating of the dose level, so that we do not need to read the MCP detector out up to 600°C unless it has been exposed to a high dose.

Figure 4: Configuration of the RADOS dosimeter with different types of TL detectors [15]

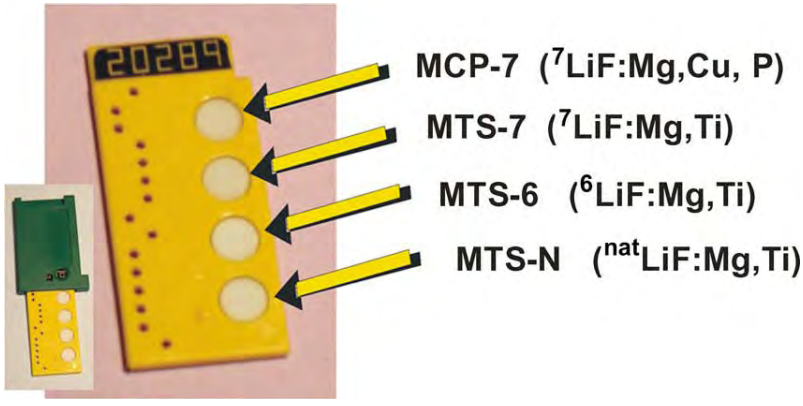

Tests and measurements

In order to test this method with a specific radiation type, blind irradiation of the detectors with 10 MeV electron beam was performed [20,21]. The doses were determined using previously fitted calibration of UHTR parameters (see Figure 3). It was observed that the parameter UHTR(350) was well suited for dose prediction above about 50 kGy, where the peak "B" was present in the glow curve, while UHTR(250) worked better in the region of tens of kilograys, as expected.

To further enhance high reliability of TL detectors, the passive dosimeter holder was proposed [15,22], which contained, in addition to four TL pellets in a RADOS dosimeter slide, alanine, a p-i-n diode and RPL detectors inserted together into polyethylene container. Such dosimeters are now applied at the LHC at CERN to measure doses at LHCb and TOTEM experiments conducted there.

Figure 5: Passive dosimeter holder [22] with four types of passive sensors: TLD, alanine, p-i-n diode and RPL detectors [15]

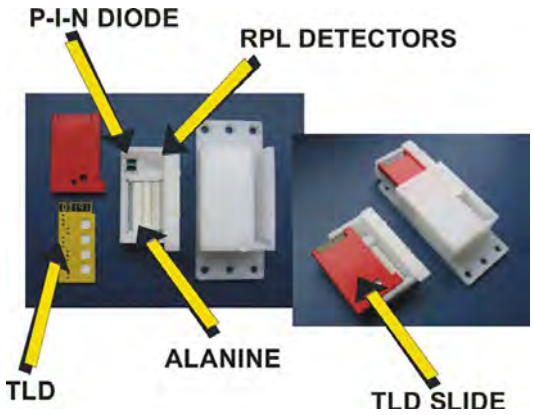

Summary and conclusions

Recent investigations and the discovery described above [14,15] could lead to great advances in thermoluminescent dosimetry technology by offering an attractive method for dosimetry of mixed radiation fields as well as a possibility of measuring a very wide range of doses with a single dosimeter [20,21]. Our results indicate that TLDs can be successfully applied to measuring of both low and high doses. Such a dosimeter constitutes a universal passive device for dosimetry around considered facilities, being not only highly reliable but cheap at the same time. This technology is already applied in dosimetry at the LHC and its experiments and is going to be applied in the hadron therapy facilities in Krakow. These applications will help spread the technology among other hadron accelerators including those devoted to medical applications.

An attempt of explaining the observed unexpected behaviour of the MCP detectors' glow curve has been made [14,15]. It was proposed that traps and recombination centres could be considered as a system of interacting clusters. With increasing dose the size of the clusters grows, simultaneously increasing the effective activation energy and shifting the TL peak towards higher temperatures. However, the nature of these "defect clusters" is unknown. Investigations are in progress as the nature of this phenomenon is still unexplained.

The new method for ultra-high dose range monitoring with a single MCP detector is a very promising tool for accident dosimetry as it does not require any dose-range prediction.

Acknowledgements

The authors would like to express high appreciation to the colleagues at CERN, especially to Maurice Glaser, Christoph Ilgner, Federico Ravotti and Dirk Wiedner, who are taking care about application of this new method there.

References

[1] Silari, M., "Workplace characterisation in mixed neutron-gamma fields, specific requirements and available methods at high-energy accelerators", *Radiat. Prot. Dosimetry* 124(3), 230-244 (2007).

[2] Bilski, P., *et al.*, "The problems associated with the monitoring of complex workplace radiation fields at European high-energy accelerators and thermonuclear fusion facilities", *Radiat. Prot. Dosimetry* 126(1-4), 491-496 (2007).

[3] Corninckx, F., *et al.*, "Comparison of high-dose dosimetry systems for radiation damage studies in collider detectors and accelerators", *Nuclear Instruments and methods in Physics Research B*, 83, 181-188 (1993).

[4] Vincke, H., *et al.*, "Response of alanine and radio-photo-luminescence dosemeters to mixed high-energy radiation fields," *Radiat. Prot. Dosimetry* 125, 340–344 (2007).

[5] Obryk, B., *et al.*, "The response of different types of TL lithium fluoride detectors to high-energy mixed radiation fields", *Radiat. Measurements*, 43, 1144-1148 (2008).

[6] Horowitz, Y.S., "LiF:Mg,Ti Versus LiF:Mg,Cu,P: The Competition Heats Up", *Radiat. Prot. Dosimetry*, 47, 135–141 (1993).

[7] Bilski, P., "Lithium fluoride: from LiF:Mg,Ti to LiF:Mg,Cu,P", *Radiat. Prot. Dosimetry*, 100, 196-206 (2002).

[8] Budzanowski, M., *et al.*, "Comparison of LiF:Mg,Cu,P (MCP-N, GR-200A) and α-Al_2O_3:C TL detectors in short-term measurements of natural radiation", *Radiat. Prot. Dosimetry*, 66, 157-160 (1996).

[9] Budzanowski, M., *et al.*, "Short-term measurements of natural radiation using high-sensitive TL detectors", *Nukleonika*, 41(2), 141-148 (1996).

[10] Budzanowski, M., *Utra-sensitive thermoluminescent detectors based on LiF:Mg,Cu,P (MCP-N) and their applicability in dosimetry of gamma radiation in environment* (in Polish), Ph.D. Thesis, IFJ Report No. 1875/D (2001).

[11] Bos, A.J.J., "High sensitivity thermoluminescence dosimetry", *Nucl. Instr. and Meth. B* 184, 3-28 (2001).

[12] Mitaroff, A., M. Silari, "The CERN-EU high-energy reference field (CERF) facility for dosimetry at commercial flight altitudes and in space," *Radiat. Prot. Dosimetry* 102, 7–22 (2002).

[13] Bilski, P., *et al.*, "High-dose characterization of different LiF phosphors", *Radiat. Measurements* 42, 582–585 (2007).

[14] Bilski, P., *et al.*, "Characteristics of LiF:Mg,Cu,P thermoluminescence at ultra-high dose range", *Radiat. Measurements* 43, 315-318 (2008).

[15] Obryk, B., *et al.*, "Development of a method for passive measurement of radiation doses at ultra-high dose range", *IEEE Trans. Nucl. Sci.* 56, No. 6, 3759-3763 (2009).

[16] Bilski, P., B. Obryk, Z. Stuglik, "Behaviour of LiF:Mg,Cu,P and LiF:Mg,Ti thermoluminescent detectors for electron doses up to 1 MGy", *Radiat. Measurements* 45, 576-578 (2010).

[17] Obryk, B., *et al.*, "The response of TL lithium fluoride detectors to 24 GeV/c protons for doses ranging up to 1 MGy", *Radiat. Measurements* 45, 643-645 (2010).

[18] Bos, A.J.J., "Theory of thermoluminescence", *Radiat. Measurements* 41, S45-S56 (2007).

[19] Mandowska, E., *et al.*, "Spectrally resolved thermoluminescence of highly irradiated LiF:Mg,Cu,P detectors", *Radiat. Measurements* 45, 579-582 (2010).

[20] Obryk, B., *Development of a method of high dose measurement using highly sensitive LiF:Mg,Cu,P detectors* (in Polish), Ph.D. Thesis, IFJ PAN (2010).

[21] Obryk, B., P. Bilski, P. Olko, "Method of thermoluminescent measurement of radiation doses from micrograys up to a megagray with a single LiF:Mg,Cu,P detector", *Radiat. Prot. Dosimetry*, in print (2010).

[22] Ilgner, C., *Passive sensor housing*, CERN online materials, available at: *http://indico.cern.ch/conferenceDisplay.py?confId=12735* (2007).

Detection of explosives and other illicit materials by a single nanosecond neutron pulses – Monte Carlo simulations of the detection process

Ryszard Miklaszewski,[1] **Krzysztof Drozdowicz,**[2] **Urszula Wiącek,**[2]
Dominik Dworak,[2] **Vladimir Gribkov**[3]
[1]Institute of Plasma Physics and Laser Microfusion, Warsaw, Poland
[2]The Henryk Niewodniczański Institute of Nuclear Physics
Polish Academy of Sciences, Krakow, Poland
[3]Institute of Theoretical and Experimental Physics, Moscow, Russia

Abstract

Recent progress in the development of a single-pulse Nanosecond Impulse Neutron Investigation System (NINIS) intended for interrogation of hidden objects (explosives and other illicit materials) by means of measuring elastically scattered neutrons is presented in this paper. The method uses very bright neutron pulses having duration of the order of few nanoseconds, generated by a dense plasma focus (DPF) devices filled with a pure deuterium or deuterium-tritium mixture as a working gas. Very short duration of the neutron pulse, its high brightness and mono-chromaticity allow to use time-of-flight method with bases of about few meters to distinguish signals from neutrons scattered by different elements.

Results of the Monte Carlo simulations of the scattered neutron field from several compounds (explosives and everyday use materials) are presented in the paper. The MCNP5 code has been used to get info on the angular and energy distributions of neutrons scattered by the above mentioned compounds assuming the initial neutron energy equal to 2.45 MeV (D-D). A new input has been elaborated that allows modelling not only a spectrum of the neutrons scattered at different angles but also their time history from the moment of generation up to detection. Such an approach allows getting approximate signals as registered by hypothetic scintillator+photomultipler probes placed at various distances from the scattering object, demonstrating a principal capability of the method to identify an elemental content of the inspected objects. Preliminary results of the MCNP modelling of the interrogation process of the airport luggage containing several illicit objects are presented as well.

Introduction

Fight against terrorism is a complicated, multidisciplinary task involving political, economical, psychological, organizational, scientific, technical, etc., issues. An efficient method of detection of explosives and other illicit materials is of principal importance. Despite of long lasting efforts of scientists and engineers such a method still does not exist. Existing prototypes are far from maturity, different methods used in such devices have they advantages and disadvantages, so still there is a space for new ideas, new inventions [1-5].

A new approach to explosives and other illicit materials detection was proposed in [6]. Taking advantage of capabilities of modern neutron generators (based on the Plasma-Focus principle) that are capable to produce flashes of very intense and very short neutron pulses (<10ns) it is possible to determine elemental content of unknown bulk samples from information existing in a field of scattered neutrons. The flush intensity reaches up to 10^9 of 2.45 MeV neutrons per shot from the D-D reaction and up to 10^{11} of 14 MeV neutrons from the D-T reaction. The time-of-flight method can be involved in the identification procedure due to the short neutron pulse duration. It seems that a single shot inspection systems can be elaborated on the basis of the method proposed, limited in time only by computer data processing

Method

The method is based on the well know fact that nuclide-specific information is present in the scattered neutron field. By detecting neutrons elastically and in-elastically scattered at different laboratory angles for two different incident neutron energies (2.45 MeV and 14 MeV), the amounts and positions of the scattering nuclides may be determined.

Figure 1: Main idea of the neutron scattering detection

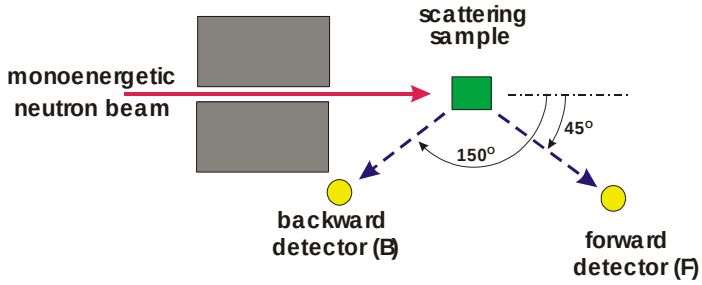

Scattering signatures of different elements (especially H, C, N and O) should be precisely determined and data basis of such signatures created. Then, using the data basis, scattering signatures measured for unknown samples are unfolded to determine their elemental composition.

The method proposed belongs to a wider group of approaches that make use of specific interaction of neutrons (fast or thermal) with different materials. As a result of such interaction the induced gamma radiation is emitted from an object irradiated as well as a field of scattered neutrons appears (due to elastic and inelastic scattering of primary neutrons). The information on elemental composition of the object can be drawn from both the gamma radiation and the scattered neutron field.

We propose to bring into play a neutron source based on a *plasma accelerator*, which generates very powerful pulses of neutrons in the nanosecond range duration. New generation of powerful neutron sources of the Plasma Focus type can generate neutron pulses not only short by its duration (in the *nanosecond range*), but provides *a very high neutron yield* in these pulses. For example our device PF-6, operating at the Institute of Plasma Physics and Laser Microfusion, Warsaw, Poland, with 7.4 kJ of energy in its capacitor storage is capable to generate in one pulse of ~10 ns duration up to 10^9 D-D neutrons (2.5-MeV) or 10^{11} D-T neutrons14-MeV). This feature gives a principal possibility to create a **"single-shot detection system"**. It means that all necessary information will be received using a single (or maximum few) very bright pulses of neutrons having duration in a nanosecond range and registered by means of the time-of-flight technique. A proposal of the general scheme of such detection system is presented in Figure 2.

Figure 2: General scheme of the detecting system

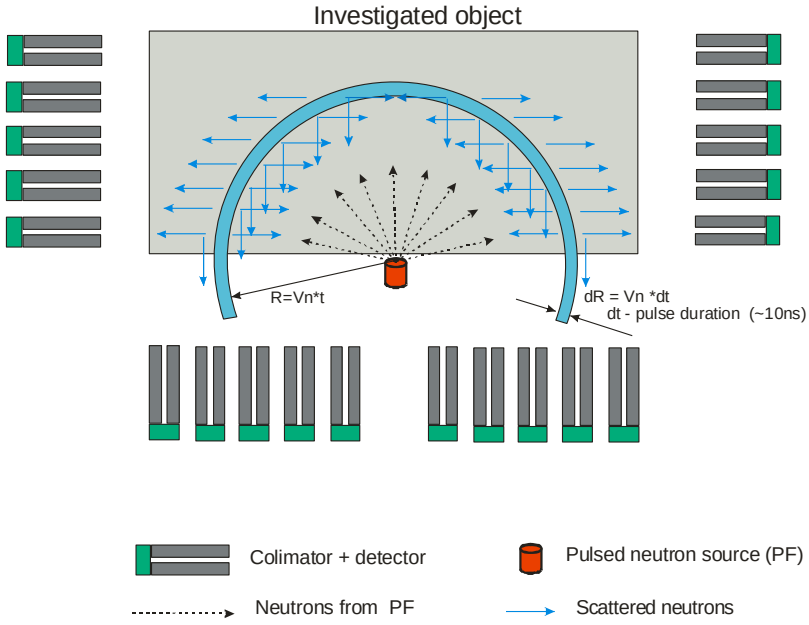

Monte Carlo modelling of the method

The MCNP (version5) standard code [7] has been used to investigate various features and properties of the method. Inputs to the MCNP code evolved in time from simple ones to more and more complicated together with increasing knowledge of the working team. The most important progress with the inputs development was an achievement of the capability of simulating scattered neutron signals as registered by factious scopes (time-amplitude signals).

Scattering from simple objects

For the start up the MCNP code was used to simulate scattering of neutrons from objects (cubes 3–5 cm) made of pure basic elements, like Oxygen, Nitrogen, Carbon, Sulphur, as well as of some compounds, *e.g.* explosives (RDX) and everyday use materials like melamine, glucose and acetamide. The aim of these investigations was to examine dependence of the registered neutron signals on angles and distances: neutron source – sample, sample – detector etc. The neutron pulse from the point D-D source (E_n = 2.45 MeV) was assumed to be Gaussian in time with the realistic full width at half maximum (FWHM) of 10 ns. The geometry of computation was as follows in Figure 3:

Figure 3: Geometry of the MCNP calculations

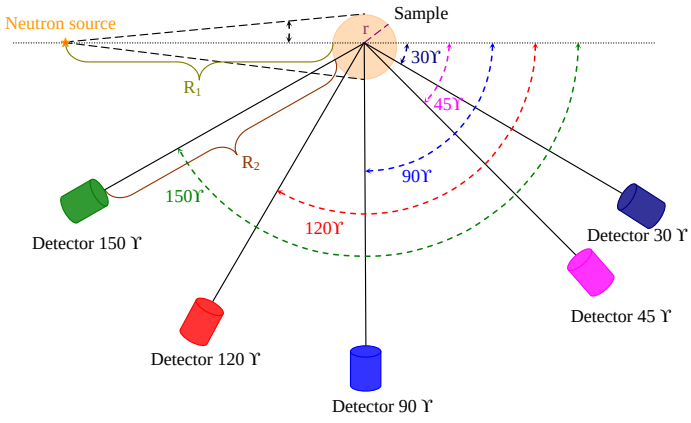

The first question was how a capability of the method to distinguish basic elements of explosives (C, N, O) depends on a scattering angle. From the results presented in Figure 4 it is evident that rather high scattering angles 150^0–170^0 should be used for the determination of the elemental content of unknown objects as for lower angles the signals originated from various elements merge gradually. In Figure 5 the time – amplitude signals from scattered neutrons for several compounds are presented showing the principal capability of the method to determine elemental content of irradiated objects. One can see from Figure 5 that for ideal conditions assumed in the computation the compounds filling the irradiated objects can be easily identified.

Figure 4: Time-of-flight signals from neutrons scattered by the sphere (r = 5cm) filed with the RDX explosive ($C_3H_6N_6O_6$)

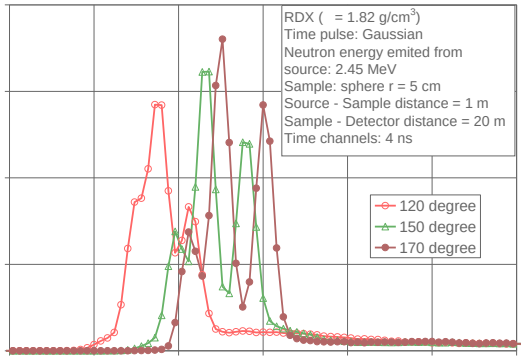

Figure 5: Comparison of the time-of-flight signals from neutrons scattered by spheres filled with various materials – a) RDX ($C_3H_6N_6O_6$), b) acetamide (C_2H_5NO), c) melamine ($C_3H_6N_6$), d) glucose ($C_3H_{12}O_6$)

a)

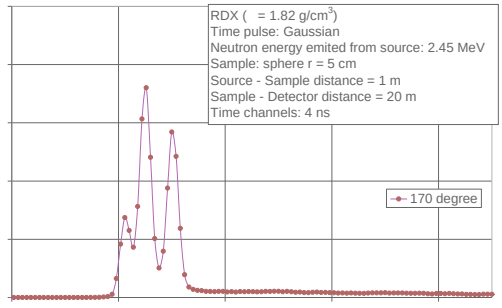

b)

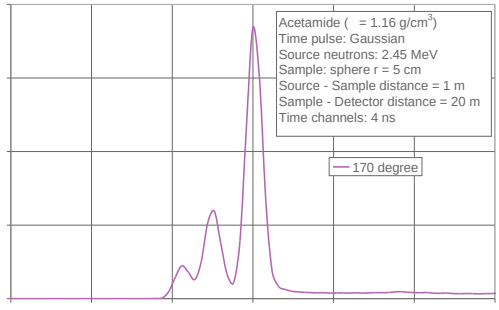

c)

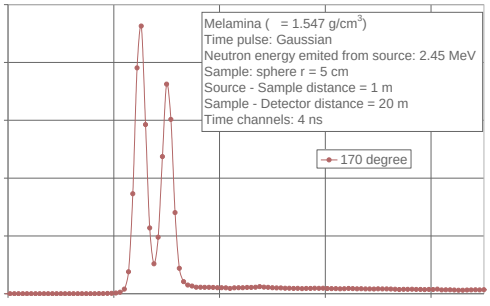

d)

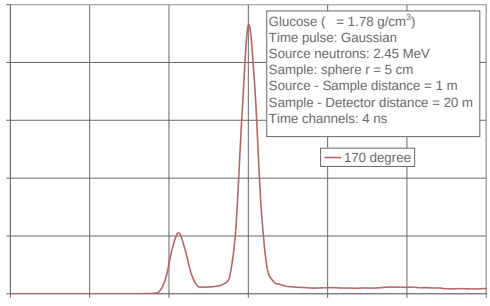

Figure 6: Geometry of the suitcase containing four spheres filled with various materials (RDX, melamine, glucose and acetamide

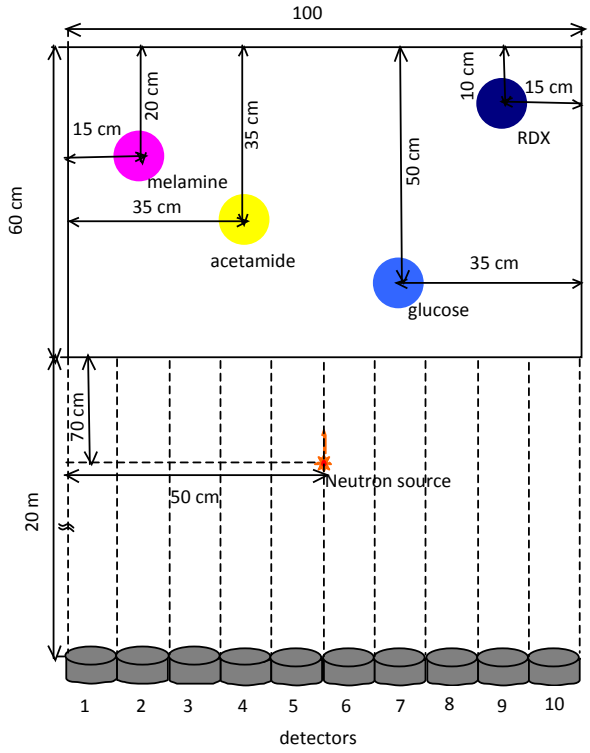

Figure 7: Signals registered by detectors (Nos. 2, 4, 7 and 9)

a) detector No. 2

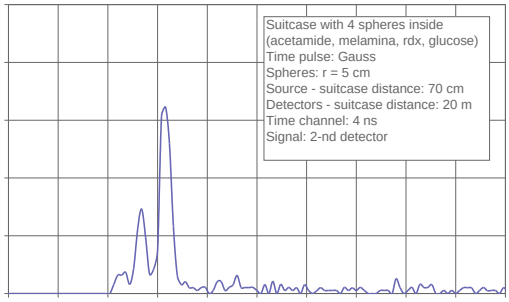

b) detector No. 4

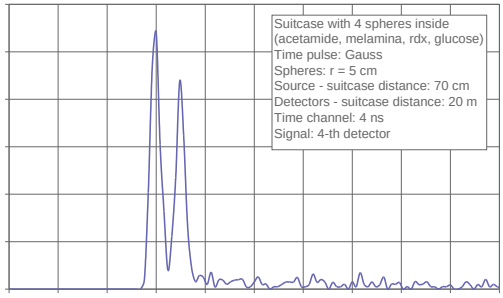

c) detector No. 7

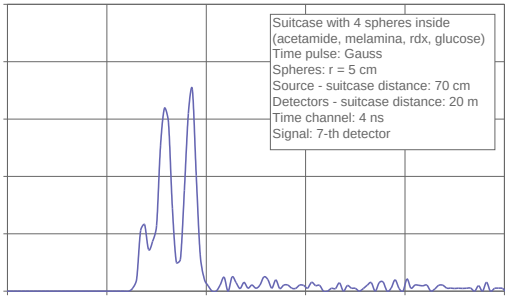

d) detector No. 9

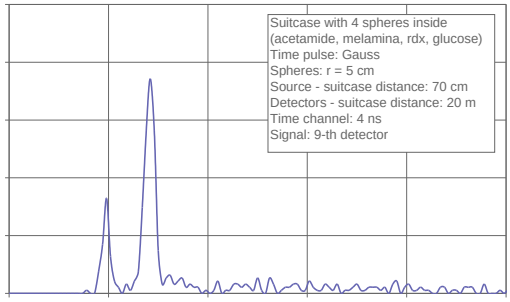

Modelling of a real luggage

The next step done in modelling of the various aspects of the method was a simulation of scattered signals from a suitcase containing objects (spheres) filled with different materials (explosive RDX and three types of everyday use materials –melamine, glucose and acetamide). Scheme of the modelling is presented in Figure 6. Collimators were modelled in front of the detectors to avoid registering neutrons from other directions. Signals registered by fictitious multichannel time analyser (detecting system) are presented in Figure 7.

From the signals presented in Figure 7 one can see that the system of detectors and collimators allows getting undisturbed signals that allow to identify the elemental content of spherical objects containing various materials. The system allows to determine position of hidden objects as well (thanks to collimators used) but several discharges associated with rotation of a luggage are necessary in order to get three dimensional positions.

Conclusions

A new method for detection and identification of hidden illicit materials was presented together with the MCNP modelling of some of its features. It seems that results of the MCNP modelling performed up to now justify a conclusion that the method passed the so called "proof of principle". An extensive programme of further theoretical (MCNP modelling) and experimental investigations of the method is now in preparation.

Acknowledgements

The work was partly sponsored from the research grant of the Polish Ministry of Science and Higher Education (MNiSzW) No. O N202 049735.

References

[1] Csikai, J, "Neutron-based techniques for the detection of concealed objects", *Proc. of the enlargement workshop on Neutron Measurements and Evaluations for Applications – NEMEA*, Budapest, Hungary, *Report EUR 21100 EN*, (2003).

[2] Buffler A., *et al.*,"Material classification by fast neutron scattering", *Nuclear Instruments and Methods in Physics Research,* B 173, pp. 483-494, (2001).

[3] Brooks, F.D., *et al.*, "Determination of HCNO concentrations by fast neutron scattering analysis", *Nuclear Instruments and Methods in Physics Research,* A 410, pp. 319-328, (1998).

[4] Nebbia, G., *et al.*, "Use of neutron based technique in the control of illicit trafficking of fissile and explosive material", *Proc. Of the Workshop on Countering Nuclear and Radiological Terrorism,* Yerevan, Armenia, pp. 271-290, (2006).

[5] Vourvopulos, G, P.C. Womble, "Pulsed fast/thermal neutron analysis: A Technique for Explosives Detection", *TALANTA*, Vol. 54, pp. 459-468, (2001).

[6] Gribkov, V.A., R. Miklaszewski, "On a possibility of the single-shot detection of hidden objects by using nanosecond impulse neutron inspection system", *Acta Phys. Chim. Debr.* XXXVIII-XXXIX, pp.185-193, (2005).

[7] X-5 Monte Carlo Team, *MCNP – A general Monte Carlo N-particle transport code, Version* 5, Los Alamos National Laboratory, *LA-UR-03-1987*, (2003).